STUDY OF ALLOY EFFECT ON ELECTROMIGRATION IN SN SOLDER ALLOYS

by

GENG NI

Presented to the Faculty of the Graduate School of

The University of Texas at Arlington in Partial Fulfillment

of the Requirements

for the Degree of

DOCTOR OF PHILOSOPHY

THE UNIVERSITY OF TEXAS AT ARLINGTON

May 2023

ACKNOWLEDGEMENTS

I would like to express my sincere gratitude to my research advisor, Prof. Choong-un Kim, for providing me with the opportunity to transfer from a master's program to a doctoral program and for guiding me with his extensive knowledge and hands-on experience in the field of microelectronics. Without his support and guidance, I would not have the bright future that I have in the semiconductor industry. I am deeply indebted to him for allowing me to be part of his exceptional research team. I would also like to thank my committee members, Dr. Ye Cao, Dr. Nancy Michael, Dr. Yaowu Hao, and Dr. Kyung Suk Yum, for their valuable time and suggestions.

I extend my heartfelt appreciation to my colleagues and group members, Dr. Po-Cheng Lu, Dr. Valery Ouvarov-Bancalero, Dr. Hossein Madanipour, Dr. Yi Ram Kim, Dr. Allison Osmanson, Kelly Claunch, Aniket Prakash Bhagwat, Sidharth Anand, Yu-Chi Cheng, Manasi Puranik, Ratan Kota, Sara Huerta, Yvoone Albert, Mohsen Tajedini, Hariram Mohanram, Chuanhao Nie, Jimmy (Bao Dang) Le, Jorge Mendoza, Hsin Hao Liang, Ross Everett, Ryan Hart, and Chuzhong Zhang, for their support and camaraderie. Thank you for all the fond memories we shared.

I would also like to acknowledge Dr. Jiechao Jiang, Dr. Yi Shen, and David Yan from Characterization Center for Materials and Biology (CCMB), Beth Robinson, Jennifer Standlee, Natalie Burden, Jose Garcia, Lashonda Burns, and Shelly Douglass from Materials Science and Engineering (MSE) administrative office, Kermit Beird, Sam Williams, and Scott Eichmann from UTA Mechanical and Aerospace Engineering (MAE) machine shop for their constant support and contagious positivity.

I am immensely grateful to my parents, Bin Ni and Yutian Zhang, for their unwavering love and encouragement during my studies. Without their support, I would not have achieved what I have today.

Finally, I congratulate and commend myself for persevering through the rigorous training of my doctoral program. There were times when I considered giving up, but with the help and support of my advisor, parents, and friends, I persevered step by step. This experience has undoubtedly been the most valuable one in my life.

This work is supported by Semiconductor Research Corporation (SRC) Task ID 2949.001.

ABSTRACT

STUDY OF ALLOY EFFECT ON ELECTROMIGRATION IN SN SOLDER ALLOYS

Geng Ni, PhD

The University of Texas at Arlington, 2023

Supervising Professor: Choong-Un Kim

This dissertation presents experimental results about the alloy effect on the Electromigration (EM) of Sn in Sn-based binary and ternary alloys. By using cross-stripe configuration, the alloy effect on EM of Sn can be characterized from marker polarity, and the migration of alloy element under EM can be measured from marker front motion. In the dissertation, the mechanism of alloy effect on EM of Sn, “Two-Phase equilibrium”, will be introduced.

Electromigration is a phenomenon where metallic atoms are migrated at the direction of electron flow under high current density. In response to the demands for greater speed and smaller size, semiconductor devices must now be designed to carry higher current densities than ever before. Which makes electromigration failure become a concern, especially in Sn-based solder interconnects due to its significant application in integrated circuits. Alloying may be the

most effective method to slow down the EM of Sn, and fundamental studies on EM of Sn are not very well understood yet. Driven by these two motivations, this project is intended to study the alloy effect on electromigration fo Sn, and Cross-stripe configuration is selected as experimental configuration in the project to study alloy effect. “Cross-stripe” was originally developed for studying Al alloying effect on electromigration of Cu. Due to the different EM rate of Sn between cross-stripe (alloyed) and stripe (metrix) areas, markers (hillock and void) induced by Kirkendall effect will initially form at boundaries of alloyed areas, and keep developing during testing. Polarity of marker formation, and motion of markers fronts thus become important parameters for characterization of alloying effect on EM rate change of Sn. Our study was initally aimed at better chatacterization about EM kinetics of alloy elements (such as Cu, Ni, Ag and Au etc.) in Sn solder interconnects, but moved further into the study about their suppression abilities on the EM rate of Sn.

Based on the expermental result achieved with various elements, all tested elements can suppress EM rate of Sn when their concentrations beyond maximum solubility limit and form inter-matellic compound (IMC) as percipiates. When alloy element concentrations are below maximum solubility, which means they exist as solute in Sn metrix, some elements like (N iand Bi) remain EM suppression of Sn, however most of elements like (Au, Ag, Cu, Pd and Co) may accelerate the EM rate of Sn. The two-phases equilibrium between Sn and Sn-based IMC is the key mechanism affecting the EM rate of Sn, not the presence of alloying elements themselves. This finding suggests that the EM reliability of Sn can be improved by either adding EM suppression elements, or producing Sn grain structure with IMC (two-phases equilibrium) by adding enough amount of alloy element beyond maximum solubility.

In the study of ternary samples, we explore the interactions between different alloying elements by applying a cross-stripe of secondary alloying elements onto an alloyed Sn stripe. Based on the result, existence of Ag will make Cu migrates faster in existing Cu-Sn system. Which is an implication to SAC alloys. Also, co-existence of Ni and Cu may further suppress the EM of Sn. Therefore, IMC stability can be increased and leads to the improvement of EM reliability of Sn in ternary systems.

The results reported in this dissertation provide a comprehensive and plausible explanation of the alloy effect on electromigration of Sn, and offer insights for improving the reliability of Sn solder interconnects against EM.

Table of Contents

List of Figures

List of Tables

Chapter 1: Introduction & Background

1.1 Research Motivation and Sn Element

As part of SRC Task 2949.001 "Metallurgical Exploration of UBM/Solder Microstructure for Suppression of Early Electromigration Failures," our research objective is to gather metallurgical evidence to aid in fundamental studies on the kinetics of early electromigration (EM) failures in typical Sn solder joints. To accomplish this research mission, two major approaches are set in the research project: First, understanding the alloy effects of various elements on electromigration behavior of Sn. Second, characterizing their EM diffusivity (Z*D) under EM of Sn. The purpose of this characterization is to gain a better understanding of the underlying kinetic mechanisms responsible for EM in Sn solder interconnects. Additionally, we hope to identify an exemplary alloying element that can be optimally located at the interface between the UBM (under bump metallization) and solder. By doing so, the EM reliability of solder interconnects can be enhanced by suppressing the inherent EM diffusivity of Sn.

Figure 1.1 Bars of pure Sn metal.

Tin, represented by the chemical symbol Sn, is a post-transition metal belonging to group 14 of the periodic table of elements. Its name originates from the Latin word "Stannum" [1]. Tin exhibits two primary oxidation states, +2 and the more stable +4.

Tin (Sn) is a soft, ductile, and highly crystalline silvery-white metal, with a melting point of 231.93°C and a boiling point of 2875°C. When a Sn bar is bent, it produces a characteristic crackling sound known as "tin-cry" as a result of twinning in Sn crystals [2]. Sn has two major allotropes: β-tin, also known as white-tin, which is stable at room temperature and has a body-centered tetragonal (BCT) crystal structure, and α-tin, also known as gray-tin, which is stable below 13.2°C and has a brittle, non-metallic form with a diamond cubic crystal structure (see Figure 1.2). The β to α Sn transformation temperature is 13.2°C, which can be lowered by impurities present in the Sn matrix. Addition of antimony (Sb) or bismuth (Bi) can even prevent this transformation from occurring at all [3]. Sn can also exist in the form of γ-tin and σ-tin at high temperatures (above 161°C) and high pressures [4].

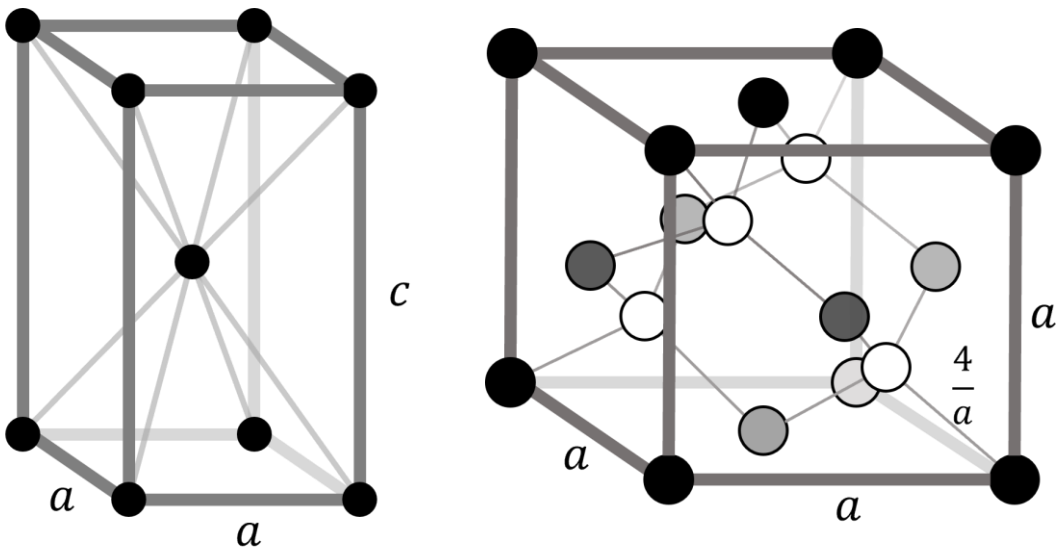

Figure 1.2 Body-centered tetragonal (left), and diamond cubic crystal structure (right).

Pure Sn was one of the first superconductors to be studied and exhibits superconductivity below a critical temperature of 3.72K [5]. In fact, the Meissner effect, one of the characteristic features of superconductors, was first observed in pure Sn crystals [6].

Tin extraction and use can be traced back to the beginnings of the Bronze Age around 3000 BC, where bronze artifacts containing a copper-tin (Cu-Sn) alloy were discovered at archaeological sites [7]. Pure metallic Sn began to be produced after 600 BC. Nowadays, Sn has become an important metal in industrial applications, with nearly half of its usage in soldering (Figure 1.3). Sn-based solders are widely used in a variety of industries, including plumbing, electronics, heating/AC, and manufacturing processes.

Initially, a general-purpose eutectic solder known as Sn-Pb solder was used widely to join two metals together. It came in ratios such as 63% tin to 37% lead, 60% tin to 40% lead, or a 50/50% ratio. Sn-Pb solder is ideal for applications where delicate temperature requirements for soldering are necessary. It is commonly used in electronics to prevent heat-sensitive components from melting, cracking, or warping at high soldering temperatures. Additionally, it provides good electrical properties and mechanical strength, ensuring that electronic components are securely joined to contact points. As the tin-lead wire is lightweight, it does not put unnecessary stress on components.

Another benefit of tin-lead solder is its corrosion resistance properties. Oxidation and other corrosive elements can severely impact soldered joints, causing them to become pitted and fail quickly, which can result in the two components entering apart, causing electronics to fail or cracks in pipes that allow steam, water, liquids, and other products to seep out [9].

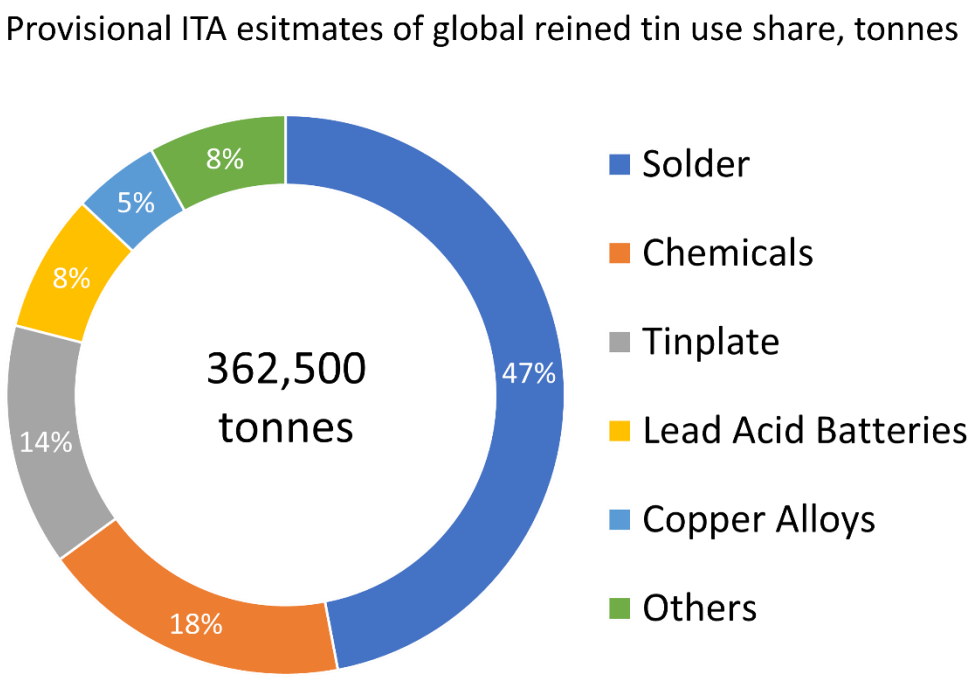

Figure 1.3 Global Tin use by application, 2017 [8].

However, the implementation of the Restriction of Hazardous Substances (RoHS) directive 2002/95/EC has restricted the use of Pb-bearing solders in most commercial electronics [10]. Since then, Sn-based Pb-free solders, such as Sn–3.0Ag–0.5Cu, Sn–3.5Ag, and Sn–1.8Ag, have been intensively investigated for their properties and applications in interconnect materials [11]. The novel solder interconnect structure is now approaching Cu pillar micro-bumps from conventional C4 bumps, showing rapid development towards interconnect miniaturization to meet the ever-increasing performance demands of electronic products [12,13]. The solder interconnect with miniaturized dimensions is thereby subjected to gradually increasing current density and confronts challenging electromigration (EM) reliability concerns (Fig 1.4) [14,15].

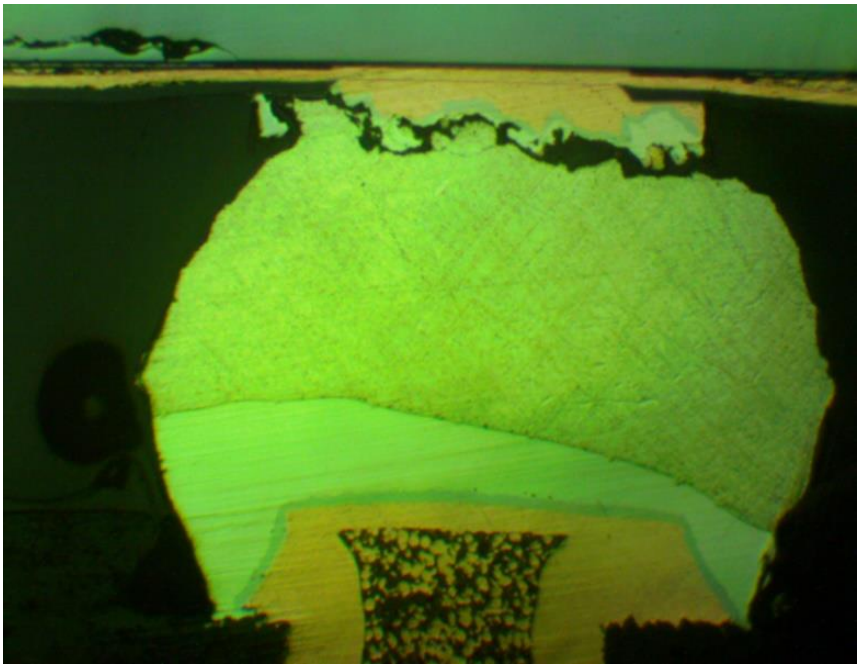

Fig 1.4 Failure induced by electromigration in Sn solder bump with Cu UBM.

A comprehensive study of electromigration in Sn-based solder interconnects is of great interest in both fundamental electromigration behavior and practical reliability aspects [16]. To date, significant efforts have been made to study the microstructure evolutions and properties variations induced by diffusion and electromigration in Sn. However, there is still a lack of understanding of the fundamental studies about solute effect on diffusion/EM in Sn [17, 18]. These gaps in knowledge have sparked interest and become our research motivations in recent years.

1.2 Diffusion

1.2.1 Mechanism of Atomic Diffusion

Atomic diffusion is a phenomenon in which atoms migrate through a solid under the influence of chemical potential, which can be related to concentration gradients for ease of

measurement [19]. One common example of atomic diffusion occurs when solute atoms diffuse through a solid solution. Depending on the type of site occupation in the crystal lattice, there are two predominant mechanisms of atomic diffusion: interstitial diffusion and substitutional diffusion.

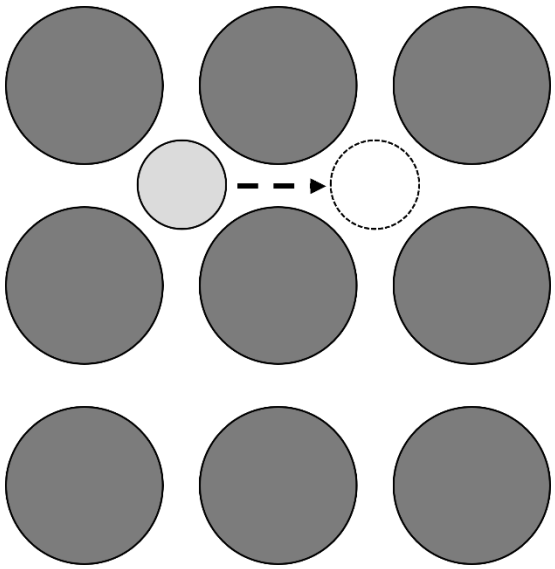

Fig 1.5 Schematic diagram of interstitial diffusion.

In interstitial diffusion, the solute atom migrates by jumping between interstitial sites in the crystal lattice. This type of diffusion occurs when the size of the solute atom is small, and it has an equal probability of jumping to all adjacent interstitial sites. In order to move an interstitial solute atom to an adjacent interstice, the atoms of the solid solution lattice must be pushed into higher energy positions (Figure 1.6). The increase of free energy of the system is known as activation energy (ΔG_m) for the migration of this atom, and the jump frequency of the atom is given by the following equation:

$$\Gamma = zv \exp\frac{-\Delta G_m}{RT} \tag{1.1}$$

where z represents the number of interstitial sites available to atom, and v stands for mean frequency of atom vibration. ΔG_m can be considered to be the sum of a large activation enthalpy ΔH_m, and a small activation entropy term $-T\Delta S_m$ [19]. Substituting

$$D = \frac{1}{6}\Gamma\alpha^2 \tag{1.2}$$

Leads to diffusion coefficient as

$$D = \left(\frac{1}{6}\alpha^2 \mathrm{z}v\exp\frac{\Delta S_m}{R}\right)\exp\frac{-\Delta H_m}{RT} \tag{1.3}$$

Simplifying equation 1.3 to an Arrhenius-type equation [19], that is

$$D = D_0\exp\frac{-Q_{ID}}{RT} \tag{1.4}$$

where

$$D_0 = \frac{1}{6}\alpha^2 \mathrm{z}v\exp\frac{\Delta S_m}{R} \tag{1.5}$$

And

$$Q_{ID} = \Delta H_m \tag{1.6}$$

Therefore, D or Γ increases exponentially with temperature at a rate determined by the activation enthalpy Q_{ID}. Equation 1.2 has been found to agree with experimental measurements of diffusion coefficients in both interstitial and substitutional diffusion [19].

In interstitial diffusion, solute atoms can migrate freely to adjacent interstices when they can overcome the energy barrier of jumping. On the other hand, substitutional diffusion is not as straightforward because an atom can only jump when there is an available adjacent vacancy site on the lattice position (figure 1.7). This diffusion is driven by a vacancy mechanism.

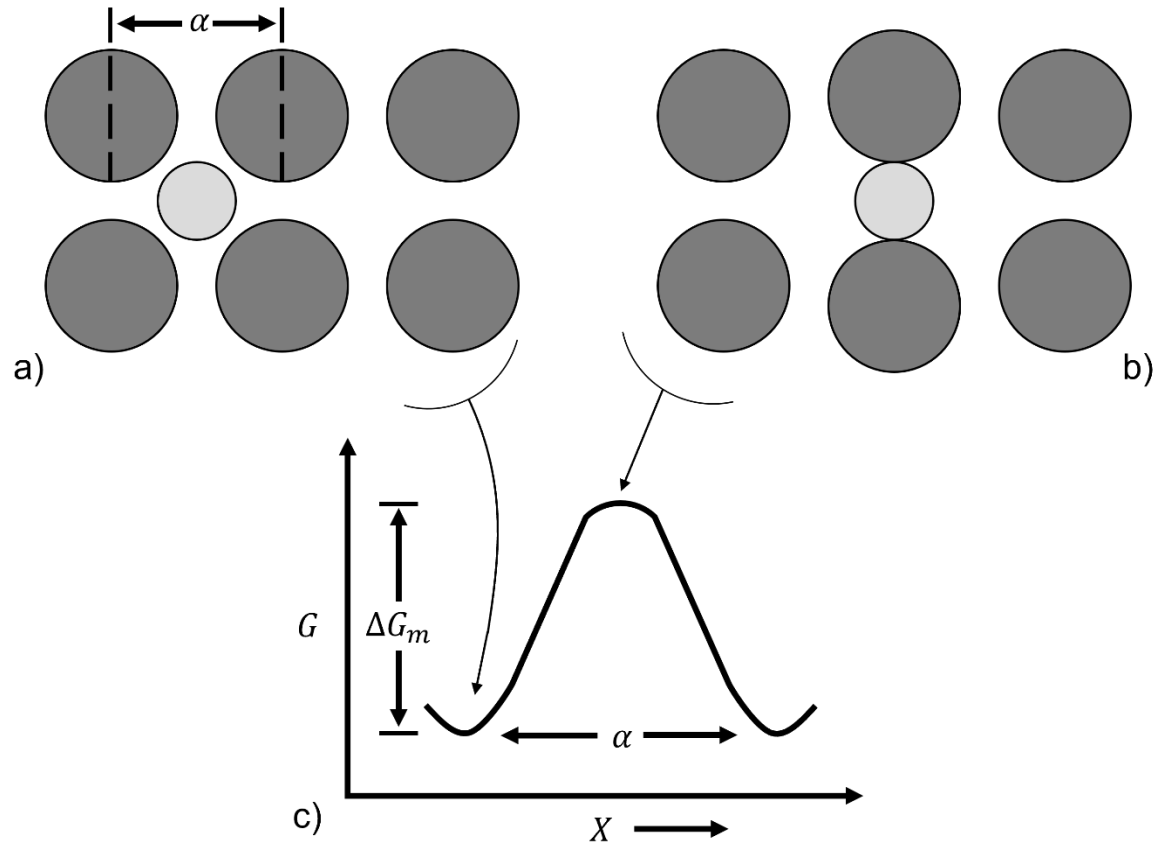

Fig 1.6 Interstitial atom, (a) in equilibrium position, (b) at the position of maximum lattice distortion, (c) Variation of the free energy of the lattice as a function of the position of atom [20].

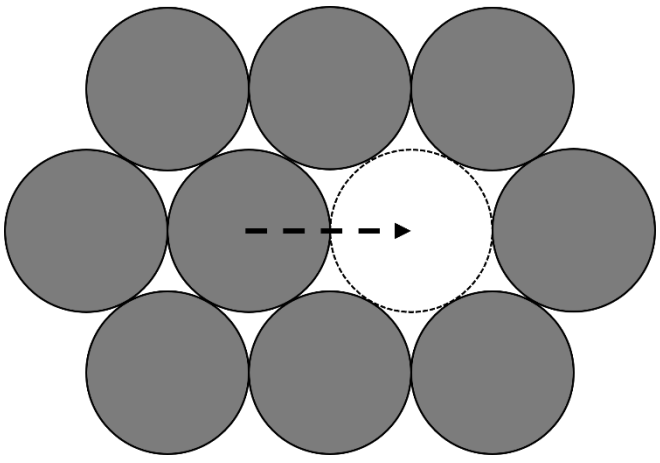

Fig 1.7 Schematic diagram of substitutional diffusion.

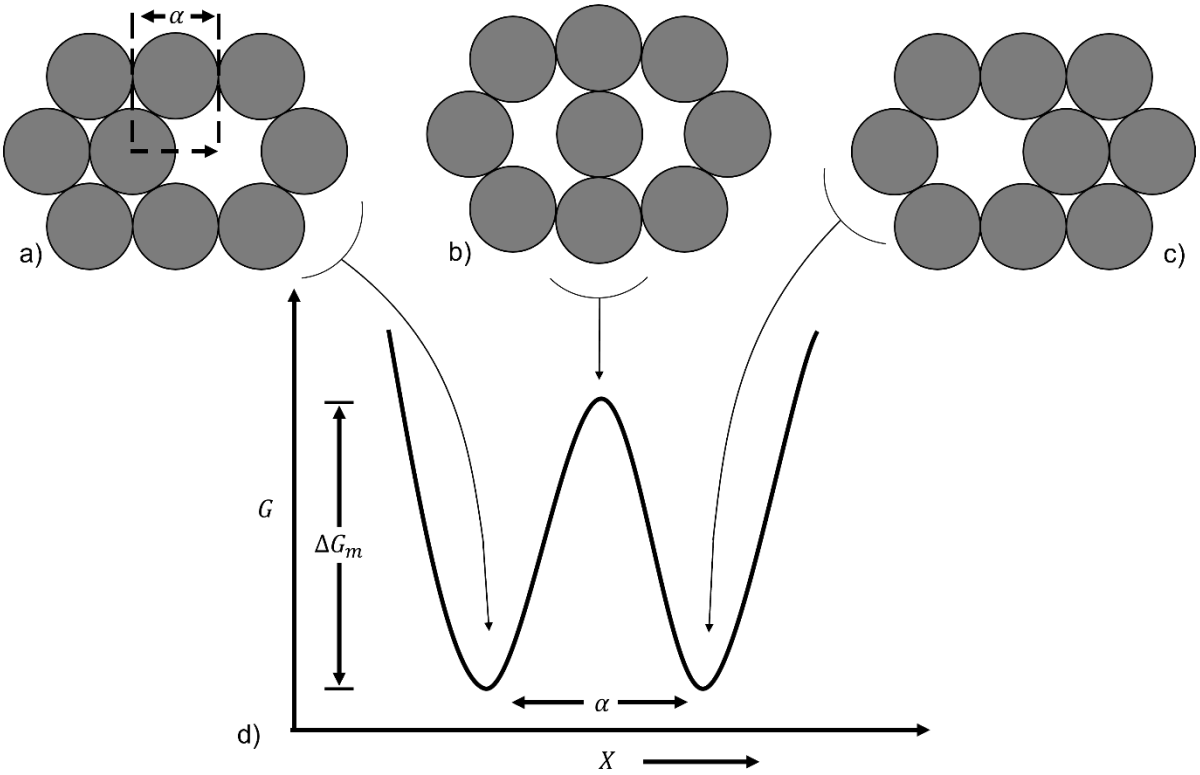

Fig 1.8 Substitutional atom, (a) in equilibrium position, (b) at the position of maximum lattice distortion, (c) in equilibrium position (after jumping), d) Variation of the free energy of the lattice as a function of the position of atom.

A simple example of substitutional diffusion is self-diffusion. As shown in Figure 1.8, an atom has adjacent vacancies can jump with enough energy to overcome the activation energy barrier ΔG_m. The jumping frequency is given by:

$$\Gamma = v\mathrm{z}X_v \exp\frac{-\Delta G_m}{RT} \tag{1.7}$$

where z is the number of nearest lattice position, v is mean frequency of atom vibration, and X_v stands mole fraction of vacancies in the lattice. Assuming all vacancies are in thermodynamic equilibrium, then X_v equals to the equilibrium vacancy concentration X_v^e, which is given by [19]:

$$X_v^e = \exp\frac{-\Delta G_v}{RT} \tag{1.8}$$

where ΔG_v is activation energy of vacancies formation in the lattice. Combing equation 1.2, 1.7 and 1.8 gives

$$D = \frac{1}{6}\alpha^2 z v \exp\frac{-(\Delta G_m + \Delta G_v)}{RT} \tag{1.9}$$

Substituting $G = H - TS$ gives

$$D = \frac{1}{6}\alpha^2 z v \exp\frac{\Delta S_m + \Delta S_v}{R} \exp\frac{-(\Delta H_m + \Delta H_v)}{RT} \tag{1.10}$$

Simplifying equation 1.10 to an Arrhenius-type equation [19], that is

$$D = D_0 \exp\frac{-Q_{SD}}{RT} \tag{1.11}$$

where

$$D_0 = \frac{1}{6}\alpha^2 z v \exp\frac{\Delta S_m + \Delta S_v}{R} \tag{1.12}$$

and

$$Q_{SD} = \Delta H_m + \Delta H_v \tag{1.13}$$

In the case of substitutional diffusion of solute (atom A) in the solid solution (atom B), the interdiffusion coefficient D_{AB} can be defined as Darken's equation [21]:

$$D_{AB} = X_B D_A + X_A D_B \tag{1.14}$$

where X_A and X_B are the mole fractions of atom A and B, respectively.

Since substitutional diffusion is vacancy-driven diffusion, the difference between diffusion through lattice, and along grain boundaries/free surfaces must be put into consideration separately. Due to the fact that grain boundaries contain more vacancy than lattice, substitutional

diffusion happens much faster at grain boundaries than in the lattice. The grain boundary diffusion makes a significant contribution to the total flux of atoms when

$$D_b\delta \gg D_l d \tag{1.15}$$

where D_b and D_l represent atomic diffusivity at grain boundary and in the lattice, δ stands for grain boundary effective thickness and d is average grain size [19].

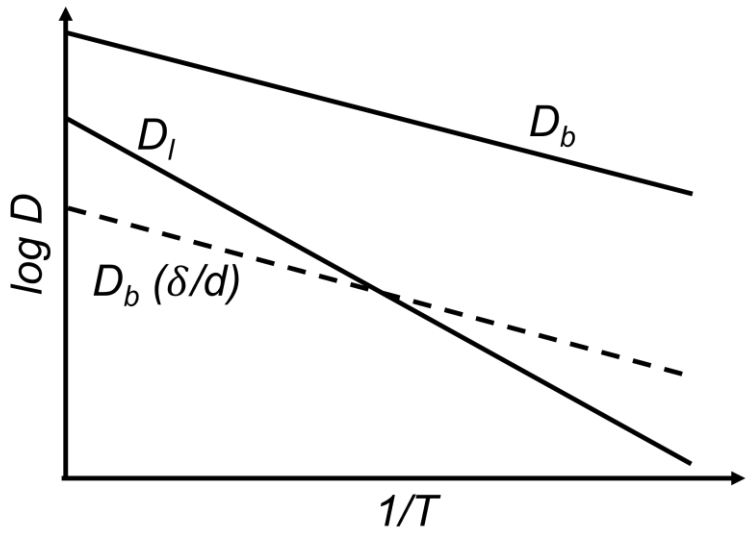

Fig 1.9 Diffusion in a polycrystalline metal.

Generally speaking, grain boundary diffusion becomes dominate when temperature below about 0.75 to 0.8 T_m, and lattice diffusion becomes dominate when temperature above 0.8 T_m (figure 1.9) [19].

1.2.2 Studies of Diffusion in Sn

Kirkendall's research in 1947 established the substitutional-vacancy driven mechanism for diffusion in binary alloy systems, which is now known as the "Kirkendall effect" [22]. This paved the way for further exploration of diffusion in Sn. In 1950, P.J. Fensham's study showed

that self-diffusion of Sn atoms in a polycrystalline structure is driven by a vacancy mechanism [23]. Later, in 1964, C. Coston and N.H. Nachtrieb proved that self-diffusion in single crystal Sn also follows a vacancy-diffusion mechanism, and were able to measure the diffusion coefficient of Sn [24]. In 1975, F.H. Huang and H.B. Huntington studied solute diffusion in Sn using radio isotopes and found that solute atoms with a large atomic size, such as Sb and Cd, followed a vacancy diffusion mechanism and diffused slowly in Sn. In contrast, solute atoms with a small atomic size, such as Zn, diffused much faster, possibly assisted by an interstitial mechanism that may exist on the C axis of Sn due to its BCT crystal structure [25]. The Cu-Sn diffusion couple is a commonly used alloy in conductors and has been extensively studied. M. Onishi and H. Fujibuchi conducted a study on the Cu-Sn binary diffusion couple using Kirkendall markers shift measurement. Their study further supported the vacancy diffusion mechanism and measured the diffusion coefficients of different phase couples [26]. Another study by A. Paul, C. Ghosh, and W.J. Boettinger focused on the intermetallic compounds in the Cu-Sn binary diffusion system. They characterized the integrated interdiffusion coefficients for intermetallic compounds and found that Sn and Cu are the faster diffusers in Cu6Sn5 and Cu3Sn, respectively [27]. Y. Yuan, Y. Gauan, D. Li, and N. Moelans also reported similar results [28]. In addition to Cu-Sn, as an important role in solder alloy design and processing, Ni-Sn diffusion couple has also been the focus of research. P. Nash and A. Nash conducted a comprehensive study on the Ni-Sn system in 1985 [29]. Based on previous studies [17, 30-36], they proposed the phase diagram of the Ni-Sn system and characterized the crystal structures of intermetallic compounds (Ni3Sn, Ni3Sn2, and Ni3Sn4) in their published results. In 1988, J. Haimovich studied the transformation behavior of the metastable phase NiSn3 using differential scanning calorimetry (DSC) and found that the decomposition of NiSn3 had a certain effect on solderability [37]. Since then, several studies [38,

39] on intermetallic compounds in the Ni-Sn system have been conducted to better understand and enhance the reliability of solder. Currently, the ternary systems of Sn-Ag-Cu (SAC) and Sn-Cu-Ni (SCN) are attracting research interests due to their applications as Pb-free solder used in solder interconnects. These studies provide a theoretical foundation for further research on the diffusion mechanism in Sn.

1.3 Introduction of Electromigration

Electromigration (EM) is a phenomenon (as shown in Figure 1.10) in which atomic diffusion in the direction of electron flow under high current density. The first observation of EM was reported by Geradin in 1861 [40]. He discovered EM in liquid alloys of lead-tin, potassium-sodium, gold, and bismuth in mercury. He was also the first to consider EM as an electrostatic interaction between the electric field and metal ions in liquid metals and molten salts.

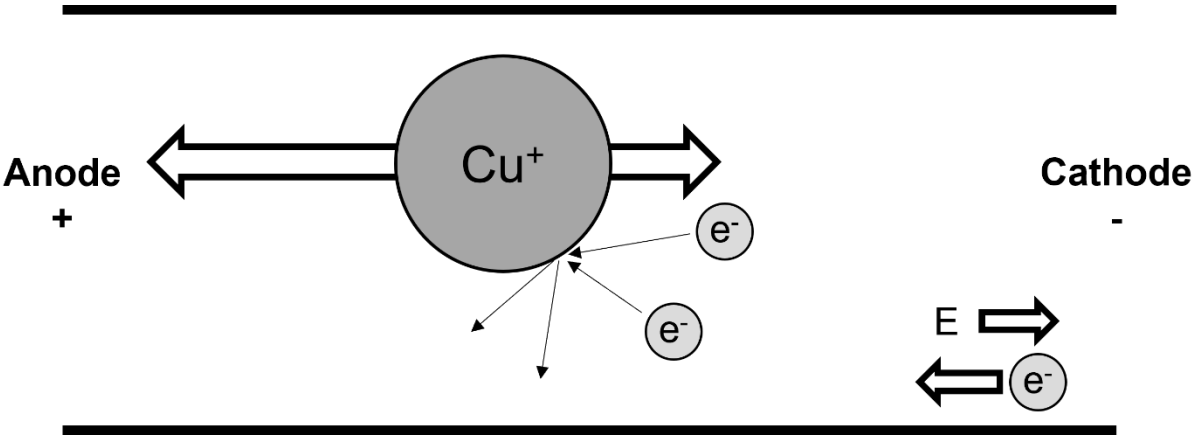

Fig 1.10 Electromigration happens in a Cu wire.

For almost a century following Geradin's initial observation of EM in liquid alloys, there was little progress made in understanding this phenomenon. It was not until 1953 that Seith and Wever conducted the first systematic studies of EM [41], measuring the mass transport of a

series of Hume-Rothery alloys and plotting it onto a phase diagram. They were able to conclude that the direction of mass transportation is correlated with the type of majority charge carrier, whether it be electrons or holes, present in the specific alloy phase. This groundbreaking finding provided the first experimental evidence for the nature of the driving force behind EM, demonstrating that the atomic motion is determined by the direction of movement of the charge carriers, rather than the electrostatic force imposed by the applied field.

In addition to their pioneering work on understanding the driving force behind EM, Seith and Wever introduced the "Marker Motion" technique, which is also known as the vacancy flux method. This technique measures EM-induced mass transport by tracking the displacement of an indentation on a metal wire, and has since become one of the standard measurements of EM.

Seith and Wever's findings prompted the development of the "Electron Wind" concept, which had been introduced by Skaupy in 1914 and laid the foundation for the basic understanding of EM [42]. Fiks mathematically formulated the concept of the EM driving force in 1959[43], while Huntington and Grone did so independently in 1961[44]. They used a semiclassical "ballistic" approach to describe the collision of moving atoms by charge carriers, and demonstrated that the driving force depended on the type of defects and the atomic configuration of the jumping path.

Their mathematical formulation of the driving force was a significant contribution to the understanding of EM, as it demonstrated the possibility of directly using electromigration of moving atoms and charge carriers. Their work generated significant interest in studying EM in metals during the 1960s, and laid the foundation for our current understanding of EM.

During electromigration inside a circuit channel, metal atoms are displaced from their original positions by electrons, migrating in the direction of electron flow. As a result, there is a

dearth of metal atoms in the direction from which the electrons are arriving, while a surplus of metal atoms accumulates in the direction from which the electrons are leaving. This gradual imbalance gives rise to voids and hillocks due to the depletion and accumulation of metal atoms, respectively (Figure 1.11).

As electromigration persists, the voids may progressively enlarge, eventually resulting in cracks that can lead to an open circuit. Similarly, hillocks may grow large enough to make contact with other channels within the device, potentially causing a short circuit. This can lead to the failure of integrated circuit (IC) devices and even pose safety concerns, such as fire hazards and electrical leakage (Figure 1.12).

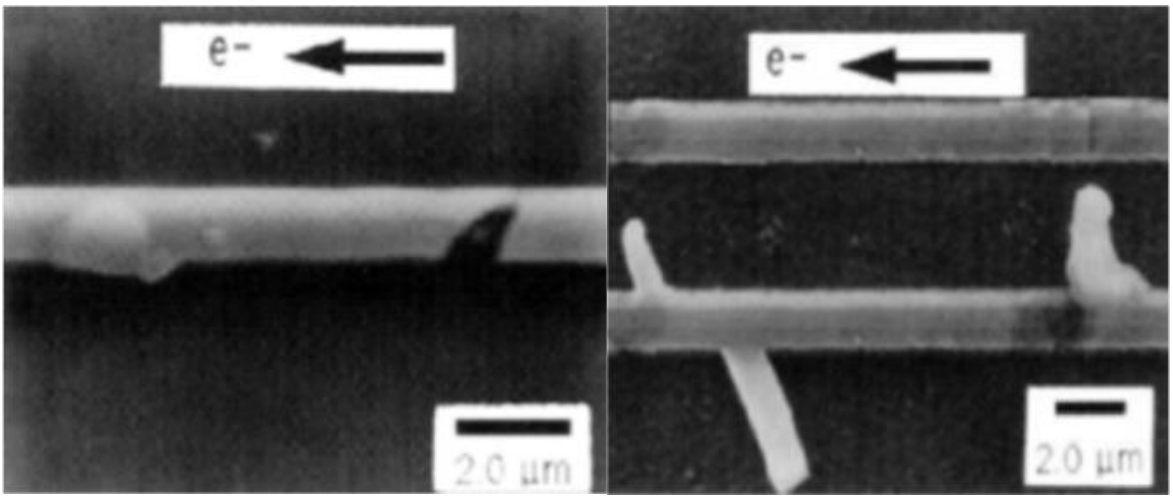

Fig 1.11 Void (left) and hillock formed during electromigration [45].

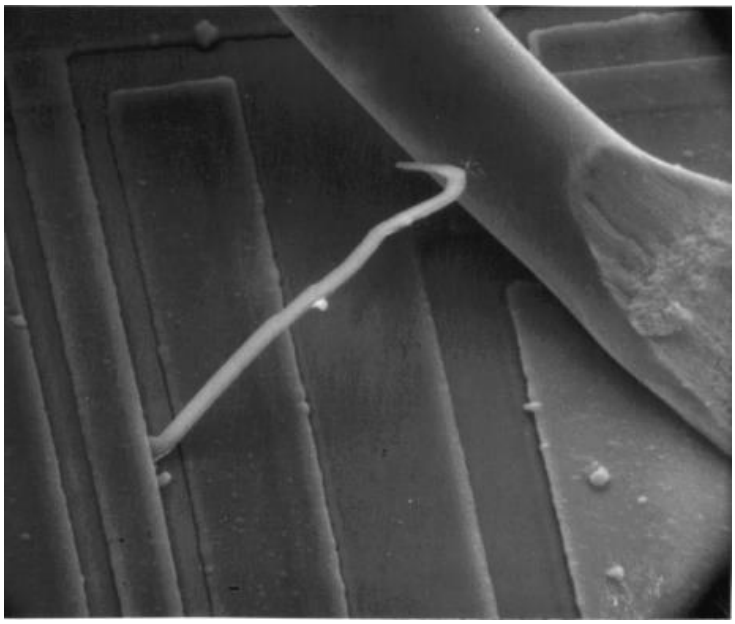

Fig 1.12 Extrusion to a bond wire causing a short circuit [46].

Furthermore, the impact of electromigration-induced semiconductor device failure is not limited to reputational damage, but also includes significant economic losses. Several cases of product failures resulting from electromigration have been documented [47]. For instance, in the late 1980s, a particular line of Western Digital's desktop drives experienced widespread failure between 12 to 18 months after field usage. Upon analysis of the returned faulty units, engineers traced the cause of failure to improper design rules in an IC controller supplied by a third party. By replacing the faulty component with one from a different supplier, Western Digital was able to rectify the issue, albeit after incurring significant damage to its reputation. Another instance was the failure of ICs in Commodore's home computers during the 1980s, caused by electromigration. In 1983, the Commodore 64 computer had a customer return rate of nearly 50%. All of these examples highlight the serious impact of electromigration damage on the semiconductor industry, and the need for robust measures to prevent it.

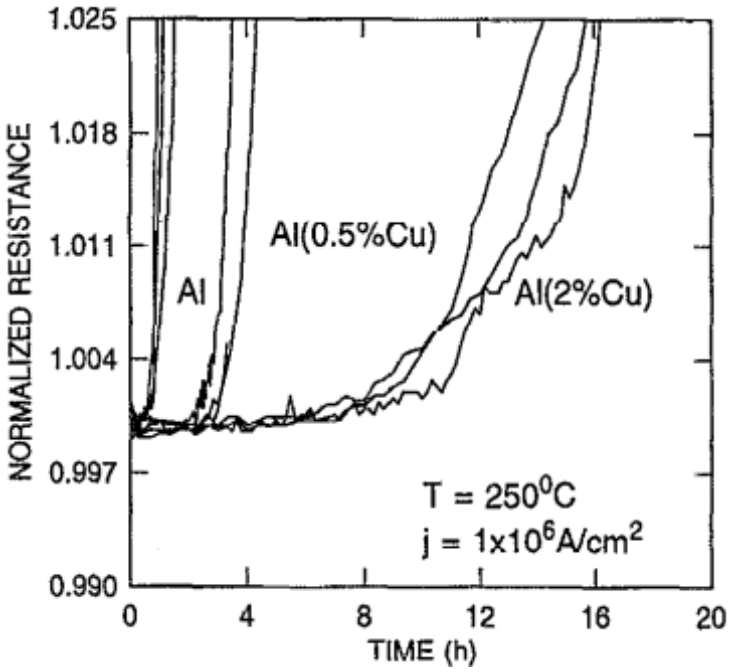

Fig 1.13 Al samples' resistance change vs time. Failure caused by electromigration will lead to resistance increase. Cu alloyed samples clearly show longer lifetime under EM than pure Al sample [48].

Alloying has been identified as an effective approach to suppress electromigration in various applications. Copper, for example, has been frequently utilized as a solute element to improve the resistance to electromigration in aluminum interconnects (Figure 1.13), as evidenced by numerous studies [48-52]. With the wide application of Sn-based solder in semiconductor interconnects, researchers have shifted their focus to investigating the solute effect on the Sn-based alloy system under electromigration in recent years. For instance, C.Y. Liu, Chih Chen, and K.N. Tu explored the electromigration behavior of Sn-Pb solders with thin film configurations [53]. They discovered that the interface between Sn and Pb, where hillock and

void formation initiated, was the fastest kinetic path of mass transport, suggesting that the EM behavior in the Sn-Pb system was driven by a vacancy-diffusion mechanism. Meanwhile, C.M. Chen and S.W. Chen investigated the effect of temperature on the EM behavior of Sn-Ag and Sn-Ni binary systems [54]. They found that under EM, Sn atoms were more prone to migrate and induce the formation of intermetallic compounds in both Sn-Ag and Sn-Ni systems, and that the effective charging number Z* of Sn was affected by the EM testing temperature. Brook Chao et al. studied Cu-Sn intermetallic compounds formed between under bump metallization and solder joints under EM, and proposed an efficient numerical method to characterize the diffusion coefficients of Cu and Sn for different intermetallic compounds [55]. Further studies have been conducted to explore the EM effect on other binary systems, such as Sn-Bi [56, 57], and ternary systems like Sn-Ag-Cu (SAC) [58-60]. Nevertheless, a comprehensive understanding of the solute effect on the EM of Sn-based solder systems is still lacking, making the establishment of a fundamental mechanism to be one of the pressing issues. Therefore, the objective of our project is to investigate the effect of solute atoms on the EM behavior of Sn and develop a comprehensive understanding of the alloy effect on EM in Sn-based solder joints.

Chapter 2: Experimental Approach

2.1 Cross-stripe Configuration

To better understand and characterize the effect of alloying on the electromigration of Sn, we have chosen to utilize the "cross-stripe" experimental configuration. This thin film testing method enables us to isolate the solute effects from other microstructural variables, such as grain size, and quantify solute behavior during electromigration [61]. The cross-stripe EM test method was developed in the 1970s as a technique for characterizing the EM diffusivity of alloying

elements in host metals, and has been proven to be an effective testing configuration in studying the electromigration of Cu alloys on Al [62]. One of the most well-studied cases involved a Cu film patterned as a cross-stripe on an Al thin-film base stripe, as there was a great desire to better understand how small amounts of Cu added to Al resulted in substantial enhancement in EM reliability, which was experimentally found to be more than two orders of magnitude. Through the use of the cross-stripe configuration, studies were able to quantify the EM diffusivity of Cu along Al grain boundaries and relate it to the suppression of Al EM.

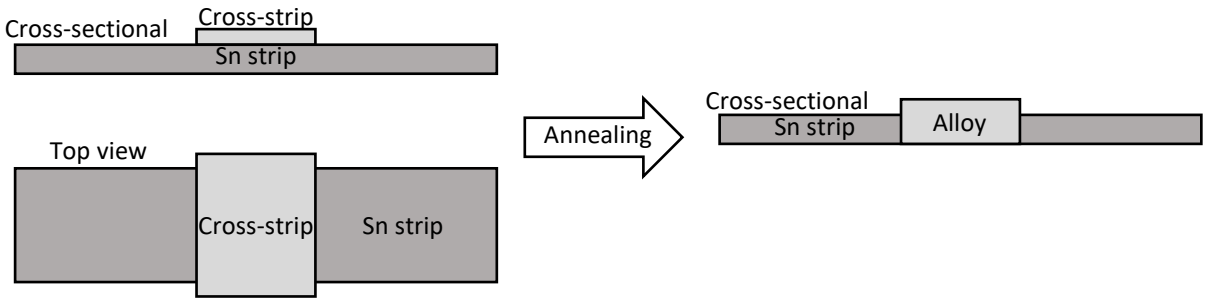

Fig 2.1 Schematic diagram of “Cross-stripe” sample preparation.

Preparing a "Cross-stripe" sample involves coating the alloy element on top of a Sn stripe in a cross shape, as shown in Figure 2.1, to create an alloyed segment situated in the middle of a pure stripe. The thickness of the coating must be carefully controlled, as it directly determines the concentration of alloy element in the resulting alloyed area. Once the coating quality and uniformity have been checked, the sample is annealed at a designated temperature to induce interdiffusion between the "Cross-stripe" (alloy element) and the Sn stripe, creating the desired alloyed area for testing.

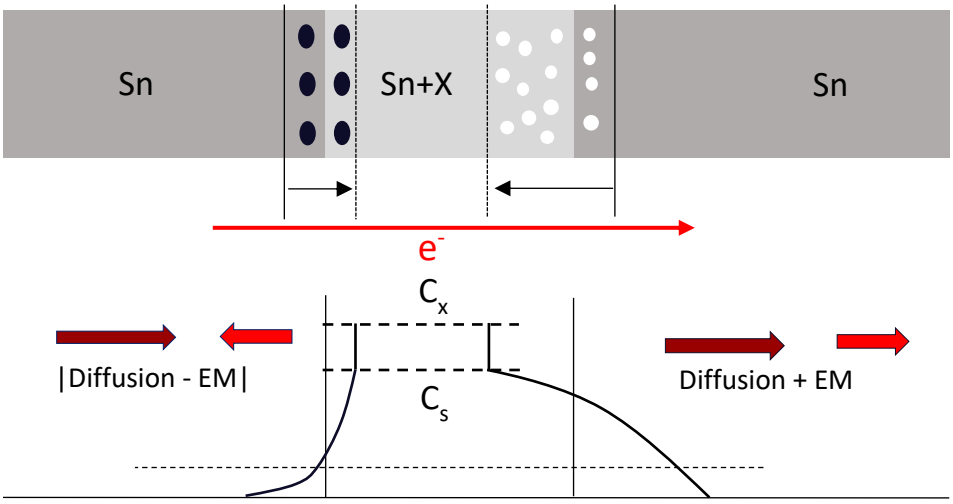

Fig 2.2 Schematic diagram shows the electromigration of Sn is suppressed by alloy element existing in alloyed cross-stripe area. Hillocks form on cathode side (electron entering side, black mark), and voids form on anode side (electron leaving side, white mark). The hillock and void front may keep advancing due to the migration of alloy element under EM. X stands for alloy element. C_o and C_s are the concentration of alloy element in Sn, and maximum solubility limit of this alloy element in Sn.

In summary, the cross-stripe configuration allows for the clear characterization of the alloy effect on electromigration of Sn. The polarity of marker (hillock and void) formation can indicate whether the alloy effect shows EM suppression or enhancement of Sn. As shown in Fig 2.2, if the presence of alloy effect in alloyed "Cross-stripe" area shows EM suppression of Sn, the EM rate of Sn on the stripe (pure Sn) area will be faster than that on the "Cross-stripe" (alloyed) area. This will lead to an excess of Sn atoms near the "Cross-stripe" boundary on cathode side (electron entering side), and a lack of Sn atoms on anode side (electron leaving side). Due to the difference of Sn EM rate, hillocks of Sn will develop near the boundary on

cathode side, and voids will appear on anode side. If alloyed cross-stripe area shows EM enhancement effect of Sn, then void and hillocks will develop on cathode and anode side, respectively. The makers with reversed polarity will appear due to the electromigration of Sn.

The "Cross-stripe" configuration offers another advantage in that it enables the characterization of the migration of the alloy element under electromigration based on the motion of markers' fronts. As depicted in Figure 2.2, the markers' fronts advance due to the migration of the alloy element under EM. By recording the position of the markers' fronts as they change over time, the migration of the alloy element under EM can be characterized, and the estimated EM diffusivity of the alloy element in Sn can be determined. This phenomenon is driven by the "Two-phase equilibrium" mechanism, which is the fundamental mechanism of the alloy effect on the EM of Sn and will be further elaborated on in subsequent chapters with solid experimental results.

2.2 Sample Preparation & Testing Cell Design

In this chapter, a detailed process of sample preparation, testing cell and circuit design/installation will be presented. Several key issues were encountered in the early stages of the research, which had a direct impact on the EM testing results. Through numerous trials and optimizations, these issues were resolved, and their solutions will be discussed in the following paragraphs.

Figure 2.3 depicts the standard "Cross-stripe" configuration sample used for all the electromigration tests in this research. It comprises three stripes with alloyed "Cross-stripe" areas. The top and bottom stripes are reference stripes, and no current will flow through them during testing. The middle stripe is the main stripe, and current will flow through it during EM

testing. By comparing the stripe surfaces between the reference stripes and the main stripe, the marker formation induced by EM can be better characterized. The optimal method for producing a standard "Cross-stripe" sample was developed after numerous trials.:

1. After cleaning, 5nm Cr is deposited on the Si wafer by sputtering as “glue layer”.
2. 2um Sn is deposited on the Cr layer by sputtering.
3. Directional annealing is applied for Sn grain growth.
4. After annealing, the Si wafer will be cut into suitable sizes with diamond cutter.
5. Alloy element is coated on the Sn stripe as “Cross-stripe”.
6. Sample is annealed in the oil bath at 200^{o}C to induce interdiffusion between alloy element and Sn. Once alloy area formation is confirmed, the sample will be ready for EM testing.

In this research, two major issues were encountered in the sample preparation process, which were subsequently resolved through various trial and process methods. The first challenge arose due to the poor adhesion between Sn and Si substrate. Initially, a 2um thick Sn layer was sputtered directly onto the Si wafer to create the EM sample, but the Sn stripe was found to be easily detached from the Si substrate, which posed challenges for subsequent "Cross-stripe" coating and testing. Further investigation revealed that the major reason for this problem was the significant difference in the thermal expansion coefficients of Sn and Si, which are 22 and 2.6, respectively [63-70]. As a result, when the sample was heated, the lattice of Sn expanded more than that of Si, resulting in compressive stress inside the Sn stripe. Conversely, during cooling, tensile stress was generated inside the Sn stripe, which contributed to the detachment issue. To overcome this challenge, a "glue layer" of Cr was added to the sample. Although the addition of Cr resulted in the development of some Sn whiskers and voids due to compressive and tensile

stress, it effectively maintained the contact between the Sn stripe and Si wafer. Moreover, the Cr layer was inert and did not diffuse into the alloy system during annealing, making it an ideal solution for this adhesion issue.

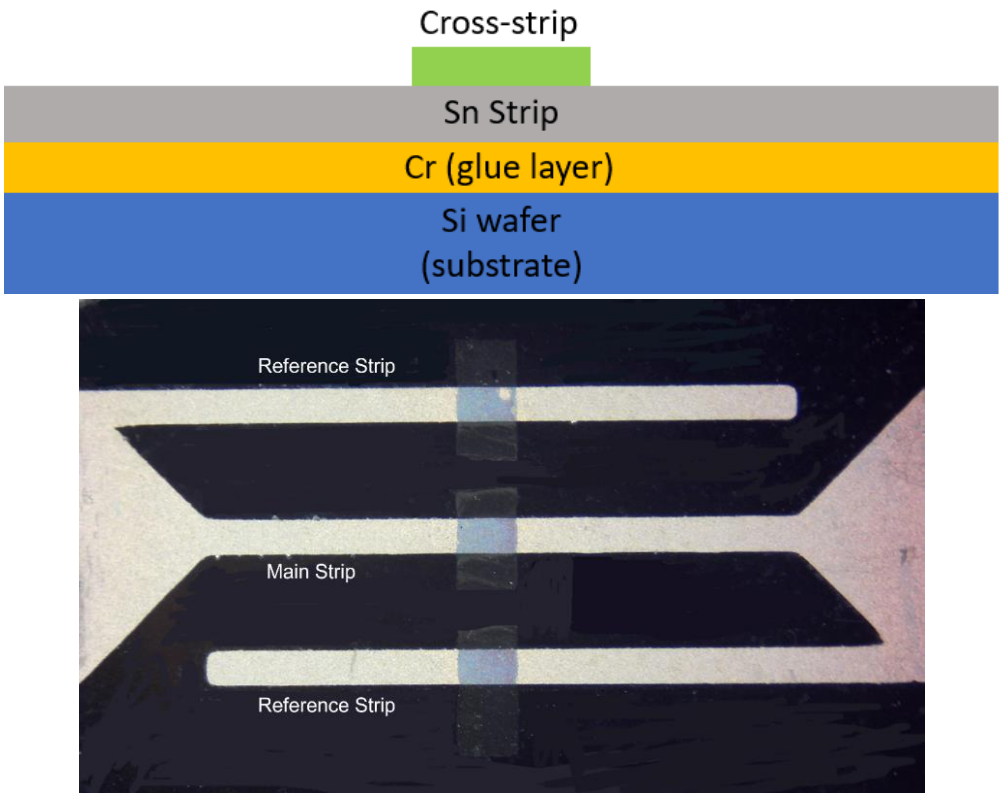

Fig 2.3 Schematic cross-sectional view of a cross-stripe sample (above), and a top view picture of Ag alloyed “Cross-stripe” sample (below).

The second issue encountered during the research was the surface oxidation of the "Cross-stripe" alloy area. As it has been demonstrated that Sn oxidizes spontaneously in the air [71], it was found that oxide was present on the surface of both the alloyed "Cross-stripe" area after annealing or testing without protection, as shown in Figure 2.4. This surface oxide prevented normal marker formation from the EM of Sn and led to measurement errors and failures in EM testing. To prevent surface oxidation, an oil bath was utilized for sample

annealing and EM testing, as shown in Figure 2.5. Additionally, the use of an oil bath ensured that the sample can be uniformly heated.

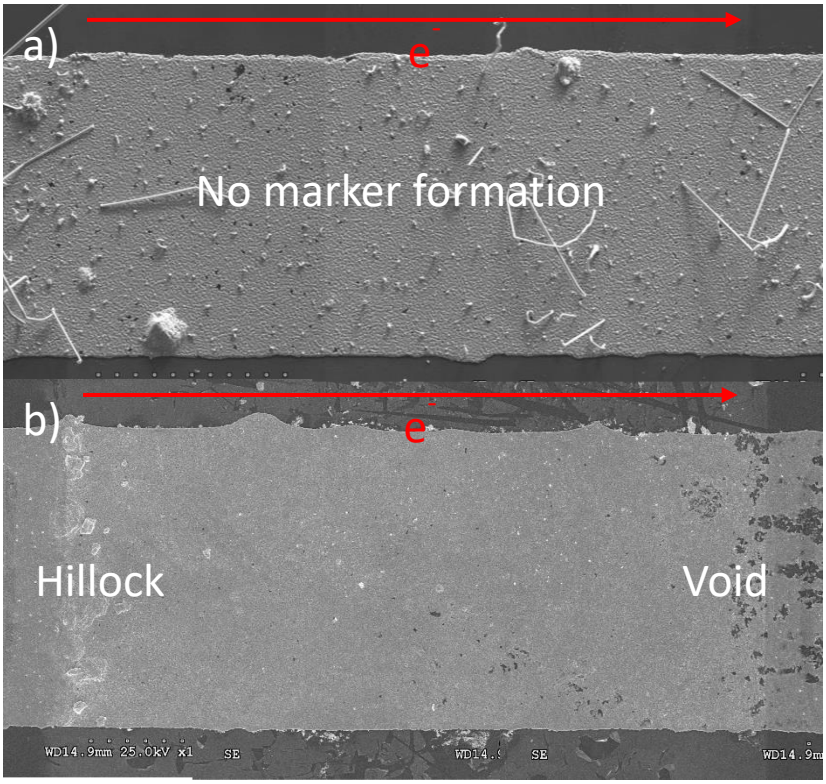

Fig 2.4 Au alloyed binary sample cross-stripe testing results. Both samples are tested at 180°C. Current density was set at $5x10^4$ A/cm^2: a) sample is fully oxidized, no marker formed during EM testing; b) sample is oxide-free, marker formation can be clearly characterized.

Figure 2.5 depicts the schematic structure of a single testing cell. In order to expedite the process of electromigration (EM) testing and achieve reliable results within a shorter duration, a heating system has been installed within the testing cell. This heating system comprises of a K-type thermocouple, a digital PID temperature controller with a solid-state relay, and a heating plate. The K-type thermocouple is always placed inside the oil bath to ensure accurate temperature control. The oil bath container is made of carbon. Furthermore, a high temperature

PCB board is utilized as the substrate after etching all metals away. The "Cross-stripe" sample is fixed onto the substrate with a stainless-steel plate, which is in direct contact with the main stripe of the sample to facilitate current flow path during EM testing. The stainless-steel plate is secured with stainless steel bolts and nuts, which provide external electrical connection access points.

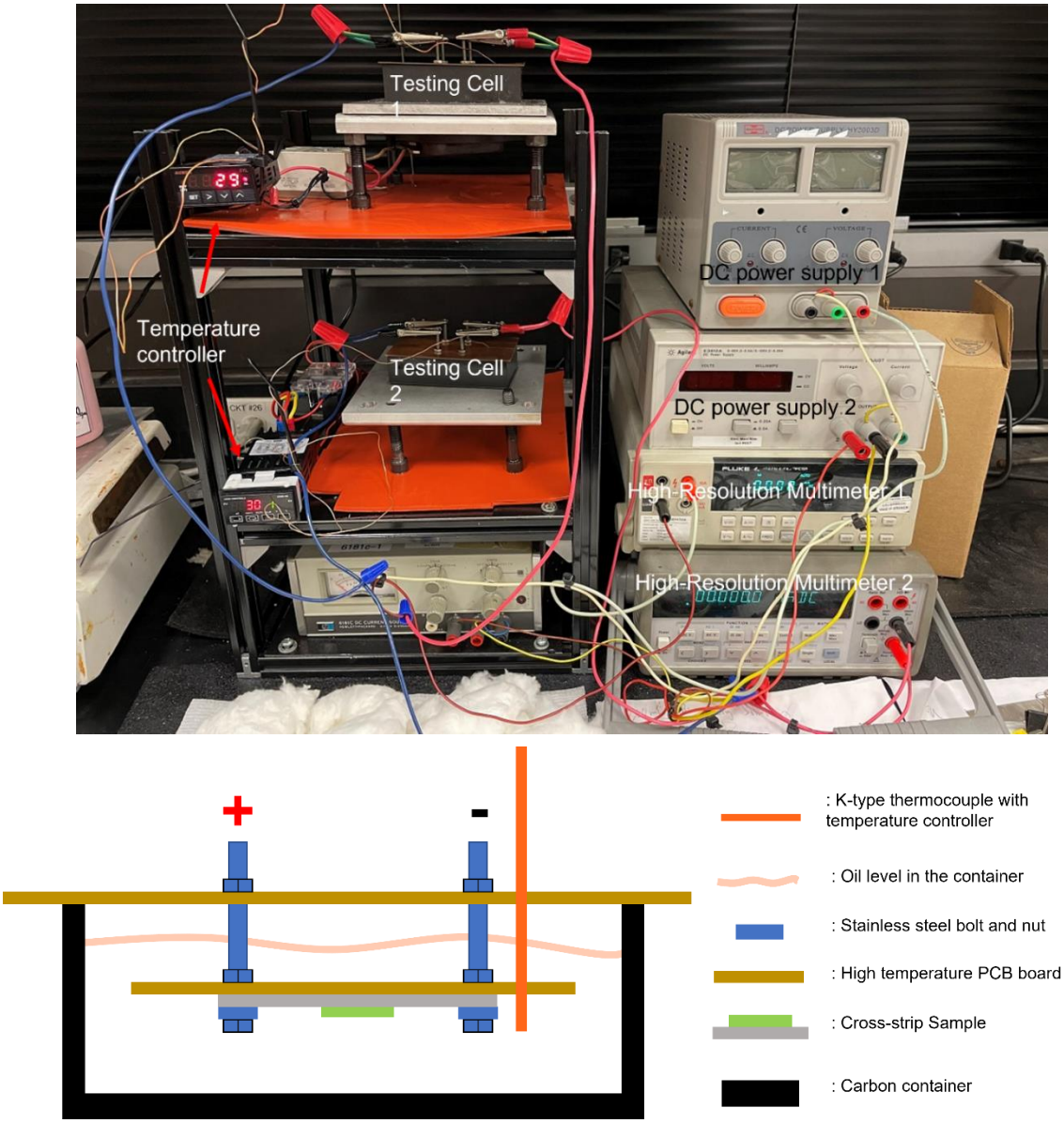

Fig 2.5 Schematic diagram of actual electromigration testing system (above), and cross-stripe sample testing cell (below).

To complete the EM testing system, a DC power supply and a high-resolution multimeter are connected to the stainless-steel bolt of the testing cell. The DC power supply provides a consistent current flow, while the high-resolution multimeter is set to current-measuring mode, allowing for precise control of the current required during the EM testing.

Chapter 3: EM Testing of Binary Samples

3.1 Gold (Au) Binary Sample

Compared to other metals, gold (Au) exhibits extremely high resistance to oxidation or corrosion. In situations where the contacts of a connector are likely to be exposed to corrosive substances or conditions, gold plating can serve as an effective barrier against oxidation and corrosion. Moreover, gold plating is an excellent finish for forming reliable solder joints as it allows for consistent and even wetting using just a mild rosin flux, without the need for acid activation. Considering the interdiffusion between gold plating and solder joint, and the fact that electromigration can drive metal atoms to move in the solder joint, potentially leading to the formation of alloy systems containing Au and Sn, it is important to investigate the effect of Au alloying on the EM of Sn.

In this section, gold (Au) is utilized as the alloying element to produce binary samples. The Sn stripe was coated with Au using a brush painting technique in a "Cross-stripe" pattern. The samples were annealed in an oil bath at 200°C for 14 hours to ensure complete alloying of the "Cross-stripe" area before being installed into the testing cell for electromigration testing at 180°C.

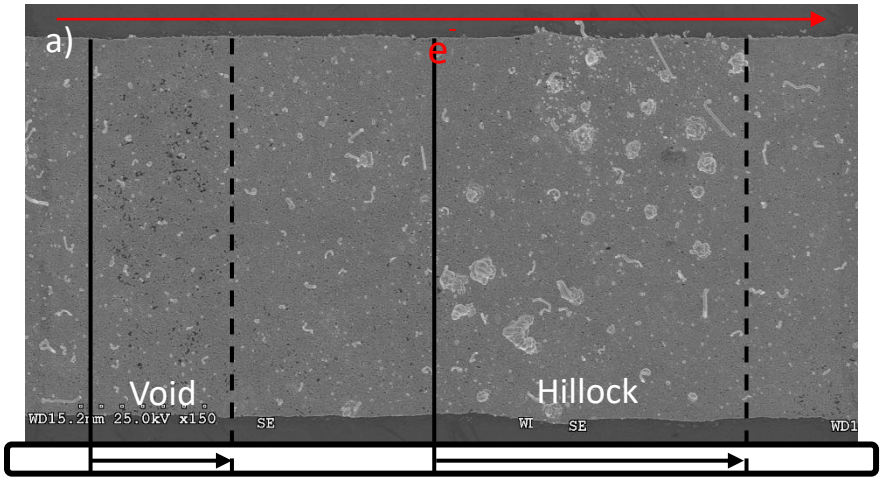
a)
e-
Void
Hillock

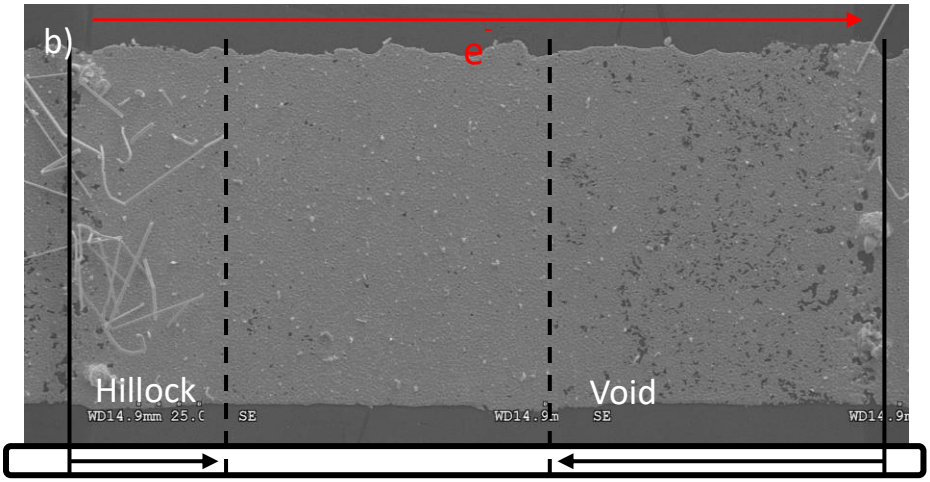
b)
e-
Hillock
Void

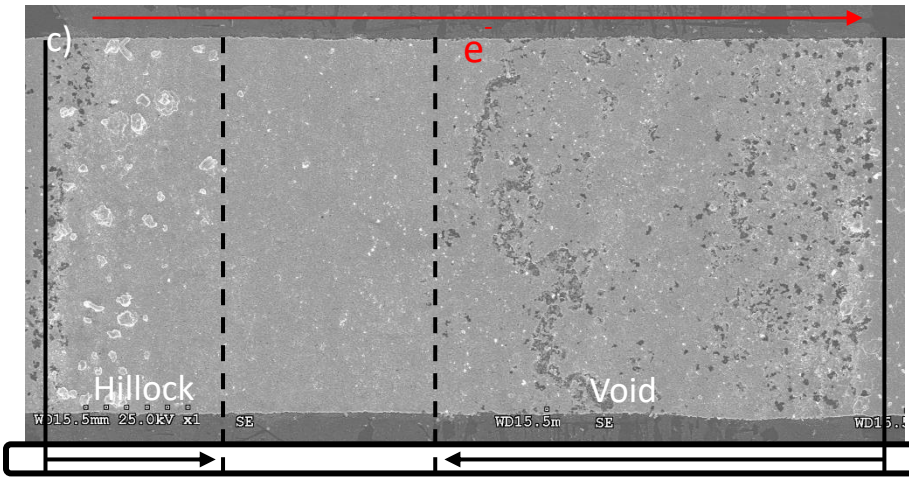
c)
e-
Hillock
Void

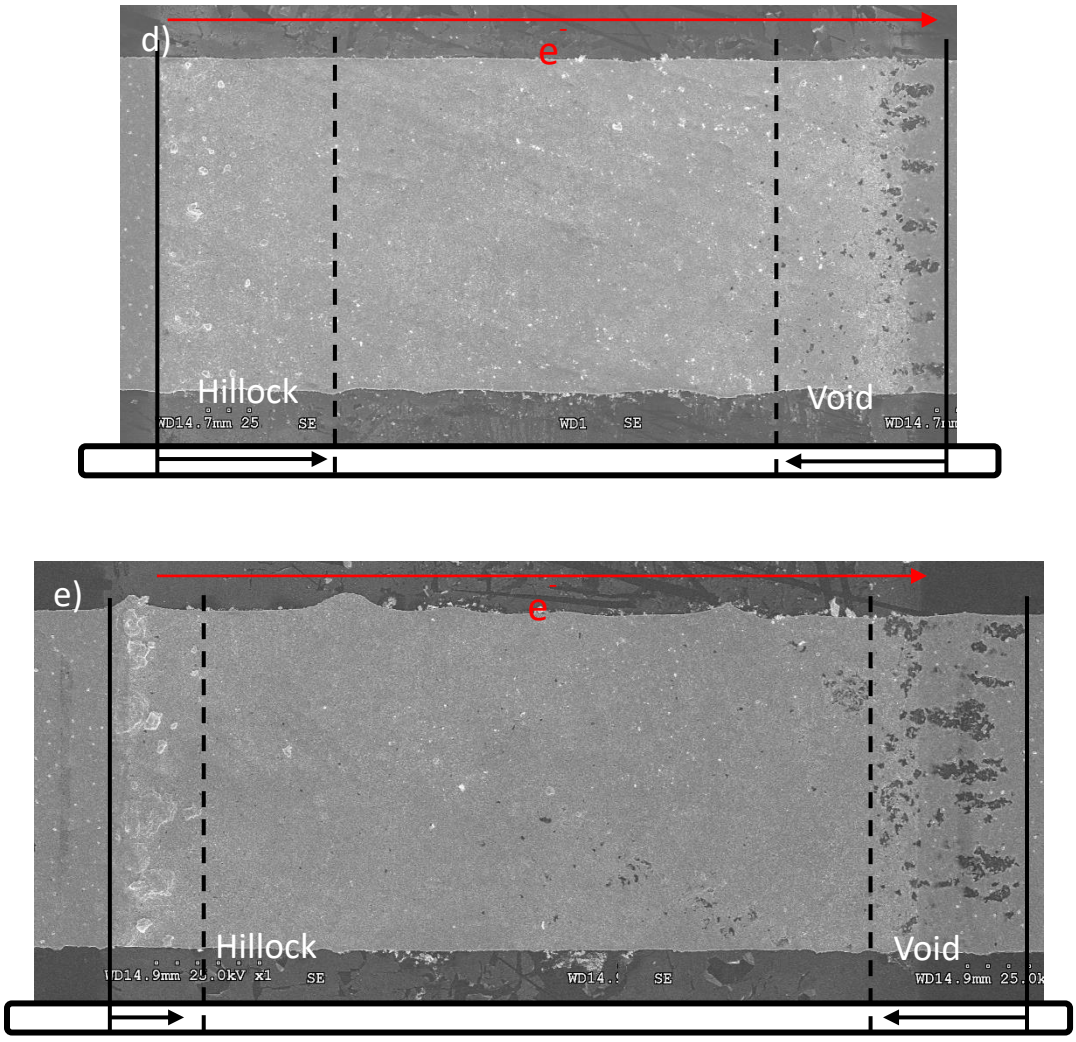

Fig 3.1 SEI images of Au alloyed binary samples after EM testing. All samples were tested at 180ºC. Current density was set at $5x10^4$ A/cm^2 for all samples except c): a) Au 1 at%, 22 hours of testing. b) Au 1.5 at%, 50.5 hours of testing, with $3x10^4$ A/cm^2. c) Au 2.6% at, 16 hours of testing. d) Au 3.78 at%, 4 hours of testing. e) Au 5.14 at%. 8 hours of testing. Arrows represent the markers front advancement from initial formation position.

Au concentration of alloyed Cross-stripe area	Result of EM of Sn
1 at%	Enhancement
1.5 at%	Suppression
2.6 at%	Suppression
3.78 at%	Suppression
5.14 at%	Suppression

Table 3.1 Summary of Au alloy effect on electromigration of Sn.

In this study, five Au binary samples with different atomic percentages of Au in the alloyed "Cross-stripe" area were prepared and successfully tested. The results of the EM testing for all five samples are shown in Figure 3.1, where clear marker formations were observed. The binary sample with 1 at% Au in the alloyed "Cross-stripe" area displayed void formation at the cathode side and hillock formation at the anode side, indicating that the EM rate of Sn in the Au alloyed area is faster than that in the pure Sn stripe. In contrast, the binary samples with 1.5 at%, 2.6 at%, 3.78 at%, and 5.14 at% of Au showed hillock formation at the cathode side and void formation at the anode side, indicating that the EM rate of Sn is slower in the Au alloyed area.

Therefore, based on experimental results, it can be concluded that in the Sn-Au binary alloy system, 1 at% Au enhances the EM of Sn, while higher atomic concentrations of Au suppress the EM of Sn. The summary of Au alloy effect is in table 3.1.

3.2 Silver (Ag) Binary Sample

The adoption of the Restriction of Hazardous Substances (RoHS) directive 2002/95/EC has resulted in the prohibition of Pb-containing solders in most commercial electronics [10]. As a

result, the Silver-Tin (Sn-Ag) alloy system has become a popular alternative to Tin-Lead solder, due to its superior mechanical strength, thermal fatigue properties, and wettability. However, despite its widespread use, there is a limited understanding of the electromigration behavior of the Ag-Sn system, and thus the impact of Ag alloying needs to be investigated.

In this section, silver (Ag) is utilized as the alloying element to produce binary samples. The Sn stripe was coated with Ag using sputtering technique in a "Cross-stripe" pattern. The samples were annealed in an oil bath at 200°C for 6 hours to ensure complete alloying of the "Cross-stripe" area before being installed into the testing cell for electromigration testing at 180°C.

In this study, four Ag binary samples with different atomic percentages of Ag in the alloyed "Cross-stripe" area were prepared and successfully tested. The results of the EM testing for all four samples are shown in Figure 3.2, where clear marker formations were observed. The binary sample with 0.06 at% Ag in the alloyed "Cross-stripe" area displayed void formation at the cathode side and hillock formation at the anode side, indicating that the EM rate of Sn in the Ag alloyed area is faster than that in the pure Sn stripe. In contrast, the binary samples with 0.20 at%, 1.90 at% and 2.72 at% of Ag showed hillock formation at the cathode side and void formation at the anode side, indicating that the EM rate of Sn is slower in the Ag alloyed area.

Therefore, based on experimental results, it can be concluded that in the Sn-Ag binary alloy system, 0.06 at% Ag enhances the EM of Sn, while higher atomic concentrations of Ag suppress the EM of Sn. The summary of Ag alloy effect is in table 3.2.

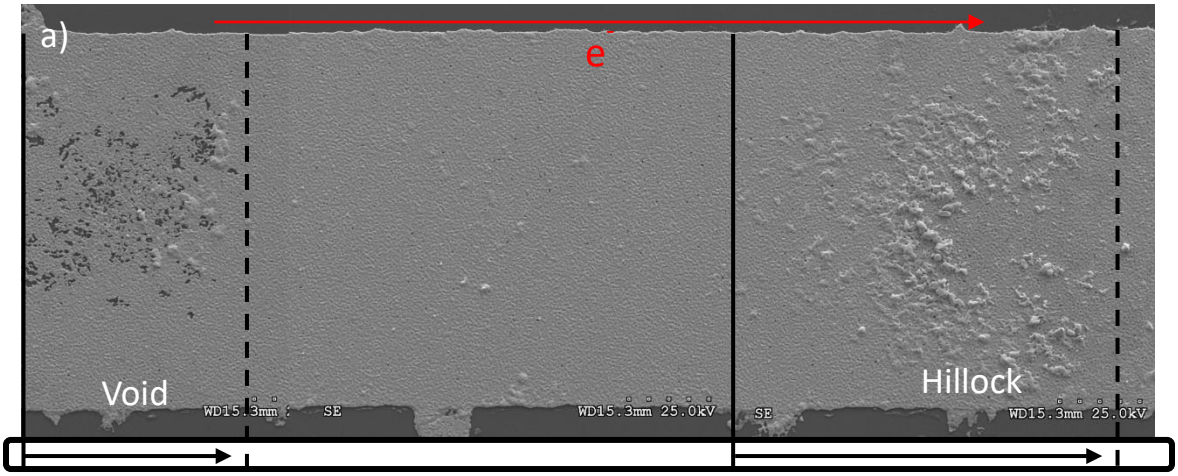
a)
e-
Void
Hillock

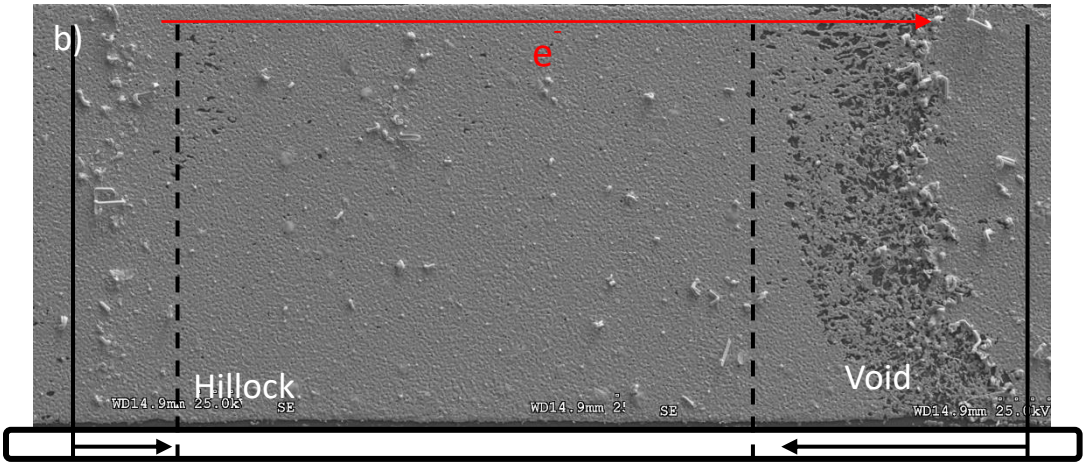
b)
e-
Hillock
Void

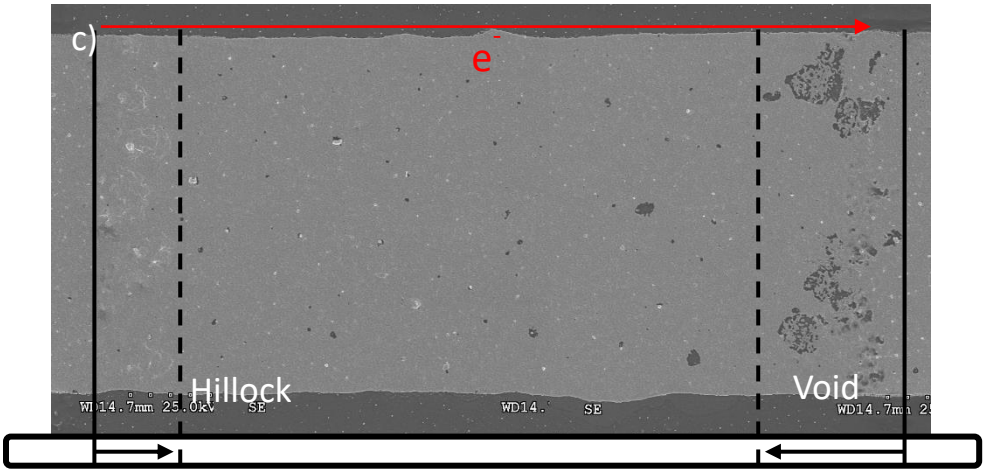
c)
e-
Hillock
Void

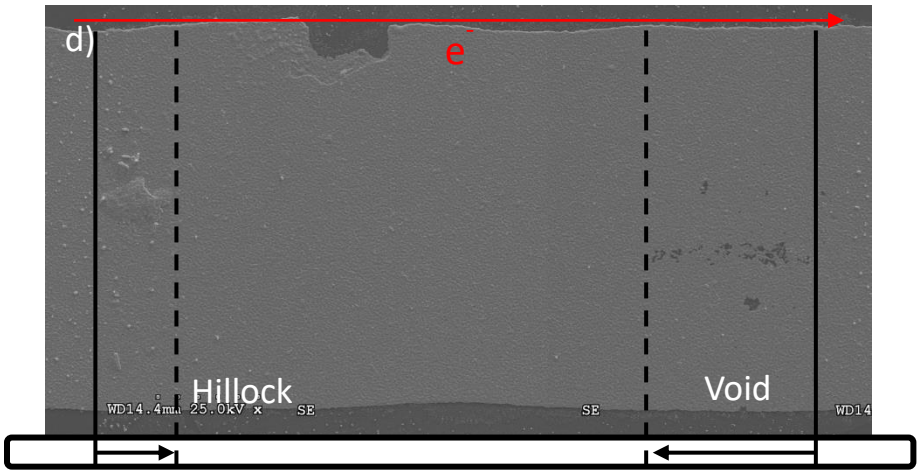

Fig 3.2 SEI images of Ag alloyed binary samples after EM testing. All samples are tested at 180^{o}C. Current density was set at 5x10^{4} A/cm^{2}: a) Ag 0.06 at%, 22 hours of testing. b) Ag 0.2 at%, 10 hours of testing. c) Ag 1.90 at%, 8 hours of testing. d) Ag 2.72 at%, 8 hours of testing. Arrows represent the markers front advancement from initial formation position.

Ag concentration of alloyed Cross-stripe area	**Result of EM of Sn**
0.06 at%	Enhancement
0.20 at%	Suppression
1.90 at%	Suppression
2.72 at%	Suppression

Table 3.2 Summary of Ag alloy effect on electromigration of Sn.

3.3 Copper (Cu) Binary Sample

As mentioned in the previous section, the prohibition of Pb-containing solders has led to the adoption of Pb-free solders such as the Sn-Ag and Sn-Ag-Cu (SAC) alloy systems as popular

alternatives for electronic assembly applications. These alloys have been shown to perform well in surface mount, wave soldering, and hand soldering. To gain a better understanding of the EM behavior of Cu in this alloy system, investigating the Cu alloy effect on the EM of Sn is included in the project.

In this section, copper (Cu) is utilized as the alloying element to produce binary samples. The Sn stripe was coated with Cu using sputtering technique in a "Cross-stripe" pattern. The samples were annealed in an oil bath at 200°C for 3 hours to ensure complete alloying of the "Cross-stripe" area before being installed into the testing cell for electromigration testing at 180°C.

In this study, three Cu binary samples with different atomic percentages of Cu in the alloyed "Cross-stripe" area were prepared and successfully tested. The results of the EM testing for all three samples are shown in Figure 3.3, where clear marker formations were observed. The binary sample with 0.69 at% Cu in the alloyed "Cross-stripe" area displayed void formation at the cathode side and hillock formation at the anode side, indicating that the EM rate of Sn in the Cu alloyed area is faster than that in the pure Sn stripe. In contrast, the binary samples with 1.35 at% and 1.93 at% of Cu showed hillock formation at the cathode side and void formation at the anode side, indicating that the EM rate of Sn is slower in the Cu alloyed area.

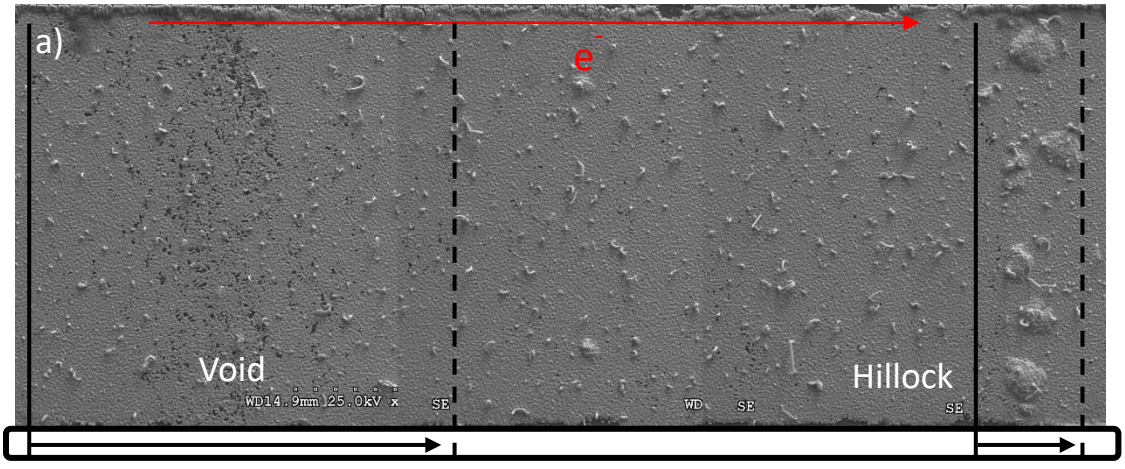

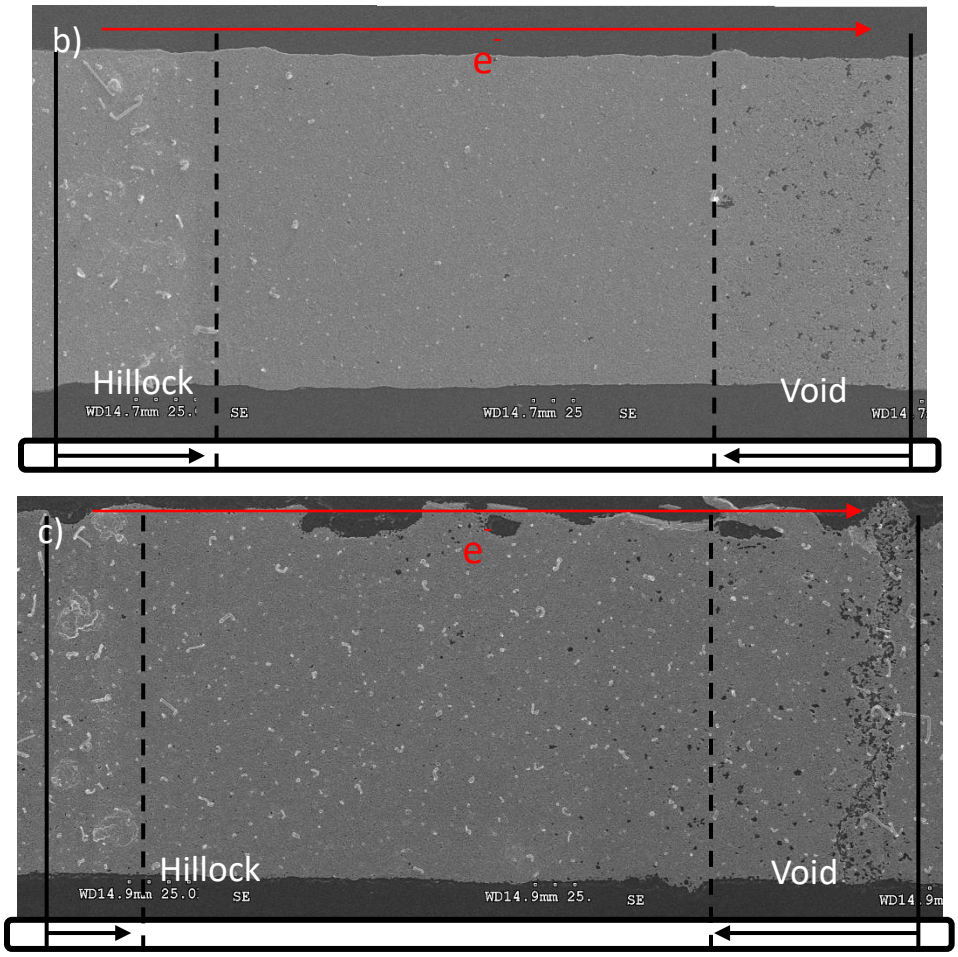

Fig 3.3 SEI images of Cu alloyed binary samples after EM testing. All samples are tested at 180°C. Current density was set at $5x10^4$ A/cm^2: a) Cu 0.69 at%, 12 hours of testing, b) Cu 1.35 at%, 8 hours of testing, c) Cu 1.93 at%, 14 hours of testing. Arrows represent the markers front advancement from initial formation position.

Cu concentration of alloyed Cross-stripe area	**Result of EM of Sn**
0.69 at%	Enhancement
1.35 at%	Suppression
1.93 at%	Suppression

Table 3.3 Summary of Cu alloy effect on electromigration of Sn.

Therefore, based on experimental results, it can be concluded that in the Sn-Cu binary alloy system, 0.69 at% Cu enhances the EM of Sn, while higher atomic concentrations of Cu suppress the EM of Sn. The summary of Cu alloy effect is in table 3.3.

3.4 Nickle (Ni) Binary Sample

In this section, Nickle (Ni) is utilized as the alloying element to produce binary samples. The Sn stripe was coated with Ni using electroplating technique in a "Cross-stripe" pattern. The samples were annealed in an oil bath at 200°C for 5 hours to ensure complete alloying of the "Cross-stripe" area before being installed into the testing cell for electromigration testing at 180°C.

In this study, two Ni binary samples with different atomic percentages of Ni in the alloyed "Cross-stripe" area were prepared and successfully tested. The results of the EM testing for all three samples are shown in Figure 3.4, where clear marker formations were observed. Unlike previous tested Au, Ag and Cu binary samples, both binary samples with 0.10 at% and 1.24% Ni in the alloyed "Cross-stripe" area showed hillock formation at the cathode side and void formation at the anode side, indicating that the EM rate of Sn is slower in the Ni alloyed area than that in pure Sn stripe.

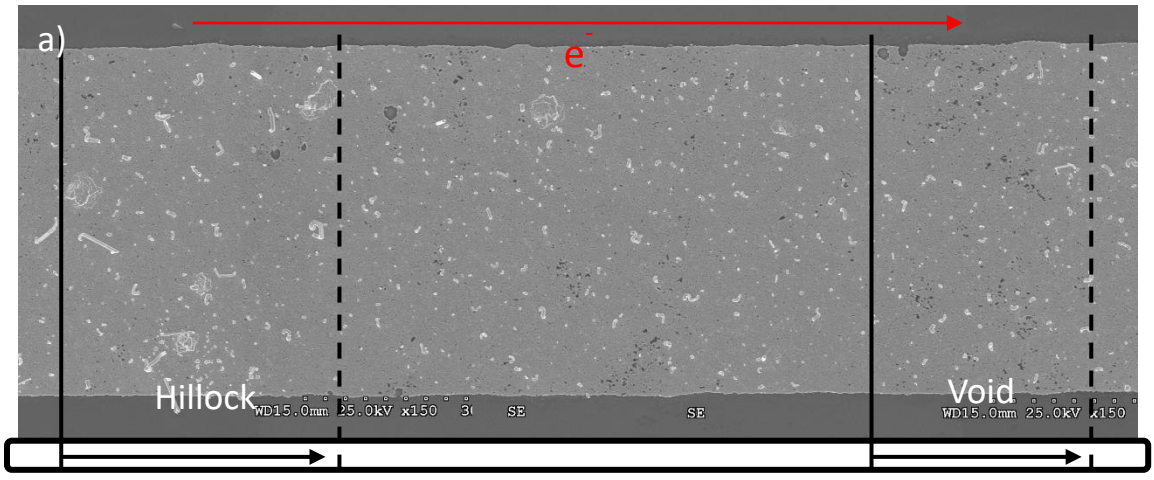

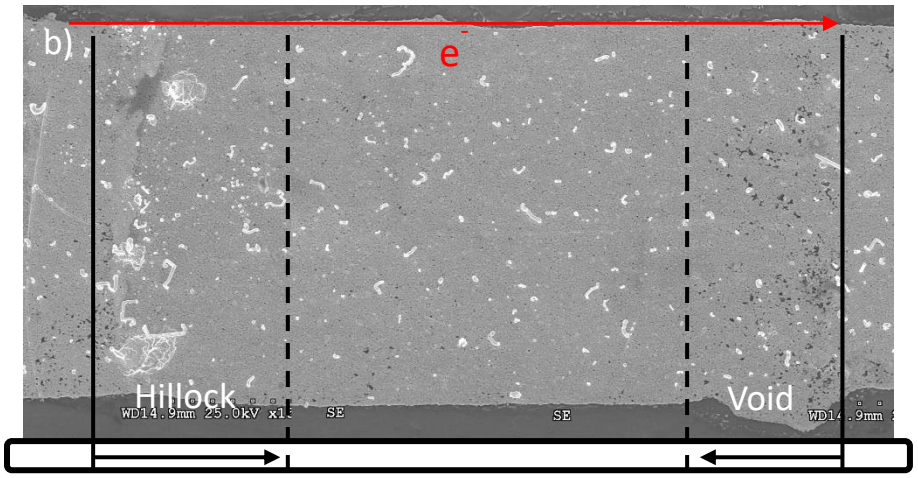

Fig 3.4 SEI images of Ni alloyed binary samples after EM testing. All samples are tested at 180^{o}C. Current density was set at 5x10^{4} A/cm^{2}: a) Ni 0.1 at%, 12 hours of testing, b) Ni 1.24 at%, 16 hours of testing. Arrows represent the markers front advancement from initial formation position.

Ni concentration in alloyed Cross-stripe area	**Result of EM of Sn**
0.10 at%	Suppression
1.24 at %	Suppression

Table 3.4 Summary of Ni alloy effect on electromigration of Sn

Therefore, based on experimental results, it can be concluded that in the Sn-Ni binary alloy system, 0.1 at% Ni suppress the EM of Sn, and higher atomic concentrations of Ni will not change the alloy effect. A summary of the Ni alloy effect is presented in table 3.4.

3.5 Bismuth (Bi) Binary Sample

In this section, Bismuth (Bi) is utilized as the alloying element to produce binary samples. The Sn stripe was coated with Bi using electroplating technique in a "Cross-stripe" pattern. The samples were annealed in an oil bath at 180°C for 2 hours to ensure complete alloying of the "Cross-stripe" area before being installed into the testing cell for electromigration testing at 180°C.

In this study, two Bi binary samples with different atomic percentages of Bi in the alloyed "Cross-stripe" area were prepared and successfully tested. The results of the EM testing for all three samples are shown in Figure 3.5, where clear marker formations were observed. Both binary samples with 2.76 at% and 8.69 at% Bi in the alloyed "Cross-stripe" area showed hillock formation at the cathode side and void formation at the anode side, indicating that the EM rate of Sn is slower in the Bi alloyed area than that in pure Sn stripe.

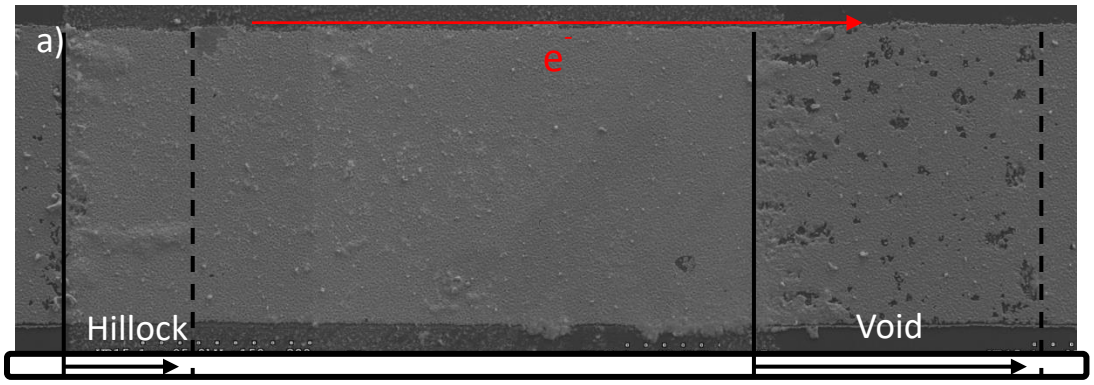

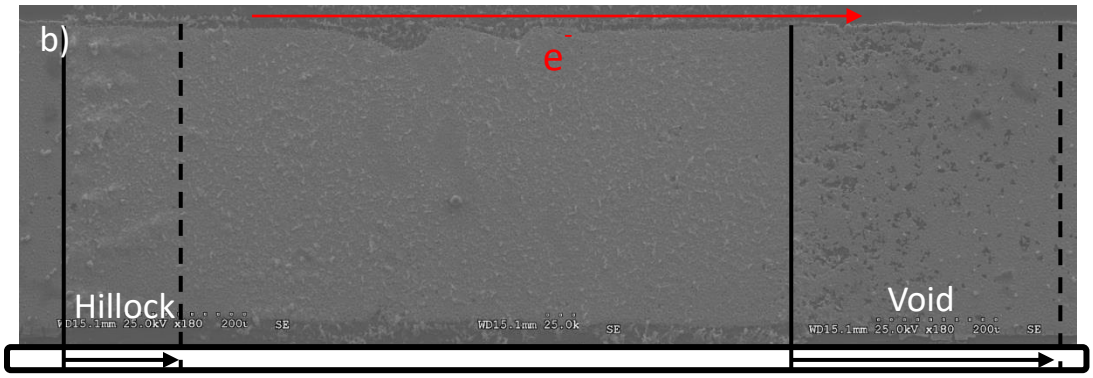

Fig 3.5 SEI images of Bi alloyed binary samples after EM testing. All samples are tested at 180^{o}C. Current density was set at 5x10^{4} A/cm^{2}: a) Bi 2.76 at%, 9 hours of testing, b) Bi 8.69 at%, 8 hours of testing. Arrows represent the markers front advancement from initial formation position.

Bi concentration in alloyed Cross-stripe area	**Result of EM of Sn**
2.76 at%	Suppression
8.69 at%	Suppression

Table 3.5 Summary of Bi alloy effect on electromigration of Sn

Therefore, based on experimental results, it can be concluded that in the Sn-Bi binary alloy system, 2.76 at% Bi suppress the EM of Sn, and higher atomic concentrations of Bi will not change the alloy effect. A summary of the Bi alloy effect is presented in table 3.5.

3.6 Palladium (Pd) Binary Sample

In this section, palladium (Pd) is utilized as the alloying element to produce binary samples. The Sn stripe was coated with Pd using sputtering technique in a "Cross-stripe" pattern.

The samples were annealed in an oil bath at 180°C for 2 hours to ensure complete alloying of the "Cross-stripe" area before being installed into the testing cell for electromigration testing at 180°C.

In this study, two Pd binary samples with different atomic percentages of Pd in the alloyed "Cross-stripe" area were prepared and successfully tested. The results of the EM testing for all three samples are shown in Figure 3.6, where clear marker formations were observed. The binary sample with 0.06 at% Pd in the alloyed "Cross-stripe" area displayed void formation at the cathode side and hillock formation at the anode side, indicating that the EM rate of Sn in the Pd alloyed area is faster than that in the pure Sn stripe. In contrast, the binary sample with 1.12 at% of Pd showed hillock formation at the cathode side and void formation at the anode side, indicating that the EM rate of Sn is slower in the Pd alloyed area.

Therefore, based on experimental results, it can be concluded that in the Sn-Pd binary alloy system, 0.69 at% Pd enhances the EM of Sn, while higher atomic concentrations of Pd suppress the EM of Sn. The summary of Pd alloy effect is in table 3.6.

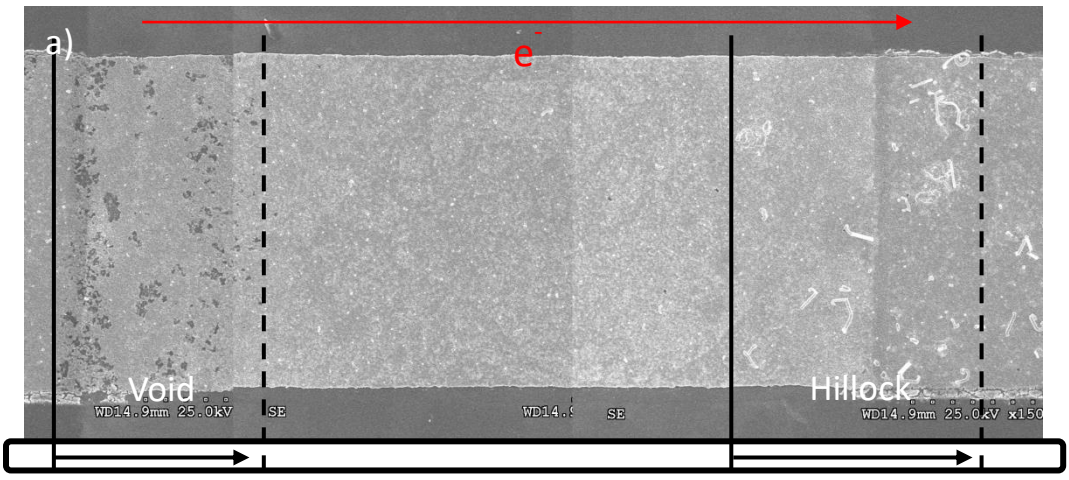

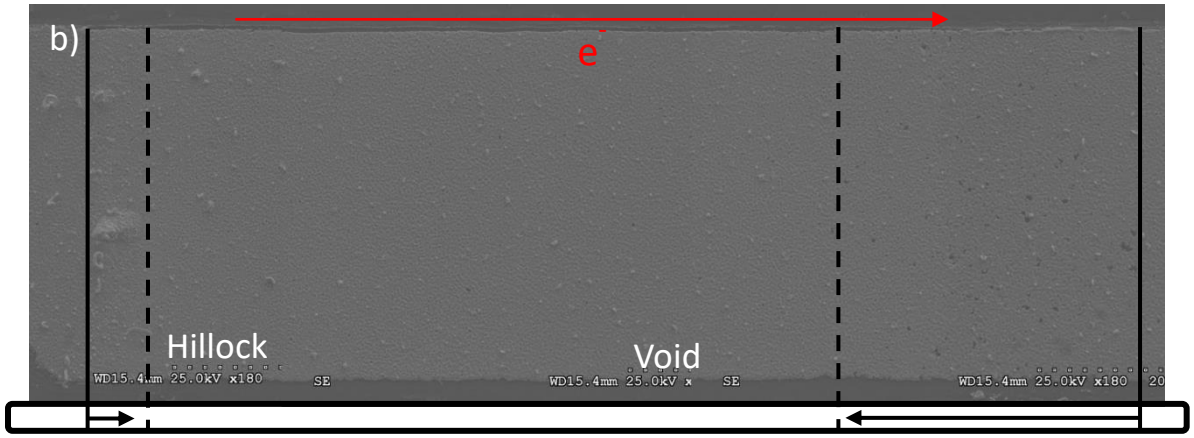

Fig 3.6 SEI images of Pd alloyed binary samples after EM testing. Samples are tested at 180°C. Current density was set at $5x10^4$ A/cm^2: a) Pd 0.06 at%, 9 hours of testing, b) Pd 1.12 at%, 8 hours of testing. Arrows represent the markers front advancement from initial formation position.

Pd concentration in alloyed Cross-stripe area	**Result of EM of Sn**
0.06 at%	Enhancement
1.12 at%	Suppression

Table 3.6 Summary of Pd alloy effect on electromigration of Sn

3.7 Cobalt (Co) Binary Sample

In this section, cobalt (Co) is utilized as the alloying element to produce binary samples. The Sn stripe was coated with Co using sputtering technique in a "Cross-stripe" pattern. The samples were annealed in an oil bath at 210°C for 12 hours to ensure complete alloying of the "Cross-stripe" area before being installed into the testing cell for electromigration testing at 180°C.

In this study, two Co binary samples with different atomic percentages of Co in the alloyed "Cross-stripe" area were prepared and successfully tested. The results of the EM testing

for all three samples are shown in Figure 3.7, where clear marker formations were observed. The binary sample with 0.36 at% Co in the alloyed "Cross-stripe" area displayed void formation at the cathode side and hillock formation at the anode side, indicating that the EM rate of Sn in the Co alloyed area is faster than that in the pure Sn stripe. In contrast, the binary sample with 1.00 at% of Co showed hillock formation at the cathode side and void formation at the anode side, indicating that the EM rate of Sn is slower in the Co alloyed area.

Therefore, based on experimental results, it can be concluded that in the Sn-Co binary alloy system, 0.69 at% Co enhances the EM of Sn, while higher atomic concentrations of Co suppress the EM of Sn. The summary of Co alloy effect is in table 3.7.

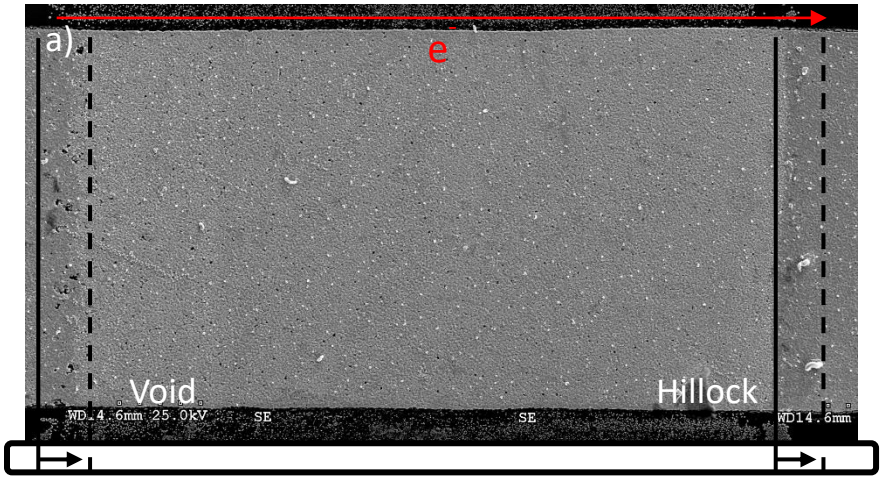

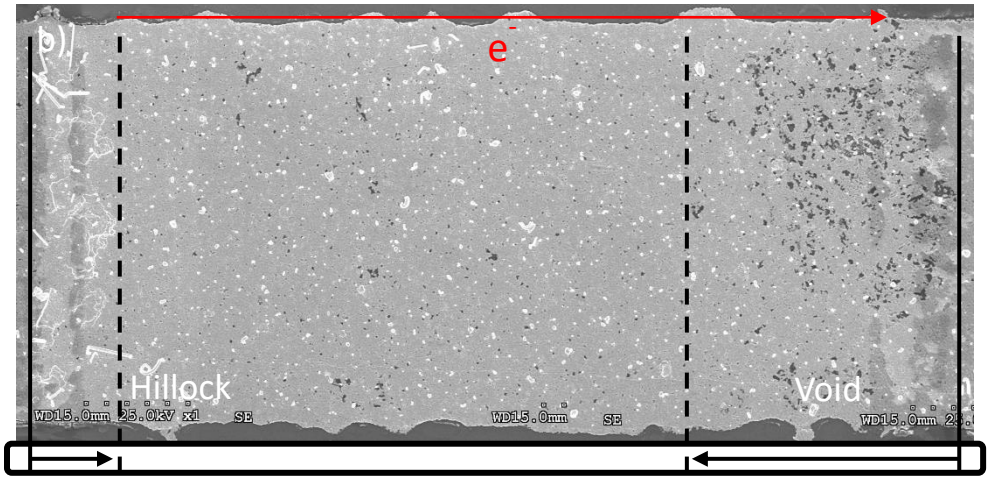

Fig 3.7 SEI images of Co alloyed binary samples after EM testing. Samples are tested at 180°C. Current density was set at $5x10^4$ A/cm^2: a) Co 0.36 at%, 4 hours of testing, b) Co 1.00 at%, 10 hours of testing. Arrows represent the markers front advancement from initial formation position.

Co concentration in alloyed Cross-stripe area	**Result of EM of Sn**
0.36 at%	Enhancement
1.00 at%	Suppression

Table 3.7 Summary of Co alloy effect on electromigration of Sn

3.8 Mechanism of Alloying Effect on EM of Sn

3.8.1 Solute Effect on EM of Sn

Based on the electromigration testing results presented in the previous chapter, two important implications can be drawn:

a) Alloying can effectively suppress the EM rate of Sn.

b) The effect of alloying on the EM of Sn may not be determined by the type of alloy element, but rather by the concentration of the alloy element in the Sn matrix.

From the EM testing results of the binary samples containing Au, Ag, Cu, Pd, and Co, it was observed that the alloy effect led to an acceleration of the EM rate of Sn in samples with low concentrations of alloy elements, while it resulted in a suppression of the EM rate of Sn in samples with increased alloy concentration. This indicates that the fundamental mechanism of the alloy effect on the EM of Sn in the binary system may be a solute-controlled mechanism.

Figures 3.8 through 3.14 illustrate the theoretical maximum solubility limit of Au, Ag, Cu, Pd, Co, Ni and Bi in the Sn matrix, respectively. These data are based on previously published experimental results and the solute atomic percent at the eutectic temperature in the phase diagram. The maximum solubilities of Ag, Cu, Pd, and Co elements are right between the concentrations of alloy elements that accelerate and suppress EM of Sn in our "Cross-stripe" EM testing results. The maximum solubility of Au is slightly different from our experimental result (0.4 at% < 0.76 at%). This discrepancy may be due to the calibration of EDS detection sensitivity and experimental limitations. These suggest that the solubility limit of the alloy element in Sn matrix may be the key factor to affect EM rate of Sn.

Au concentration in alloyed Cross-strip area	Alloy effect of EM of Sn
0.76 at%	Enhancement
0.4 at% at 217°C	**Maximum Solubility**
1.5 at%	Suppression
2.6 at%	Suppression
3.78 at%	Suppression
5.14 at%	Suppression

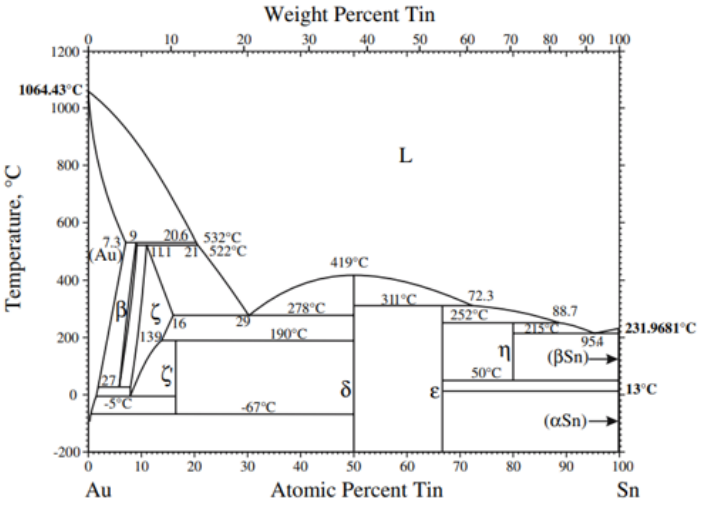

Fig 3.8 Summary of Au alloy effect on EM of Sn with maximum solubility (left) and corresponding Au-Sn phase diagram [72, 73].

Ag concentration in alloyed Cross-strip area	Alloy effect of EM of Sn
0.06 at%	Enhancement
0.09 at% at 221°C	**Maximum Solubility**
0.2 at%	Suppression
1.90 at%	Suppression
2.72 at%	Suppression

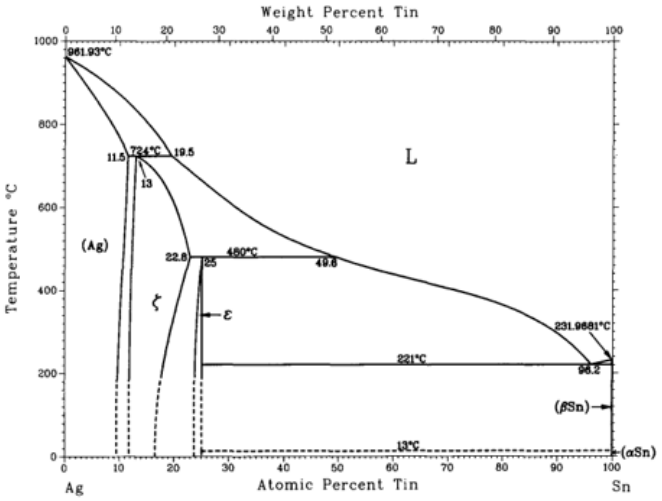

Fig 3.9 Summary of Ag alloy effect on EM of Sn with maximum solubility (left) and corresponding Ag-Sn phase diagram [73, 74].

Cu concentration in alloyed Cross-strip area	Alloy effect of EM of Sn
0.69 at%	Enhancement
1.32 at% at 227°C	**Maximum Solubility**
1.35 at%	Suppression
1.93 at%	Suppression

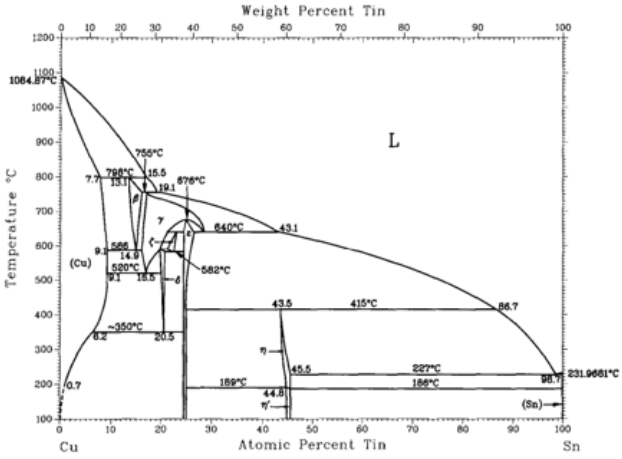

Fig 3.10 Summary of Cu alloy effect on EM of Sn with maximum solubility (left) and corresponding Cu-Sn phase diagram [75].

Pd concentration in alloyed Cross-strip area	Alloy effect of EM of Sn
0.06 at%	Enhancement
1 at% at 229°C	**Maximum Solubility**
1.12 at%	Suppression

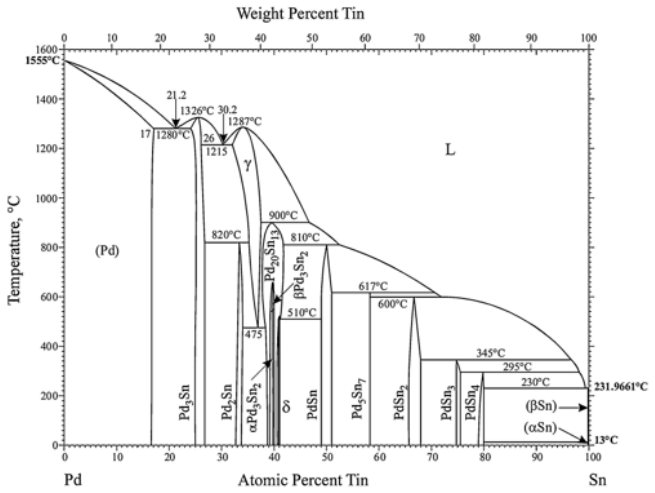

Fig 3.11 Summary of Pd alloy effect on EM of Sn with maximum solubility (left) and corresponding Pd-Sn phase diagram [76, 77].

Co concentration in alloyed Cross-strip area	Alloy effect of EM of Sn
0.36 at%	Enhancement
0.5 at% at 229°C	**Maximum Solubility**
1.00 at%	Suppression

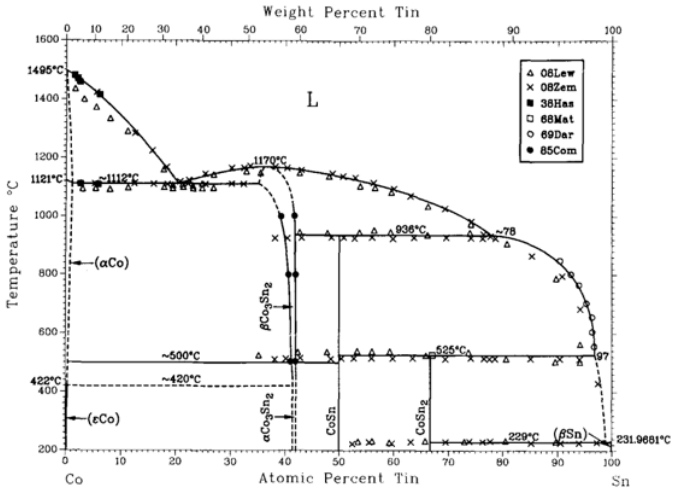

Fig 3.12 Summary of Co alloy effect on EM of Sn with maximum solubility (left) and corresponding Co-Sn phase diagram [78, 79].

However, a complication is found among the tested alloy elements. As depicted in Figures 3.13 and 3.14, the addition of Ni to Sn in binary samples suppresses the EM of Sn both

below and above Ni's maximum solubility. Bi exhibits a similar effect to Ni, with EM suppression of Sn observed in binary samples with Bi concentration below the solubility limit. These behaviors are inconsistent with those of other alloy elements. In summary, there may be two types of alloy elements in the Sn binary alloy system. The first type of elements accelerates the EM of Sn at low concentrations when they exist as solutes in Sn solid solution. When their concentrations exceed the solubility limit, new phases form as intermetallic compounds (IMC) in the Sn matrix, suppressing the EM of Sn. In contrast, the second type of elements always suppress the EM of Sn, regardless of their concentration. Thus far, Au, Ag, Cu, Pd, and Co belong to the first type, while Ni and Bi belong to the second type.

Ni concentration in alloyed Cross-strip area	Alloy effect of EM of Sn
0.10 at%	Suppression
0.33 at% at 231.15°C	**Maximum Solubility**
1.24 at%	Suppression

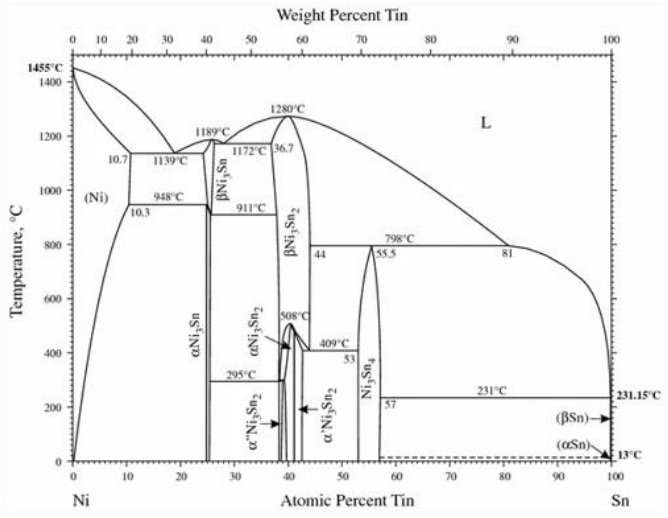

Fig 3.13 Summary of Ni alloy effect on EM of Sn with maximum solubility (left) and corresponding Ni-Sn phase diagram [80-83].

Bi concentration in alloyed Cross-strip area	Alloy effect of EM of Sn
2.76 at%	Suppression
8.69 at%	Suppression
13at% at 138°C	**Maximum Solubility**

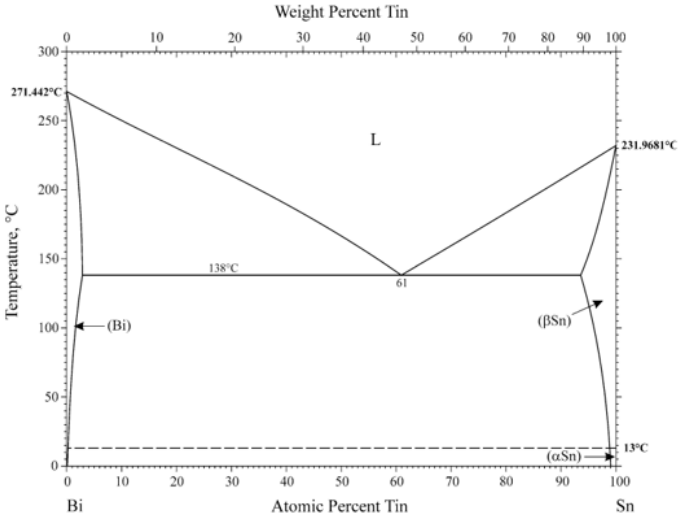

Fig 3.14 Summary of Bi alloy effect on EM of Sn with maximum solubility (left) and corresponding Bi-Sn phase diagram [84, 85].

Figure 3.15 illustrates the marker motions observed during EM testing of binary samples containing the first type (Au) and second type (Bi) alloy elements as solute. The advancing directions of the hillock and void are in the direction of electron flow, consistent with the vacancy-driven diffusion mechanism in Sn discussed in Chapter 1 [25]. The EM testing temperature used in this project for all samples was 180°C, equivalent to 453.15 K. Since the melting temperature of pure Sn is 505.08 K, the EM testing temperature is clearly above 0.8Tm of Sn, which is 404.06 K. Under this condition, the diffusivity of lattice diffusion will be much higher than that of grain boundary diffusion (Figure 1.9) [19], indicating that lattice (bulk) diffusion will be the dominant diffusion mechanism for both Sn and solute atoms in the alloy system.

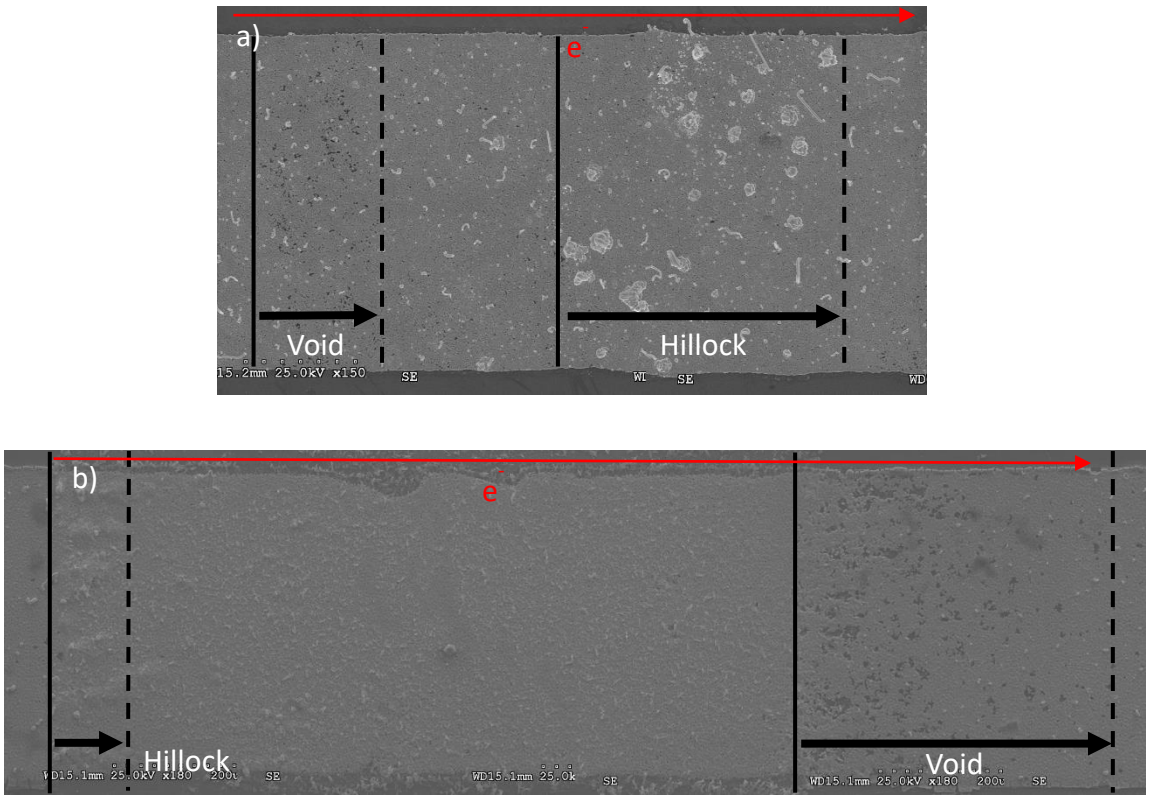

Fig 3.15 Markers motion of sample with a) Au solute (0.75 at%), b) Bi solute (8.69 at%). Arrows represent the markers front advancement from initial formation position.

While we have not yet obtained definitive evidence to prove the detailed mechanism underlying the effect of first and second type elements on the EM of Sn, we believe it is related to the binding energy between solute atoms and vacancies, as well as changes in the activation energy of Sn atom diffusion. For the first type of solute atoms (Au, Ag, Cu, Pd and Co), their presence in the Sn matrix can decrease the activation energy required for Sn atom migration, possibly due to their low binding energy to vacancies. Which drives vacancies away from solute atoms to become available to Sn atoms for jumping, leading to an acceleration effect on the EM of Sn. On the other hand, for the second type of solute atoms (Ni and Bi), their binding energy to

vacancies is higher than that of Sn atoms, making vacancies more likely to remain next to solute atoms and unavailable for Sn atom jumping. This leads to a suppression effect on the EM of Sn.

3.8.2 IMC Effect - Two Phase Equilibrium

Based on the EM testing results and the maximum solubility limit of the alloy element, a "Two-phase equilibrium" mechanism is proposed, as shown in Figure 3.16. When the alloy element exists as a solute in the Sn solid solution, the electromigration rate of Sn is accelerated or enhanced by the first or second type of solute atoms, and in this case, the concentration of the alloy element is below its maximum solubility limit in the Sn matrix. However, when the alloy element concentration exceeds the maximum solubility limit in the Sn matrix, alloy element induced intermetallic compound (IMC) will form as new phase (precipitates), inducing the "Two-phase equilibrium" and suppressing the EM rate of Sn for both first and second type of atoms.

The SEM micrographs in Figures 3.17 show the markers motion of samples with IMC induced by both types of elements. The advancing directions of the hillock are in the direction of electron flow, and void is in the opposite direction of electron flow. This phenomenon is driven by the IMC dissolution process, which is driven by the migration of alloy elements under EM. Again, this result is consistent with the vacancy-driven diffusion mechanism in Sn. The underlying mechanism is not fully understood, but it is believed to be related to two facts. First, the total number of sites in the lattice consists of three parts: the number of solution atoms, the number of solute atoms, and the number of vacancies. The existence of two-phase equilibrium limits the vacancy concentration at its equilibrium level. Additional solute atoms are ready to be supplied into lattice for controlling the number of vacancies by dissolving the IMC precipitates

(second phase), which act as a source and sink for vacancies, as well as solutes. Second, the precipitated IMC will attract vacancies at grain boundaries, and block the diffusion path to further suppress the EM of Sn. This suggests that the existence of the two-phase equilibrium plays an essential role in suppressing the Sn-EM rate.

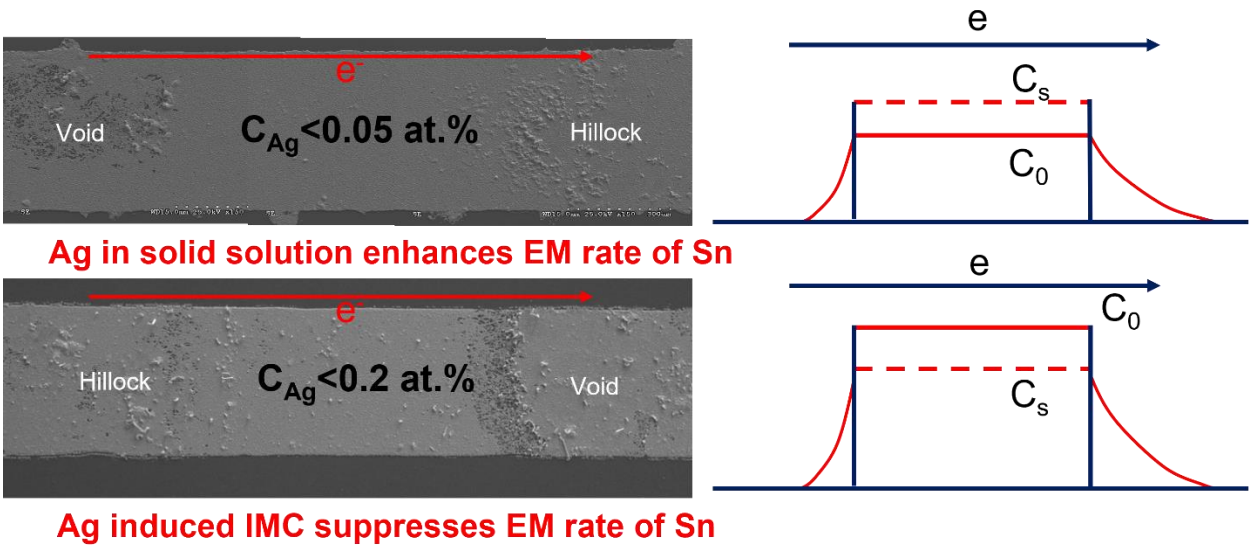

Fig 3.16 Schematic diagram shows Two-phase Equilibrium mechanism of alloy effect. "Cross-stripe" sample is Ag sample. C_0 stands for concentration of alloy elements in Sn matrix. C_s stands for the maximum solubility limit of alloy elements in Sn matrix.

The result with binary sample contains Bi beyond solubility limit is currently unavailable due to the high joule heating generated during EM testing. Which leads to the partial melting of "Cross-stripe" area, abnormal migration of alloy elements, and possible open circuit failure.

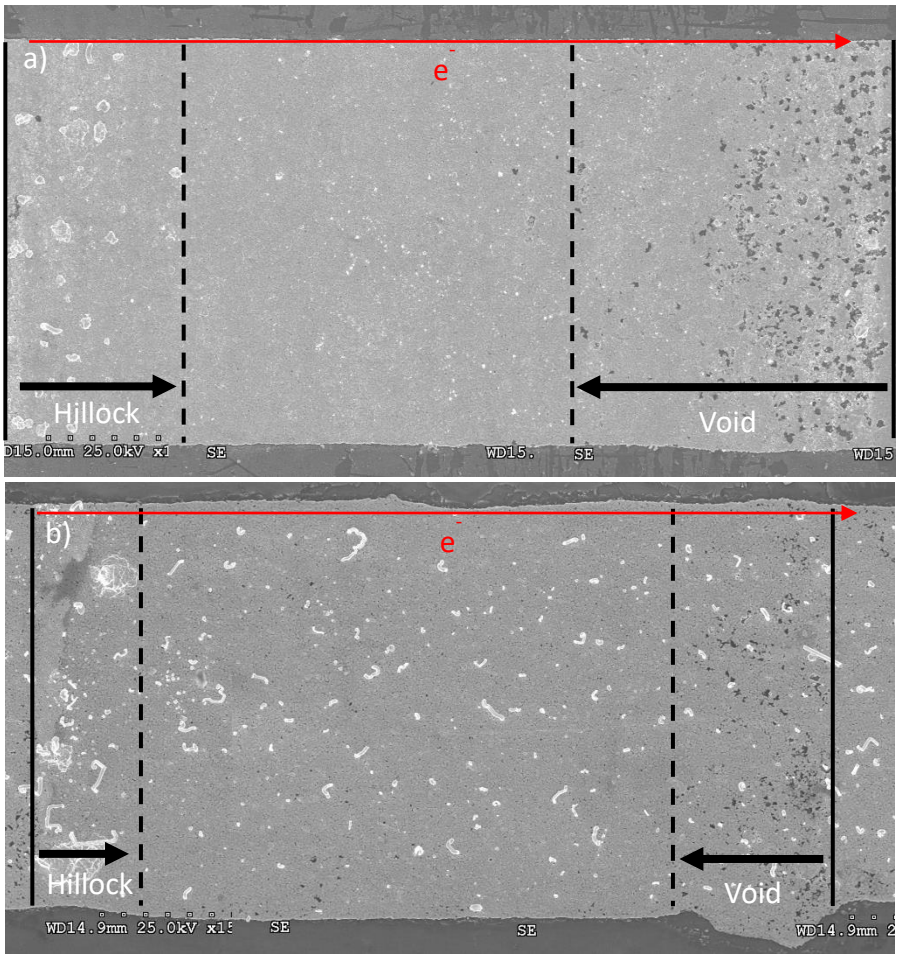

Fig 3.17 Markers motion of sample with a) Au IMC (2.60 at%), b) Ni IMC (1.24 at%). Arrows represent the markers front advancement from initial formation position.

3.8.3 Marker Front Motion and Estimated Electromigration Diffusivity (Z*D)

The task of describing solute electromigration is extremely challenging due to the fact that the position of the boundary between the Sn stripe and the alloyed area changes with time. This is known as the Stefan problem [86], which involves a diffusion system with a moving boundary or frame of reference (Figure 3.18).

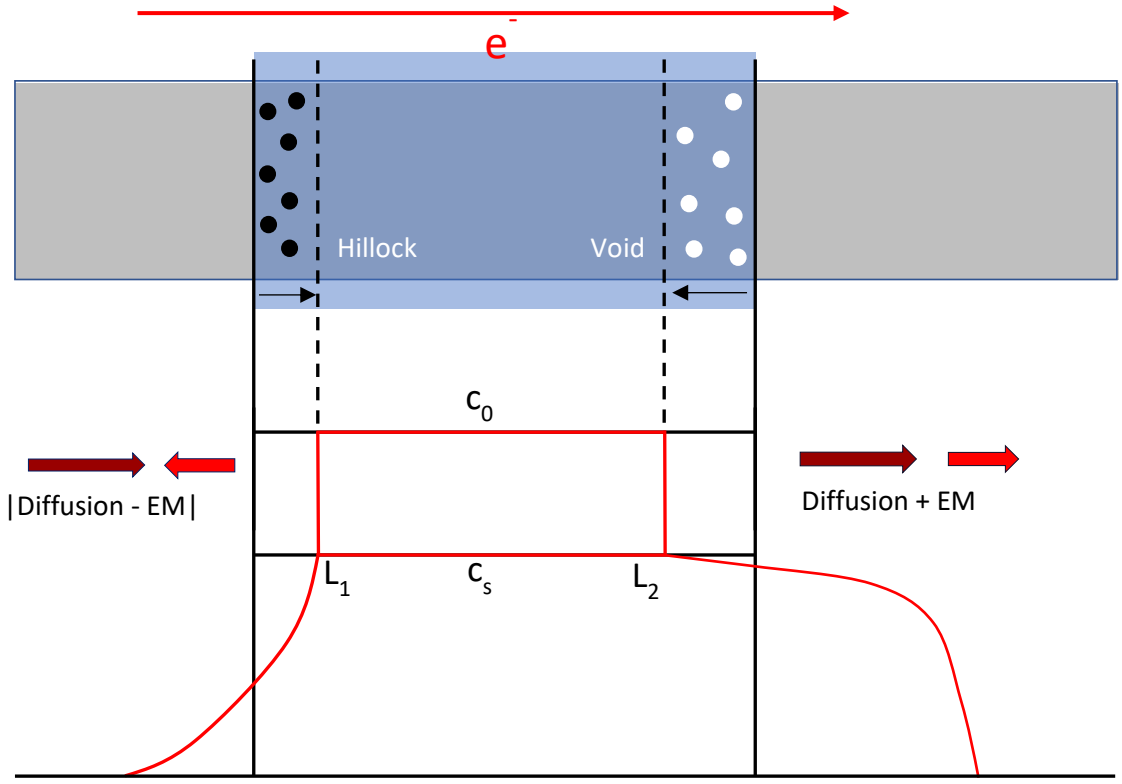

Fig 3.18 Schematic diagram shows marker front boundary L1 and L2 movement under EM.

As shown in Figure 3.18, Maker front L1 (hillock) and L2 (void) are defined as boundaries that separate the two-phase and signal phase regions within the stripe. The alloyed area begins with an initial solute amount (Co) that exceeds its solubility limit (Cs) to Sn, resulting in the area being in a state of two-phase equilibrium. The removal of solute from a local area, at a rate of (Co-Cs), leads to complete dissolution of the IMC, causing the L1 and L2 boundaries to advance with EM, in the direction determined by the flux divergence at the boundaries.

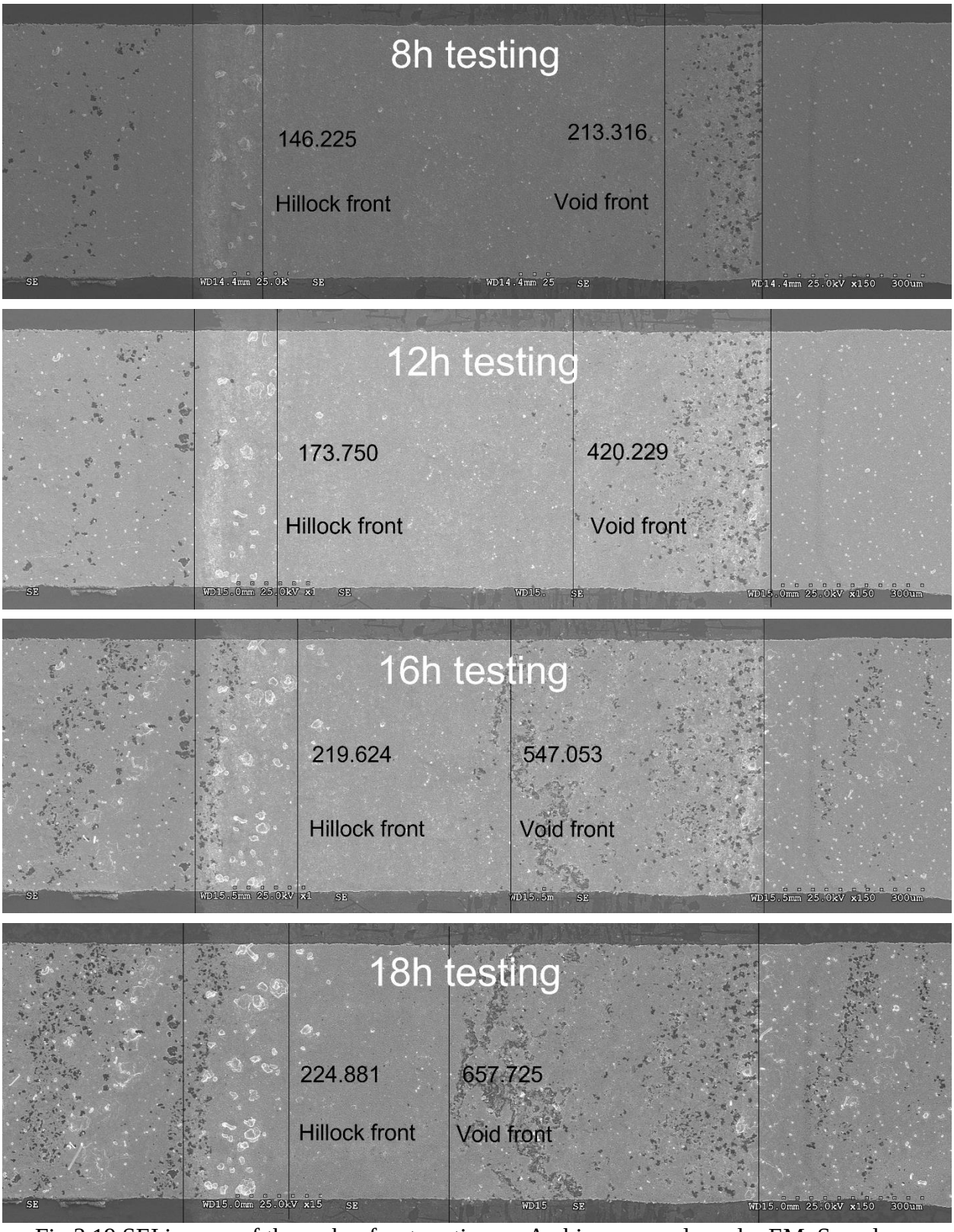

Fig 3.19 SEI images of the maker front motion on Au binary sample under EM. Sample was tested at 180^{o}C with 5x10^{4} A/cm^{2}. This sample contains 2.6 at% Au with induced IMC.

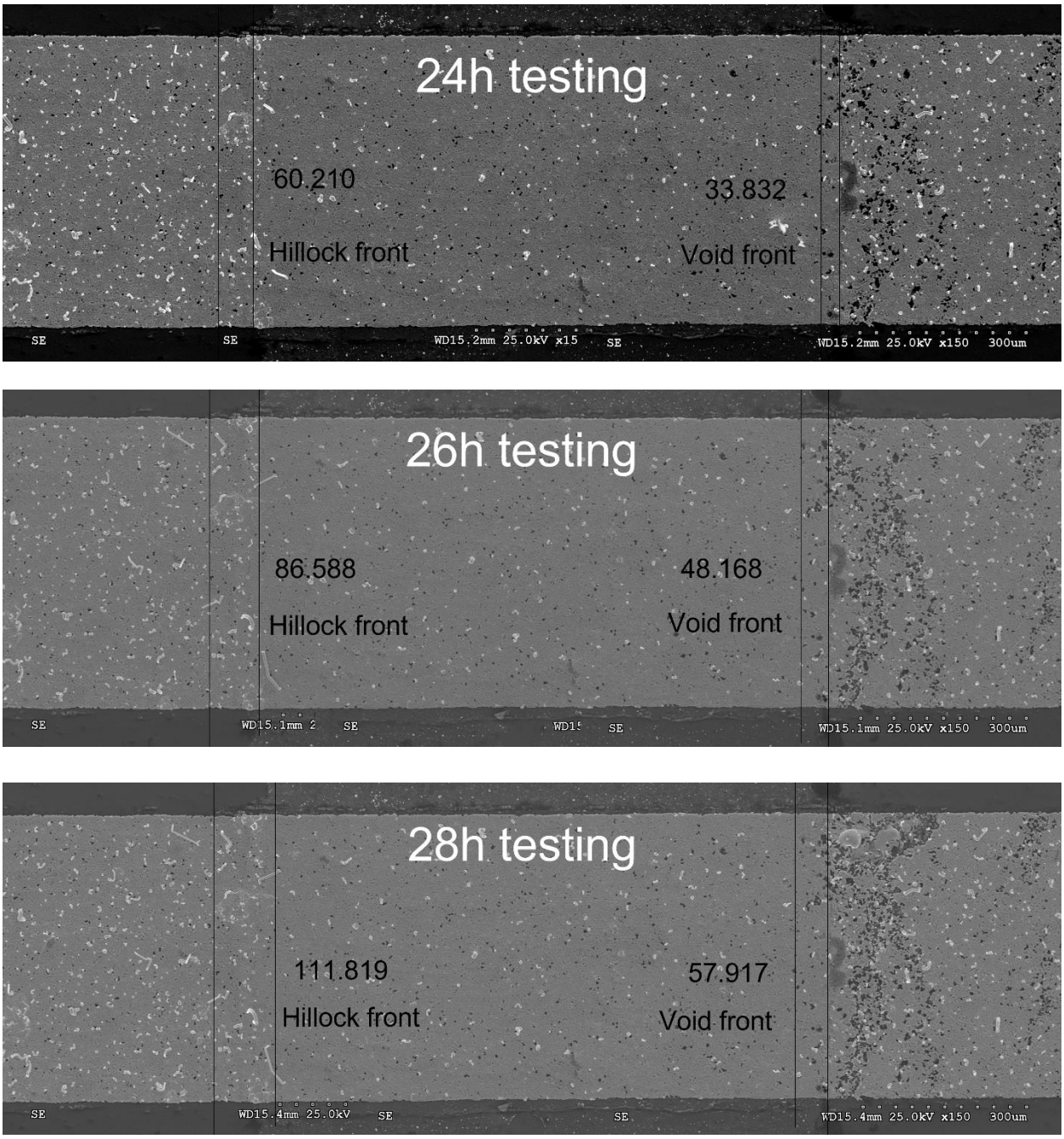

Fig 3.20 SEI images of the maker front motion on Ag binary sample under EM. Sample was tested at 180ºC with $5x10^4$ A/cm^2. This sample contains 1.77 at% Ag with induced IMC.

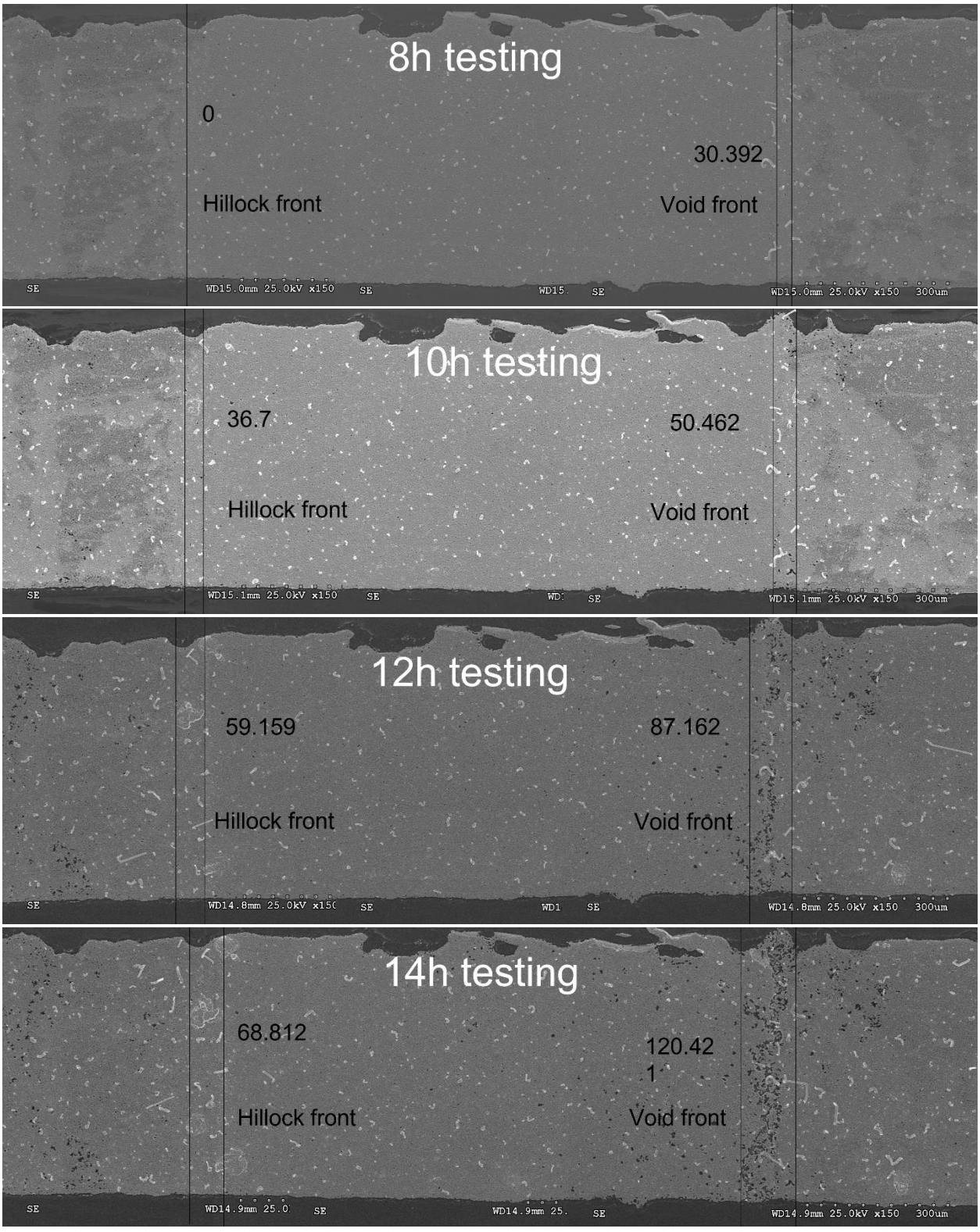

Fig 3.21 SEI images of the maker front motion on Cu binary sample under EM. Sample was tested at 180^{o}C with 5x10^{4} A/cm^{2}. This sample contains 1.93 at% Cu with induced IMC.

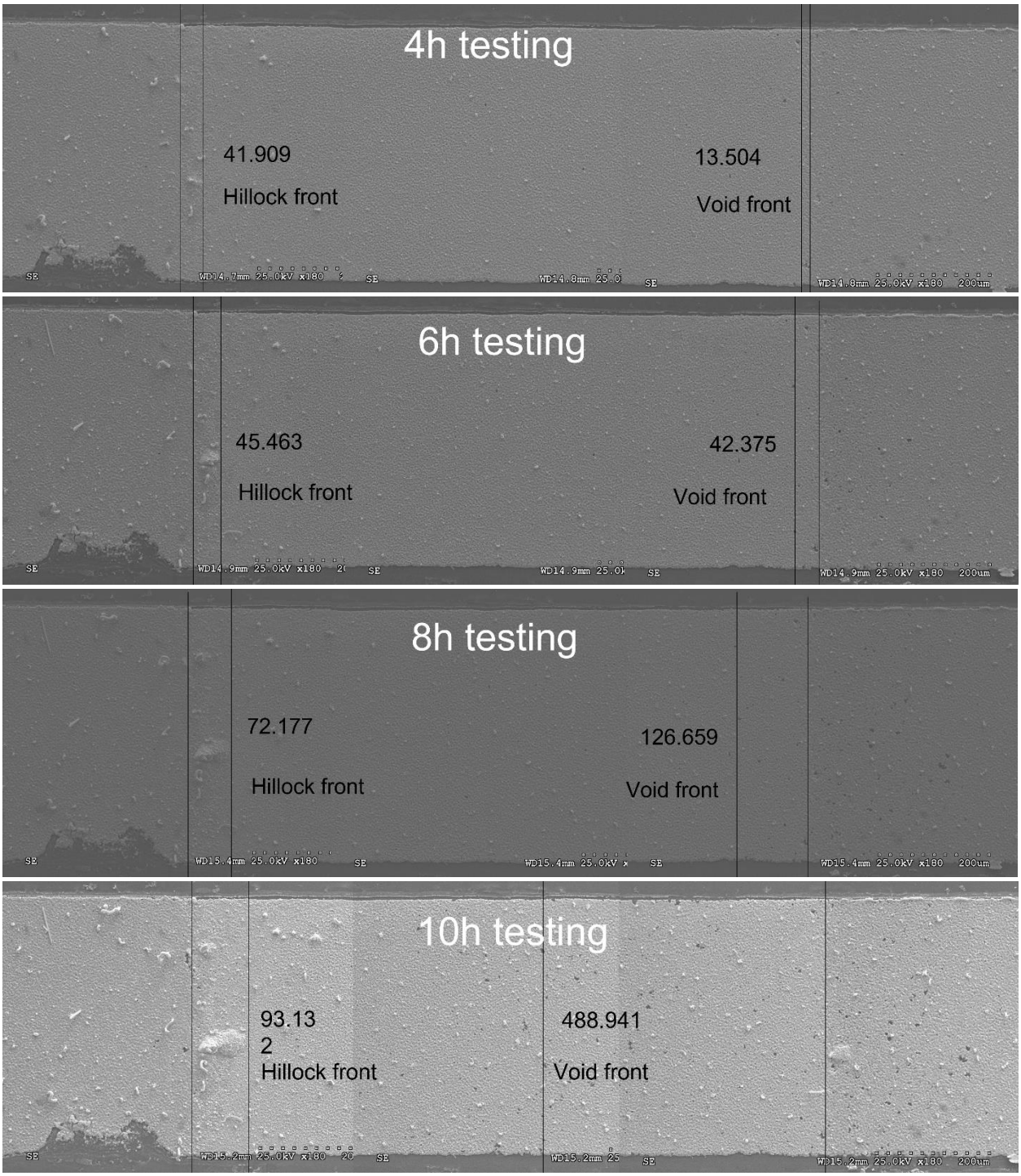

Fig 3.22 SEI images of the maker front motion on Pd binary sample under EM. Sample was tested at 180ºC with $5x10^4$ A/cm^2. This sample contains 1.12 at% Pd with induced IMC.

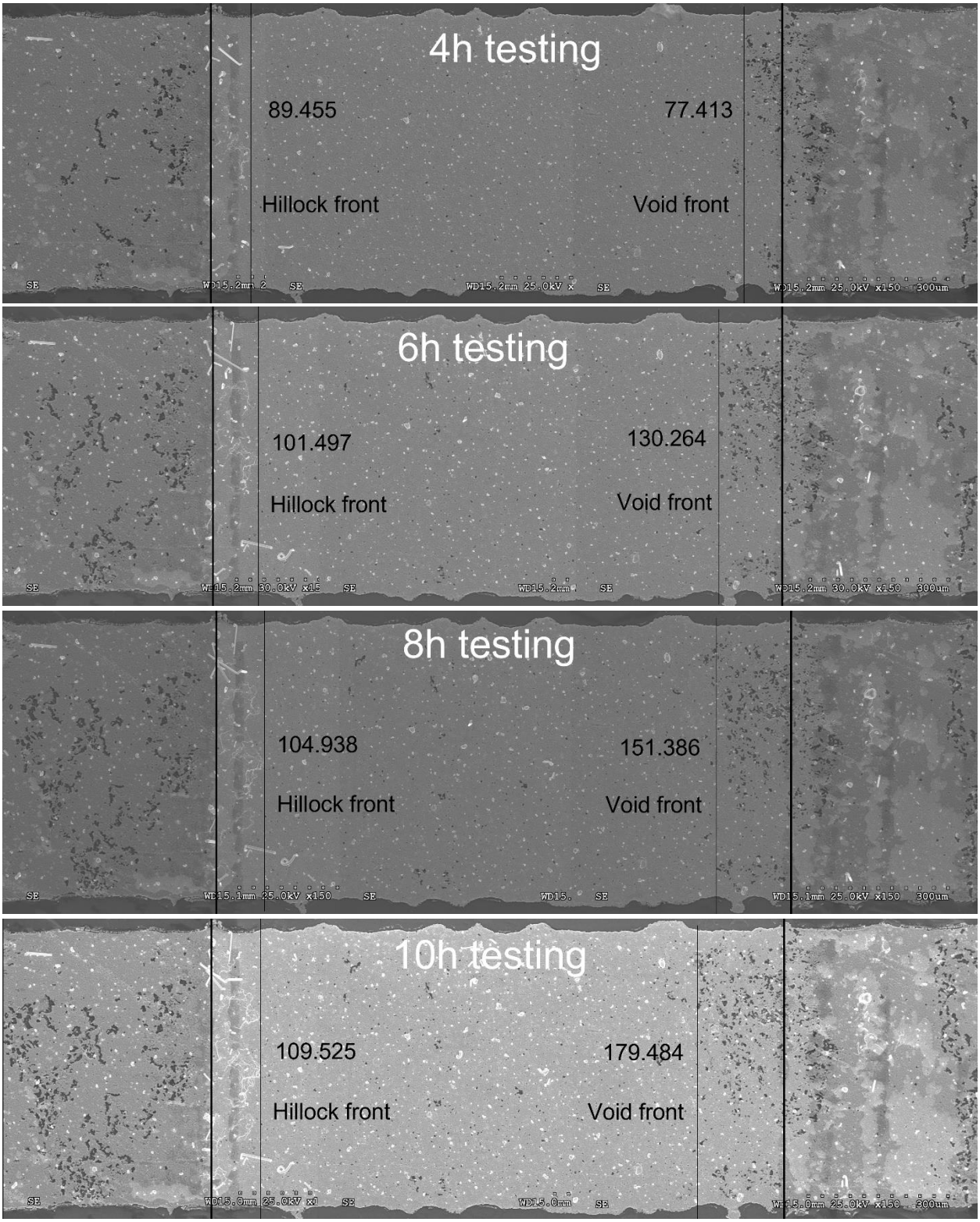

Fig 3.23 SEI images of the maker front motion on Co binary sample under EM. Sample was tested at 180ºC with $5x10^4$ A/cm^2. This sample contains 1.00 at% Co with induced IMC.

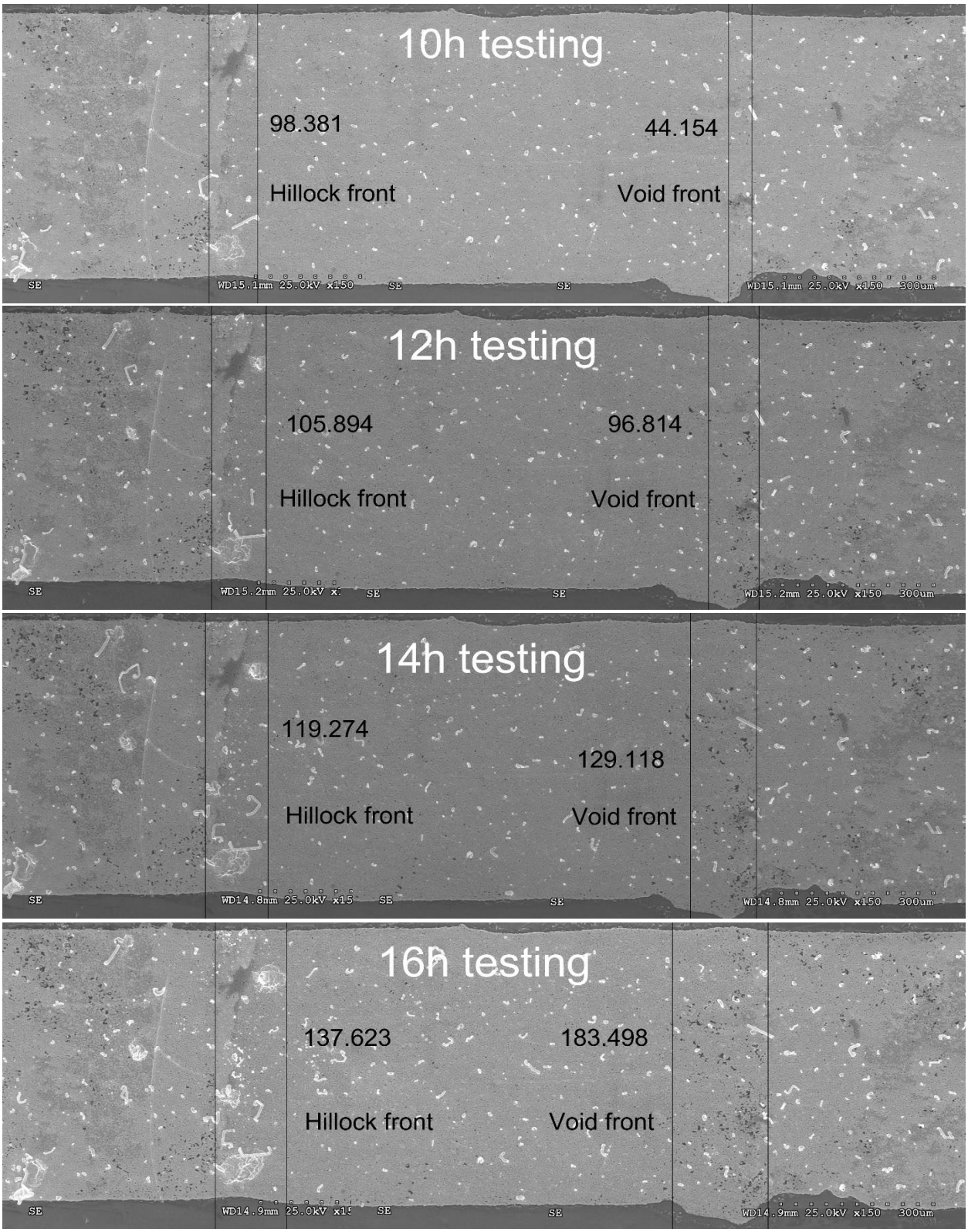

Fig 3.24 SEI images of the maker front motion on Ni binary sample under EM. Sample was tested at 180^{o}C with 5x10^{4} A/cm^{2}. This sample contains 1.24 at% Ni with induced IMC.

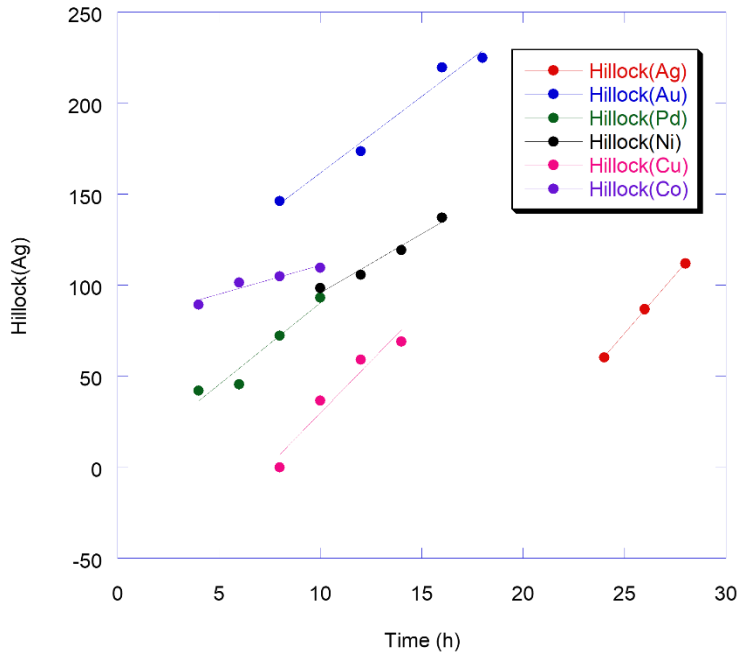

Fig 3.25 Summary of Hillock front motion (L1) on alloy "Cross-stripe" samples.

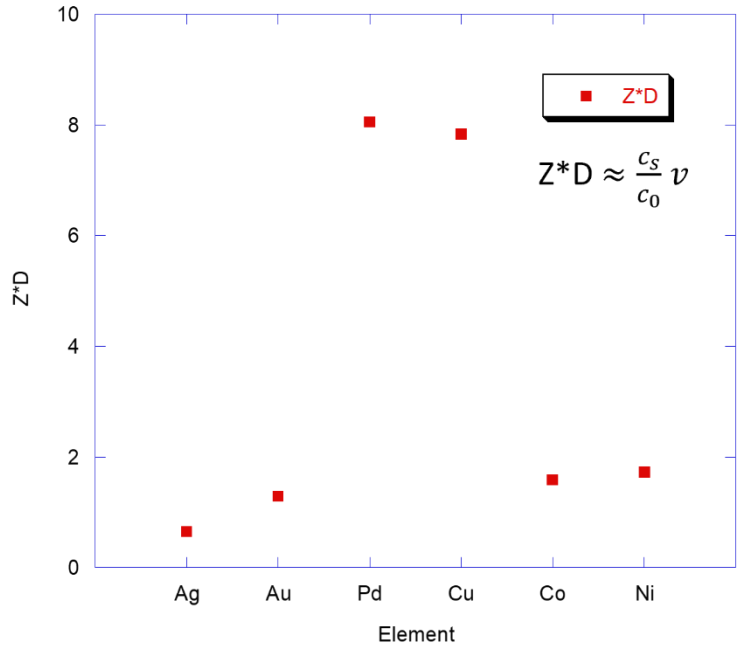

Fig 3.26 The estimated EM diffusivity (Z*D) of solute elements determined by fitting the marker advancement data to the approximation. Z* stands for effective charge numbers.

Figures 3.19 to 3.24 depict the movement of the marker under EM in binary samples of Au, Ag, Cu, Pd, Co, Ni, and Bi on the "Cross-stripe." In figures 3.25 and 3.26, we provide a summary of the hillock front advancement observed during the EM testing and the estimated electromigration diffusivity (Z*D) of alloyed elements. Unfortunately, we were unable to obtain the Z*D value of Bi. Because the mathematical solution mode proposed above is designed for two-phase with existence of IMC, and testing result with binary samples contain Bi IMC is currently unavailable due to joule heating.

The results of our study suggest that most of the elements tested exhibit high electromigration (EM) mobility, particularly Pd and Cu, indicating that they are EM active. However, an exception is observed in the case of Ag, which is not very EM active, implying that it does not move as much as other elements when subjected to EM conditions. Therefore, to suppress EM in Sn and enhance the EM reliability of Sn-based solder joints, two types of alloy elements can be added to the Sn matrix: Ag, due to its low EM activity, and Ni, owing to its permanent EM suppression ability.

Chapter 4: EM Testing of Ternary Samples

4.1 Secondary Element Effect on Sn-Ni System

4.1.1 Ag Effect on Sn-Ni System

In industrial applications of Sn-based solder, such as a Sn-Ag solder joint with a thin layer of Ni as a diffusion barrier, the situation is often more complex than a simple binary alloy system. This has led to a growing interest in understanding the EM behavior of Sn-based ternary and even quaternary systems in industry. Our research aims to address this need by investigating the EM behavior of Sn-based ternary alloy systems. In addition to understanding the solute effect

on EM of Sn and building fundamental knowledge about the alloying effect on EM of Sn in binary systems, we aim to explore the secondary alloy element effect on existed alloy system, and characterize the possible effects of two different solute atoms on Sn under EM in ternary alloy systems. Specifically, we investigate the EM behavior of Sn-based ternary alloy systems by adding a secondary alloy element on top of a Sn binary alloy stripe as a "Cross-Stripe." After annealing, an Sn-based ternary alloy system can be formed, allowing us to identify the effect of the secondary alloy element on the EM of the existing Sn binary system through marker polarity and motion. We also aim to characterize possible interactions between two different solute atoms using SEM and EDS.

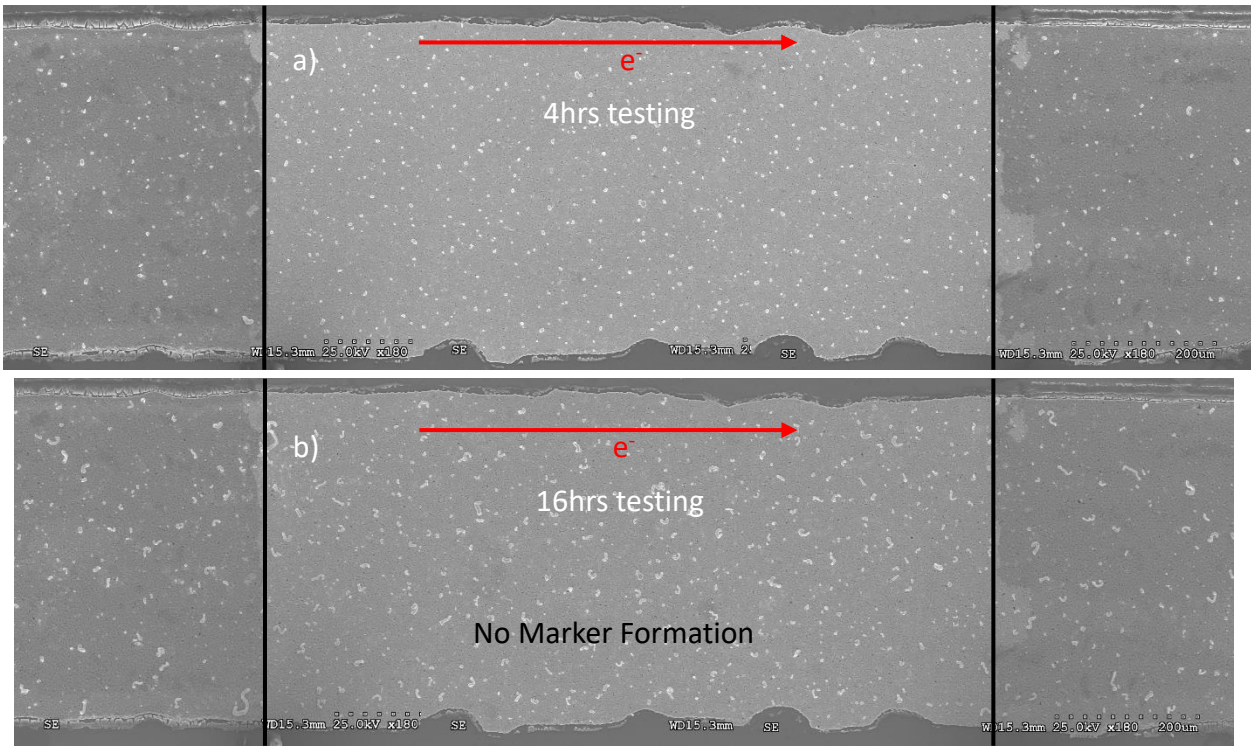

Fig 4.1 SEI image of ternary sample (Ag as cross-stripe on Sn-Ni). Ni is around 0.43 at%. Ag is around 0.09 at%. Sample was tested at 180°C, with $5x10^4$ A/cm^2: a) sample after 4 hours testing, b) sample after 16 hours testing.

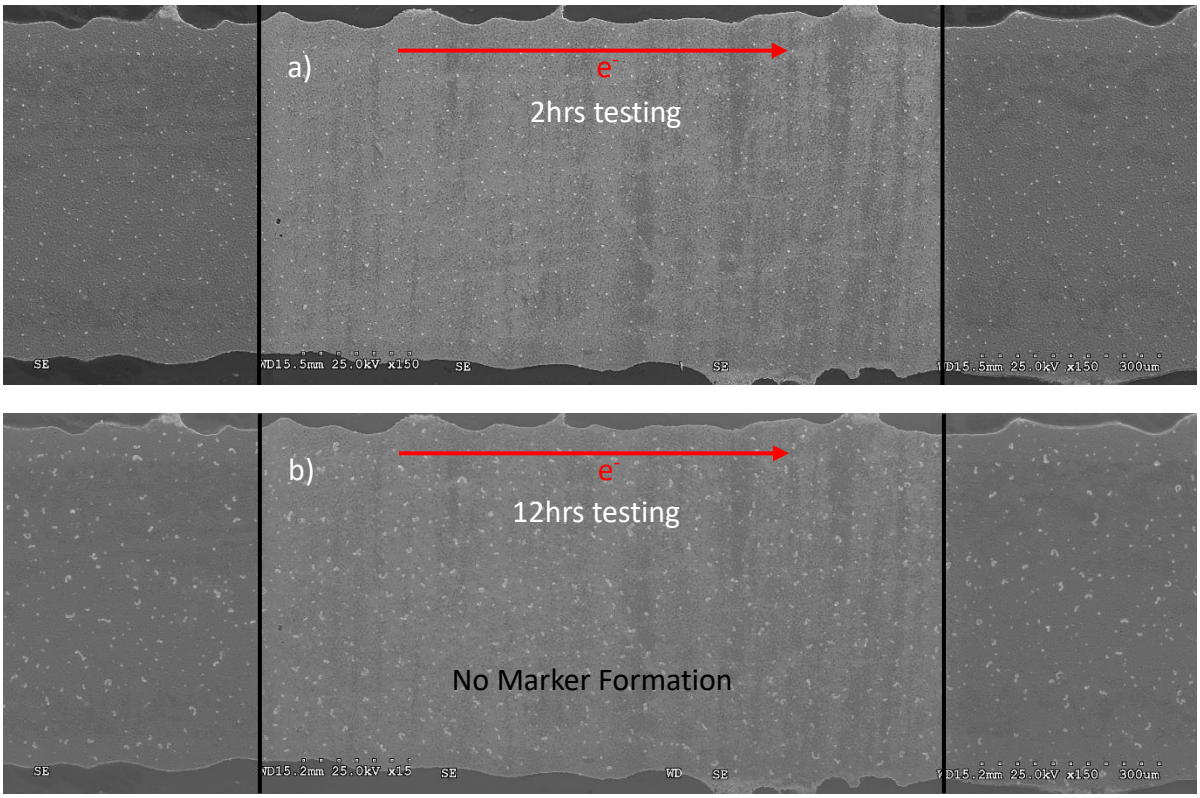

Fig. 4.2 SEI image of ternary sample (Ag as cross-stripe on Sn-Ni). Ni is around 2.41 at%. Ag is around 0.79 at%. Sample was tested at 180^{o}C, with 5x10^{4} A/cm^{2}: a) sample after 2 hours testing, b) sample after 12 hours testing.

In this section, we investigated the electromigration (EM) behavior of the Sn-Ag-Ni ternary alloy system. By sputtering an Ag layer as a "Cross-stripe" on top of the Sn-Ni stripe, we were able to study the effect of Ag as a secondary alloy element on the Sn atoms in the existing Sn-Ni alloy system under EM. Surprisingly, as shown in Figures 4.1 and 4.2, we observed no formation of hillocks or voids during the electromigration test for both ternary samples. This suggests that the presence of Ag did not alter the electromigration behavior of Sn in the ternary alloy system. Furthermore, this indicated that Ag exists independently in the system as a secondary element and does not interact with the Sn atoms. We also observed the development

of pure Sn whiskers on the sample after a certain time of electromigration testing, which may have resulted from residual compression stress generated during the repeated cooling/heating process when the sample was taken out from the oil bath for SEM inspection. In conclusion, our findings suggest that adding Ag to an existing Sn-Ni system will not have any additional impact on the EM of Sn.

4.1.2 Cu Effect on Sn-Ni System

In this section, we investigated the EM behavior of the Sn-Cu-Ni ternary alloy system, commonly known as SCN solder alloy. To explore the impact of Cu as an additional element on the existing Sn-Ni alloy system under EM, we applied a Cu "Cross-stripe" on top of the Sn-Ni stripe. The polarity and motion of the marker were used to evaluate the effect of the Cu element on the EM behavior of Sn.

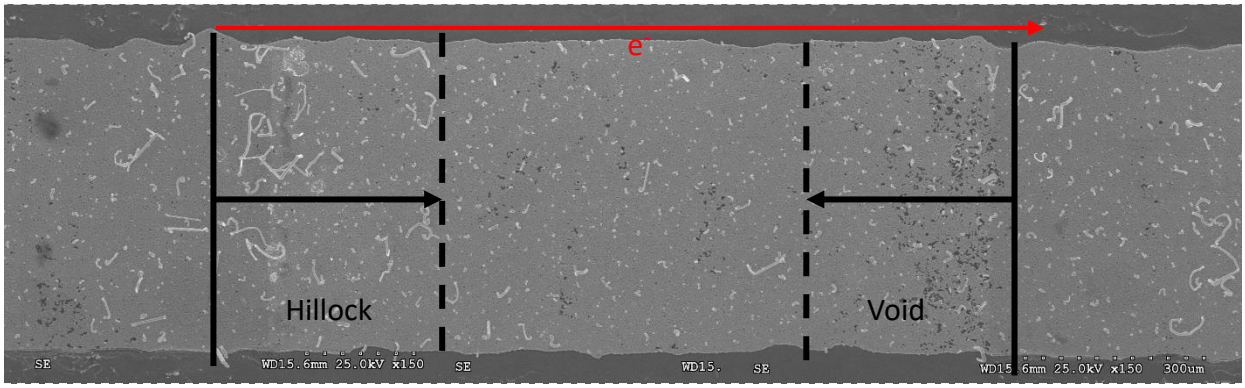

Fig 4.3 SEI image of ternary sample (Cu as cross-stripe on Sn-Ni). Cu is 0.10 at%, Ni is 0.86 at%. Sample was tested at 180^{o}C for 14 hours, with 5x10^{4} A/cm^{2}.

After the electromigration (EM) testing, clear marker formation was observed at the boundary area of the Sn-Cu-Ni ternary sample, as shown in Figure 4.3. Hillocks were formed at the cathode side, and voids were formed at the anode side, indicating that the presence of Cu

element further suppressed the EM rate of Sn in the system. The direction of marker advancement suggested that the Cu and Ni atoms migrated under EM, which is consistent with the "Two-phase Equilibrium" mechanism observed in EM testing of binary samples. This indicated that the EM was still driven by vacancy diffusion, and the intermetallic compounds (IMCs) induced by Cu and Ni may also control the vacancy concentration in the Sn-Cu-Ni system, similar to what was observed in the binary system. Therefore, this result further supported the "Two-phase Equilibrium" mechanism proposed in our research.

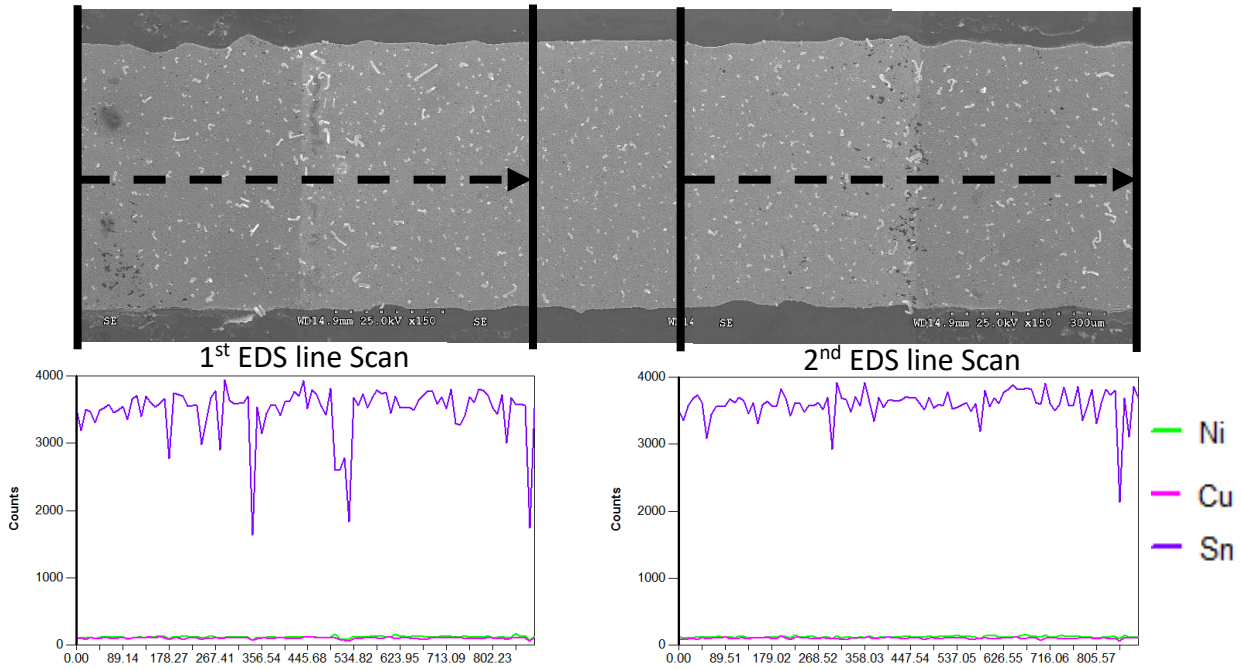

Fig 4.4 EDS line scan on the ternary sample (Cu as cross-stripe on Sn-Ni). Cu is 0.10 at%, Ni is 0.86 at%. Sample was tested at 180°C for 10 hours, with $5x10^4$ A/cm^2.

The migration of element atoms under EM was characterized using DS technique. Figure 4.4 presents the EDS line scan results obtained from the Sn-Cu-Ni ternary sample. The data indicated no major peak of Ni and Cu, suggesting that the presence of Cu did not have any effect on the Ni atoms under EM and vice versa. However, the EDS line scan results of Sn displayed

some fluctuations and several absences of Sn in counts, which may be due to voids generated by residual tensile stress induced during the repeated cooling/heating process when the sample was taken out from the oil bath for SEM inspection.

4.2 Secondary Element Effect on Sn-Cu System

4.2.1 Ag Effect on Sn-Cu System

In this section, we investigated the EM behavior of the Sn-Ag-Cu ternary alloy system, which is commonly known as the SAC solder alloy. To characterize the effect of the Ag element on the existing Sn-Cu alloy system under EM, Ag was applied as a "Cross-stripe" on top of the Sn-Cu stripe and the polarity and motion of the marker were analyzed.

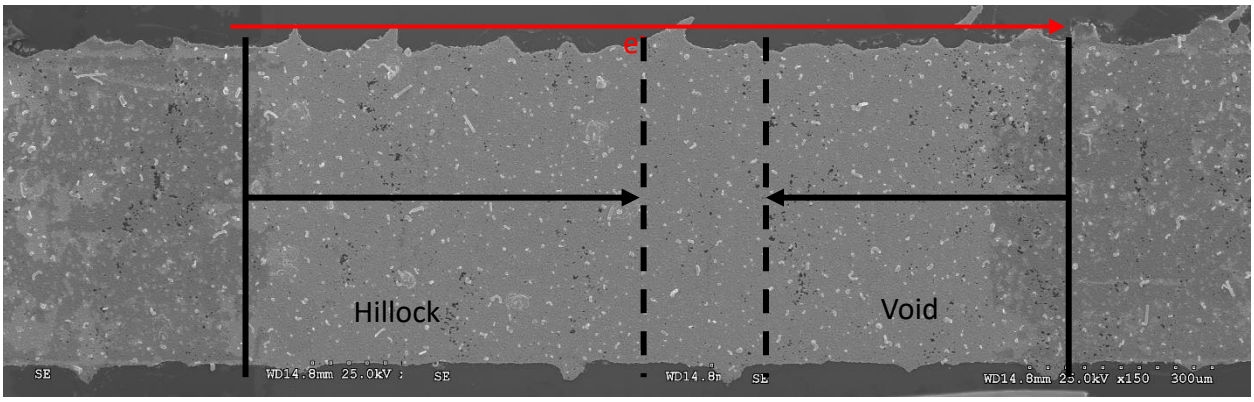

Fig 4.5 SEI image of ternary sample (Ag as cross-stripe on Sn-Cu). Cu is 0.96 at%, Ag is 0.56 at%. Sample was tested at 180ºC for 8 hours, with $5x10^4$ A/cm^2.

As demonstrated in Figure 4.5, hillocks were observed at the cathode side and voids at the anode side on the SAC ternary sample, indicating that the Ag element's presence suppressed the Sn electromigration rate in the existing Sn-Cu system. The direction of marker advancement suggested the occurrence of vacancy diffusion under electromigration in the alloy system, further

supporting the proposed "Two-Phase Equilibrium" mechanism. The intermetallic compounds (IMCs) induced by Ag and Cu may also govern the vacancy concentration in the Sn-Ag-Cu system.

Subsequent to the EM testing, an EDS line scan was conducted on the ternary sample. Figure 4.6 illustrates that high counts of Cu element were detected at the anode side boundary of the cross-stripe area. This finding was confirmed with several EDS line scan results on two Ag on Cu-Sn ternary samples. However, Cu was not observed to migrate and accumulate near the cross-stripe boundary in previous binary sample testing. This outcome suggested that the Ag element may trigger Cu migration during electromigration in the Sn-Ag-Cu system, which could pose a concern for SAC alloy applications.

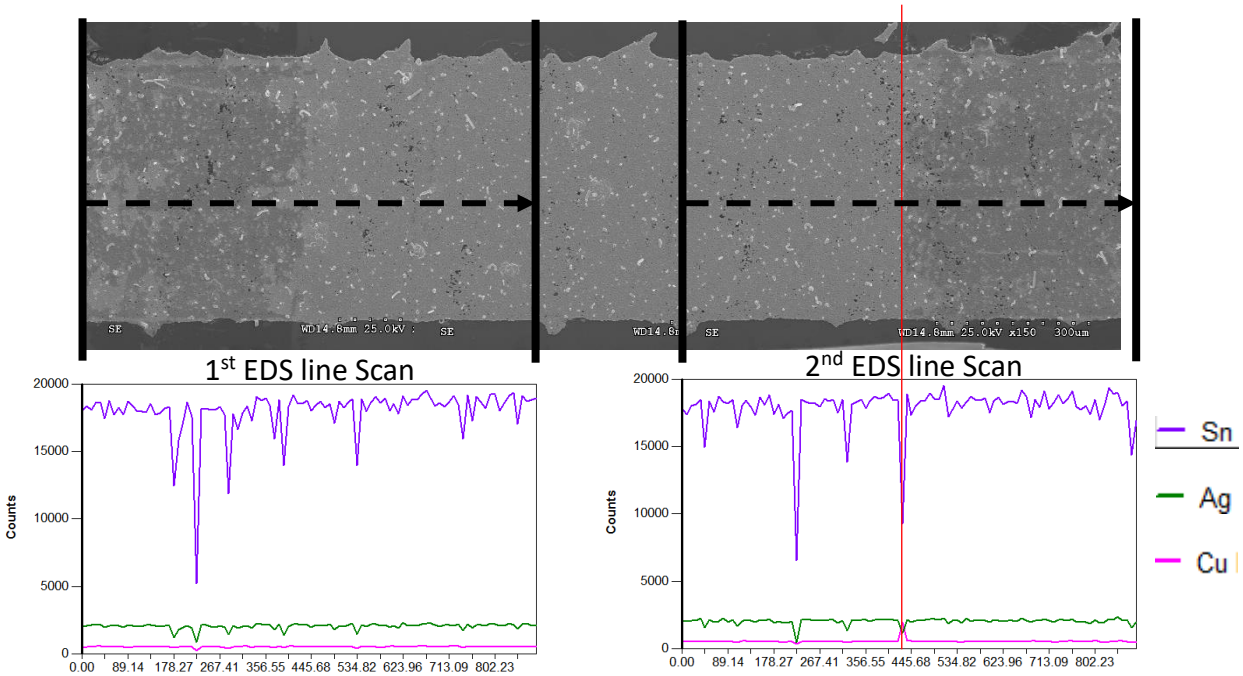

Fig 4.6 EDS line scan on ternary sample (Ag as cross-stripe on Sn-Cu): Cu is 0.96 at%, Ag is 0.56 at%, sample surface after 10 hours test.

4.2.2 Ni Effect on Sn-Cu System

A similar EM testing in SCN system like section 4.1.1was performed in this section. This time a Ni "Cross-stripe" was applied on top of the Sn-Cu stripe to study the presence of Ni atoms on the existing Sn-Cu alloy system under EM.

Figure 4.7 shows the marker formation and motion in Sn-Ni-Cu system under EM testing. Hillocks and voids were observed at the cathode and anode sides, respectively. This indicated that the presence of Ni element has a suppressive effect on the electromigration of Sn in the existing Cu-Sn system. Again, the direction of marker advancement was consistent with the proposed "Two-phase Equilibrium" mechanism.

However, an interesting phenomenon was observed in the EDS mapping and line scan performed on this Sn-Ni-Cu ternary sample (Figure 4.8). Several locations with high Ni and Cu signals, and low Sn signal were detected under EDS mapping scan. The backscattered scanning electron (BSE) images revealed that these locations may have a different phase than the surrounding areas. All these suggest that the additional Ni atoms may react with Cu to form a new phase without Sn element.

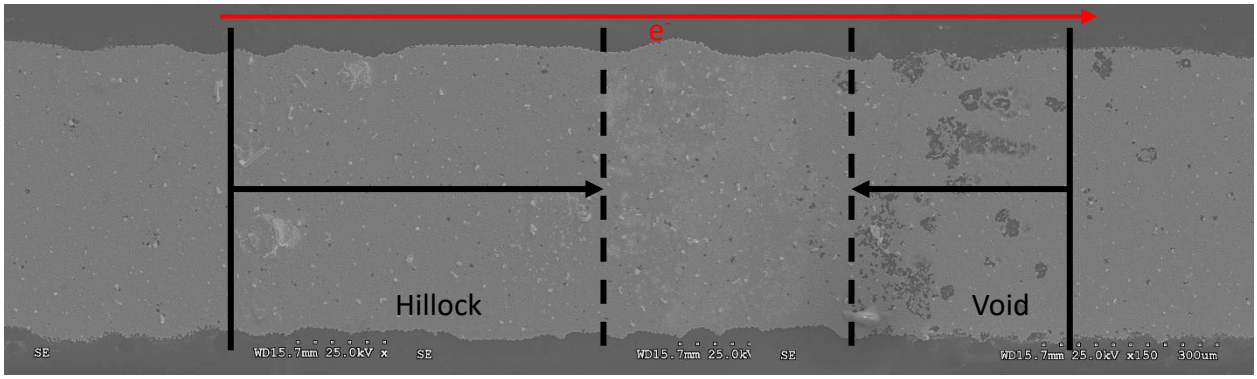

Fig 4.7 SEI image of ternary sample (Ni as cross-stripe on Sn-Cu). Ni is 3.47 at%, Cu is 1.92 at%. Sample was tested at 180^{o}C for 16 hours, with 5x10^{4} A/cm^{2}.

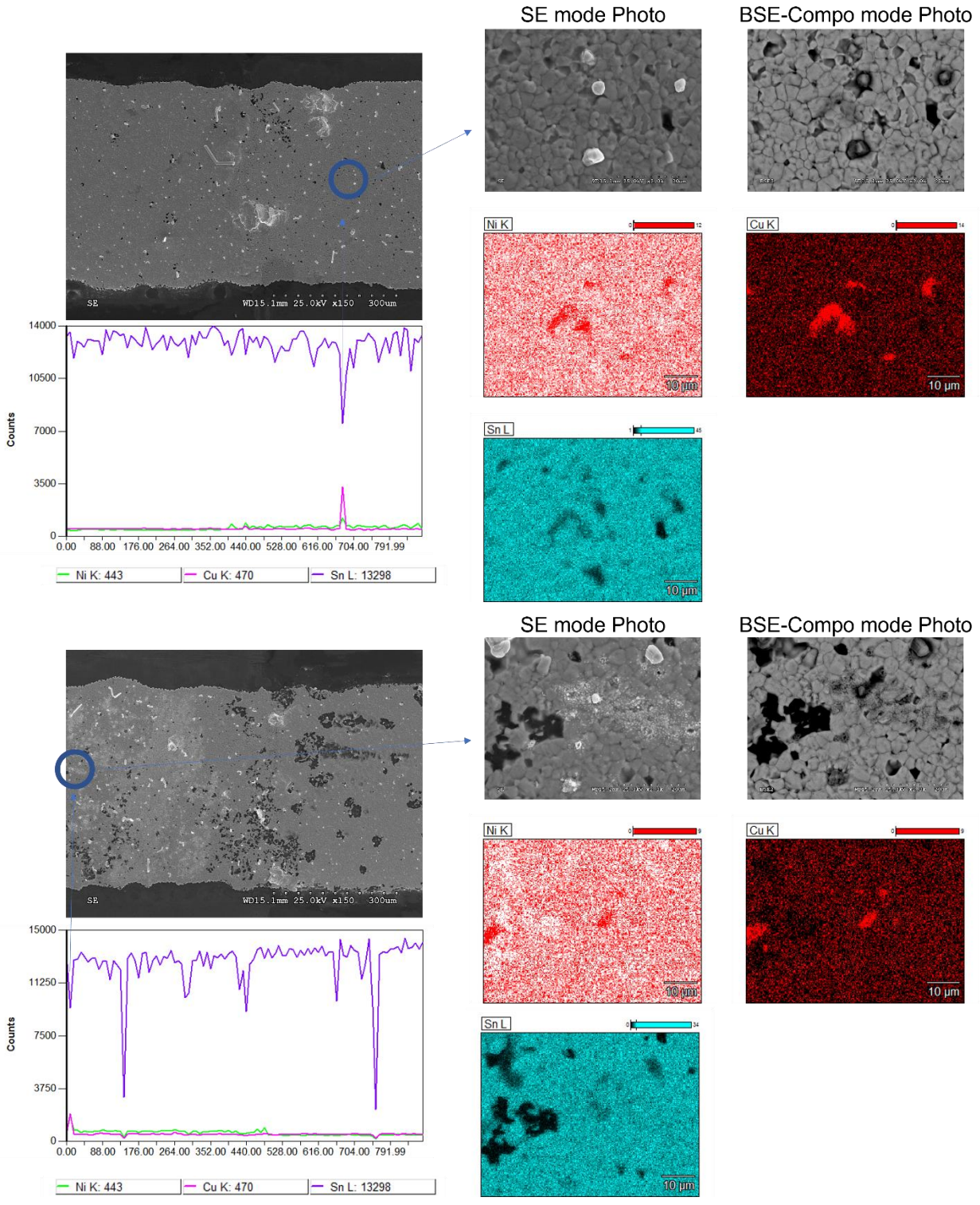

Fig 4.8 EDS line scan on ternary sample (Ni as cross-stripe on Sn-Cu) Cu is 0.10 at%, Ni is 0.86 at%. Sample was tested at 180^{o}C for 24 hours, with 5x10^{4} A/cm^{2}.

4.3 Mechanism of Secondary Element Effect

Based on the electromigration testing results result of ternary samples, two important implications can be drawn:

a) In the Sn-Ag-Cu system, the existence of Ag further suppresses the EM of Sn, and may accelerate Cu migration under EM.

b) In the Sn-Ni-Cu system, co-existence of Ni and Cu further suppress the EM of Sn, but they trend to form a new phase without Sn.

The Sn-Ag-Cu system, commonly known as the SAC alloy, is a widely used lead-free solder that has a melting point below 220^{o}C [87]. As the EM testing temperature for all ternary samples is 180^{o}C, lattice diffusion is the primary mechanism in the SAC system ($T > 0.8T_m$). While we do not yet have enough experimental data to fully explain the observed phenomenon in EM testing of the SAC system, we believe that the further suppression of the EM of Sn is caused by the formation of multiple IMCs, such as Ag_3Sn and Cu_6Sn_5, induced by alloy elements. This results in better control over the concentration of vacancies in the system. Additionally, the fast migration of Cu in the SAC system may be attributed to the presence of Ag solute atoms, which can lower the activation energy required for Cu atoms to jump, allowing Cu solutes to migrate quickly through the C axis in the Sn matrix under the force of EM.

The Sn-Ni-Cu system, also known as SCN alloy, is another popular lead-free solder with a melting point around 227^{o}C [88]. Similar to the SAC system, lattice diffusion is the dominant diffusion mechanism in the SCN system at the EM testing temperature ($T > 0.8T_m$). The observed further suppression of the EM of Sn in the SCN system is attributed to the formation of multiple IMCs, which helps to control the concentration of vacancies in the system.

Interestingly, we have observed the formation of a new phase in the SCN system that contains only Cu and Ni without Sn. We postulate that this Cu-Ni phase has a lower Gibbs free energy than other phases under electromigration, which drives its continuous development until an equilibrium concentration is reached. This finding could be a concern for SCN solder applications under electromigration and warrants further investigation.

Chapter 5: Conclusion and Future Plan

5.1 Conclusion

The presented results have shed light on the impact of alloy elements on the electromigration behavior of Sn. The binary sample testing results enabled the establishment of a "Two-Phase Equilibrium" mechanism, while the ternary sample testing allowed for the examination of the secondary alloy element effect on the existing Sn alloy system.

Three conclusions can be concluded from the research project:

a) Electromigration (EM) reliability of solder joint can be improved by two methods: 1) adding EM suppressing elements (such as Ni and Bi); 2) producing Sn grain with “Two-phase equilibrium”.

b) Fundamental EM properties of alloy elements can be characterized from marker polarity, and motion by using “Cross-stripe” configuration.

c) Ag may accelerate Cu migration under EM in Sn-Ag-Cu alloy system. Co-existence of Ni and Cu may further suppress the EM of Sn.

Results have been published and present at TechCon 2022 [89].

5.2 Future Work

The subsequent phase of this study will entail "Cross-stripe" testing with new alloy elements that could potentially exert a significant impact on Sn electromigration. The following test objectives have been established:

a) Conduct further "Cross-stripe" EM testing to explore the effects of additional alloy elements on Sn electromigration.

b) Conduct EM testing with low-temperature solder alloys.

Currently, EM testing of indium (In) with "Cross-stripe" configuration on Sn stripe is underway. As demonstrated in Fig 5.1 and Table 5.1, In displays acceleration on Sn electromigration when it exists as a solute in the Sn matrix, and suppression when it forms intermetallic compounds (IMC). This promising result further supports the proposed "Two-phase Equilibrium" mechanism. Upon completion of the EM testing, the marker motion measurement and EM diffusivity will be reported.

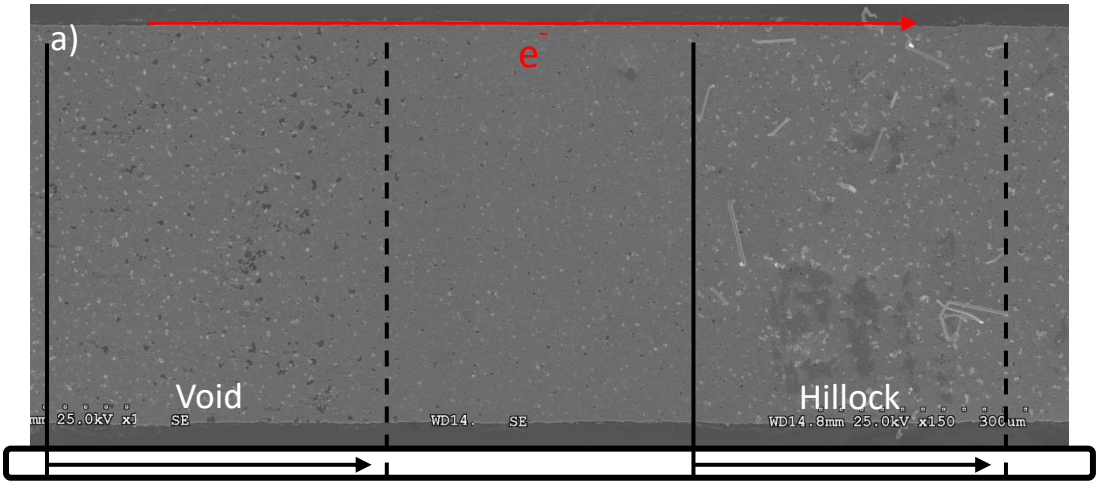

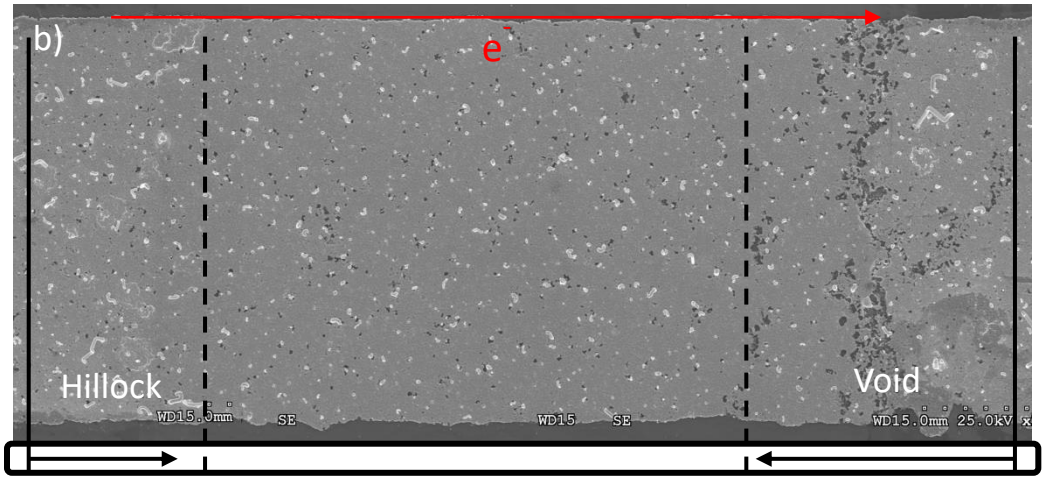

Fig 5.1 SEI images of In alloyed binary samples after EM testing. All samples are tested at 180^{o}C. Current density was set at 5x10^{4} A/cm^{2}: a) In is 0.69 at%, 64 hours of testing. b) In is 1.33 at%, 24 hours of testing.

In concentration in alloyed Cross-strip area	Alloy effect of EM of Sn
0.69 at%	Enhancement
1 at% at 222.6°C	**Maximum Solubility**
1.33 at%	Suppression

Table 5.1 Summary of In alloy effect on EM of Sn with maximum solubility [90-92].

As to the low-temperature solder alloy, it's a type of solder that has a melting temperature significantly lower than traditional solder alloys, typically below 150°C (302°F). This makes them particularly useful for soldering electronic components that are sensitive to heat, such as those found in modern microelectronics.

The most common type of low temperature solder alloy is a eutectic mixture of tin (Sn) and bismuth (Bi), often with small amounts of other metals added to improve its properties. This alloy has a melting temperature of around 138°C (280°F), which is significantly lower than traditional lead-tin (Pb-Sn) solder alloys that melt at around 183°C (361°F). Other low temperature alloys include tin-silver (Sn-Ag) and tin-zinc (Sn-Zn) alloys.

Low temperature solder alloys have several advantages over traditional solder alloys. They produce less thermal stress on the components being soldered, which can reduce the risk of damage to sensitive electronic components. They also tend to have a higher wetting ability, meaning they can form stronger bonds with the surfaces they are soldered to. Additionally, low temperature solder alloys are generally considered to be more environmentally friendly than traditional Pb-Sn alloys, which contain toxic lead.

Low temperature solder alloys are an important development in the field of electronics manufacturing, allowing for the soldering of increasingly complex and sensitive electronic components. All these becomes our research motivation on low-temperature solder alloys, which will be targeted at Sn-Bi binary alloy system.

Reference

[1] "Stannum": Peter van der Krogt, "Elementa chemica" apud situm Elementymology & Elements Multidict. Nomen Latinum mediaevale

[2] Holleman, Arnold F.; Wiberg, Egon; Wiberg, Nils (1985). "Tin". Lehrbuch der Anorganischen Chemie (in German) (91–100 ed.). Walter de Gruyter. pp. 793–800

[3] Schwartz, Mel (2002). "Tin and alloys, properties". Encyclopedia of Materials, Parts and Finishes (2nd ed.). CRC Press.

[4] Molodets, A.M.; Nabatov, S.S. (2000). "Thermodynamic potentials, diagram of state, and phase transitions of tin on shock compression". High Temperature. 38 (5): 715–721.

[5] Dehaas, W.; Deboer, J.; Vandenberg, G. (1935). "The electrical resistance of cadmium, thallium and tin at low temperatures". Physica. 2 (1–12): 453.

[6] Meissner, W.; R. Ochsenfeld (1933). "Ein neuer effekt bei eintritt der Supraleitfähigkeit". Naturwissenschaften. 21 (44): 787–788.

[7] Cierny, J.; Weisgerber, G. (2003). "The "Bronze Age tin mines in Central Asia". In Giumlia-Mair, A.; Lo Schiavo, F. (eds.). The Problem of Early Tin. Oxford: Archaeopress. pp. 23–31.

[8] "Tin demand to decline – International Tin Association". Mining.com. 18 October 2019. Retrieved 2021-07-03.

[9] https://www.belmontmetals.com/tin-lead-wire-common-solder-for-a-wide-range-of-applications/

[10] S. Menon, E. George, M. Osterman, M. Pecht, High lead solder (over 85%) solder in the electronics industry: RoHS exemptions and alternatives,, J. Mater. Sci. Mater. Electron. 26 (2015) 4021–4030.

[12] K.N. Tu, Reliability challenges in 3D IC packaging technology, Microelectron. Reliab. 51 (2011) 517–523.

[13] C.L. Liang, K.L. Lin, J.W. Peng, Microstructural evolution of intermetallic compounds in TCNCP Cu pillar solder joints,, J. Electron. Mater. 45 (2016) 51–56.

[14] K.N. Tu, Recent advances on electromigration in very-large-scale-integration of interconnects,, J. Appl. Phys. 94 (2003) 5451–5473.

[15] C. Chen, H.M. Tong, K.N. Tu, Electromigration and thermomigration in Pb-free flip-chip solder joints, Ann. Rev. Mater. Res. 40 (2010) 531–555.

[16] Liao, Yi-Han, et al. "A comprehensive study of electromigration in pure Sn: Effects on crystallinity, microstructure, and electrical property." Acta Materialia 200 (2020): 200-210.

[17] Abtew, M.; Selvaduray, G. Lead-Free Solders in Microelectronics. Mater. Sci. Eng. R Rep. 2000, 27, 95–141.

[18] Suganuma, K. Advances in Lead-Free Electronics Soldering. Curr. Opin. Solid State Mater. Sci. 2001, 5, 55–64.

[19] Porter, David A., Kenneth E. Easterling, and Mohamed Y. Sherif. Phase transformations in metals and alloys. CRC press, 2021. Porter, David A., Kenneth E. Easterling, and Mohamed Y. Sherif. Phase transformations in metals and alloys. CRC press, 2021.

[20] Cahn, R. W. "Recovery and Recrystallization, Chap. 19,“Physical Metallurgy, Cahn, RW, 2nd Ed." (1974).

[21] Darken, L.S. (February 1948). "Diffusion, Mobility, and Their Interrelation through Free Energy in Binary Metallic Systems". Trans. AIME. 175: 194.

[22] Smigelskas, A. D.; Kirkendall, E. O. (1947). "Zinc Diffusion in Alpha Brass". Trans. AIME. 171: 130–142.

[23] Fensham, P. (1950). Self-Diffusion in Polycrystalline Tin. Australian Journal of Chemistry, 3(1), 105.

[24] Coston, C., & Nachtrieb, N. H. (1964). Self-Diffusion in Tin at High Pressure. The Journal of Physical Chemistry, 68(8), 2219–2229.

[25] Huang, F. H., and H. B. Huntington. "Diffusion of Sb 124, Cd 109, Sn 113, and Zn 65 in tin." Physical Review B 9.4 (1974): 1479.

[26] Onishi, M., & Fujibuchi, H. (1975). Reaction-Diffusion in the Cu–Sn System. Transactions of the Japan Institute of Metals, 16(9), 539–547.

[27] Paul, A., Ghosh, C. & Boettinger, W.J. Diffusion Parameters and Growth Mechanism of Phases in the Cu-Sn System. Metall Mater Trans A 42, 952–963 (2011).

[28] Yuan, Y., Guan, Y., Li, D., & Moelans, N. (2016). Investigation of diffusion behavior in Cu–Sn solid state diffusion couples. Journal of Alloys and Compounds, 661, 282–293.

[29] Nash, P., Nash, A. The Ni−Sn (Nickel-Tin) system. Bulletin of Alloy Phase Diagrams 6, 350–359 (1985).

[30] H. Gautier, "Metallic Alloys," Bull. Soc. Encour. Ind. Natl., 1, 1313 (1896).

[31] M.G. Charpy, "Microscopic Study of Metallic Alloys," Bull. Soc. Encour. Ind. Natl., 2, 384-419 (1897).

[32] M. L. Guillet, “On the Ni−Sn Alloys”, Rev. Met., 4, 535–551 (1907).

[33] G. Voss, “The Ni−Sn Alloys,” Z. Anorg. Chem. 57, 35–45 (1908).

[34] D. Hanson, E.S. Sandford, and H. Stevens, “The Constitution of Alloys of Tin with Nickel. Ni−Sn System,” J. Inst. Met., 55, 117–119 (1934).

[35] W. Mikulas and L. Thomassen, “Equilibrium Relations in the Ni−Sn System,” Trans. AIME, Inst. Metal Div., 124, 111–137 (1937).

[36] T. Heumann, “The Equilibrium State in the Ni−Sn System,” Z. Metallkd., 35, 206–211 (1943) in German.

[37] HAIMOVICH, JOSEPH. "Intermetallic compound growth in tin and tin-lead platings over nickel and its effects on solderability." Proceedings of the Twelfth Annual Electronics Manufacturing Seminar. 1988.

[38] Bader, S., Gust, W., & Hieber, H. (1995). Rapid formation of intermetallic compounds interdiffusion in the Cu Sn and Ni Sn systems. Acta Metallurgica et Materialia, 43(1), 329–337.

[39] Labie, R., Ruythooren, W., & Van Humbeeck, J. (2007). Solid state diffusion in Cu–Sn and Ni–Sn diffusion couples with flip-chip scale dimensions. Intermetallics, 15(3), 396–403.

[40] Ho, Paul S., and Thomas Kwok. "Electromigration in metals." Reports on Progress in Physics 52.3 (1989): 301.

[41] W. Seith and H. Wever, Z. Elecktrochem. 59 (1953), 891–900.

[42] Skaupy, Fr. "Electrical conduction in metals." Verband Deutscher Physikalischer Gesellschaften 16 (1914): 156-157.

[43] V. B. Fiks, Sov. Phys. Solid State 1, 14 (1959)

[44] Huntington, H. B., and A. R. Grone. "Current-induced marker motion in gold wires." Journal of Physics and Chemistry of Solids 20.1-2 (1961): 76-87.

[45] B. Geden, “Understand and avoid electromigration (em) & ir-drop in custom ip blocks,” Nov 2011

[46] Lloyd, J. R. (1999). Electromigration in integrated circuit conductors. Journal of Physics D: Applied Physics, 32(17), R109–R118.

[47] https://en.wikipedia.org/wiki/Electromigration

[48] C.-K. Hu, M. B. Small, and P. S. Ho, J. Appl. Phys. 74 (2), 969-978 (1993).

[49] C.-K. Hu, K. Y. Lee, K. L. Lee, Jr. Cabral, C., E. G. Colgan, and C. Stanis, J. Electrochem. Soc. 143 (3), 1001-1006 (1996).

[50] Kim, Choongun, and J. W. Morris Jr. "The influence of Cu precipitation on electromigration failure in Al-Cu-Si." Journal of applied physics 72.5 (1992): 1837-1845.

[51] Ames, I. "FM dHeurle, and RE Horstmann." IBM J. Res. Develop 14 (1970): 461.

[52] Blech, Ilan A. "Copper electromigration in aluminum." Journal of Applied Physics 48.2 (1977): 473-477.

[53] C. Y. Liu, Chih Chen, K. N. Tu; Electromigration in Sn–Pb solder strips as a function of alloy composition. Journal of Applied Physics 15 November 2000; 88 (10): 5703–5709.

[54] Chen, C.-M., & Chen, S.-W. (2002). Electromigration effect upon the Sn/Ag and Sn/Ni interfacial reactions at various temperatures. Acta Materialia, 50(9), 2461–2469.

[55] Chao, B., Chae, S.-H., Zhang, X., Lu, K.-H., Im, J., & Ho, P. S. (2007). Investigation of diffusion and electromigration parameters for Cu–Sn intermetallic compounds in Pb-free solders using simulated annealing. Acta Materialia, 55(8), 2805–2814.

[56] Zhang, R., Xu, G., Wang, X. et al. Electromigration in Sn-Bi Modified with Polyhedral Oligomeric Silsesquioxane. J. Electron. Mater. 39, 2513–2521 (2010).

[57] Gu, Xin, and Yan Cheong Chan. "Electromigration in line-type Cu/Sn-Bi/Cu solder joints." Journal of electronic materials 37 (2008): 1721-1726.

[58] Lee, K., Kim, K., Tsukada, Y., Suganuma, K., Yamanaka, K., Kuritani, S., & Ueshima, M. (2011). Effects of the crystallographic orientation of Sn on the electromigration of Cu/Sn–Ag–Cu/Cu ball joints. Journal of Materials Research, 26(3), 467-474.

[59] Jian-Qiang Chen, Jing-Dong Guo, Kai-Lang Liu, Jian-Ku Shang; Dependence of electromigration damage on Sn grain orientation in Sn–Ag–Cu solder joints. *Journal of Applied Physics* 21 October 2013; 114 (15): 153509.

[60] Lee, K., Kim, K.-S., Tsukada, Y., Suganuma, K., Yamanaka, K., Kuritani, S., & Ueshima, M. (2011). Influence of crystallographic orientation of Sn–Ag–Cu on electromigration in flip-chip joint. Microelectronics Reliability, 51(12), 2290–2297.

[61] Kim, Choong-Un, et al. "Influence of solute additions on electromigration in aluminum." MRS Online Proceedings Library (OPL) 428 (1996).

[62] P.S. Ho and J.K Howard, J. Appl. Phys. 45, p. 3 229 (1974).

[63] Touloukian, Y. S., Thermophysical Properties of Matter, Vol. 12, Thermal Expansion, IFI/Plenum, New York, 1975.

[64] David R. Lide (ed), CRC Handbook of Chemistry and Physics, 84th Edition. CRC Press. Boca Raton, Florida, 2003; Section 4, Properties of the Elements and Inorganic Compounds; Physical Properties of the Rare Earth Metals

[65] Beaudry, B. J. and Gschneidner, K.A., Jr., in Handbook on the Physics and Chemistry of Rare Earths, Vol. 1, Gschneidner, K.A., Jr. and Eyring, L., Eds., North-Holland Physics, Amsterdam, 1978, 173.

[66] McEwen, K.A., in Handbook on the Physics and Chemistry of Rare Earths, Vol. 1, Gschneidner, K.A., Jr. and Eyring, L., Eds., North-Holland Physics, Amsterdam, 1978, 411.

[67] D.R. Lide, (Ed.) in Chemical Rubber Company handbook of chemistry and physics, CRC Press, Boca Raton, Florida, USA, 79th edition, 1998.

[68] A.M. James and M.P. Lord in Macmillan's Chemical and Physical Data, Macmillan, London, UK, 1992.

[69] G.W.C. Kaye and T. H. Laby in Tables of physical and chemical constants, Longman, London, UK, 15th edition, 1993.

[70] J.A. Dean (ed) in Lange's Handbook of Chemistry, McGraw-Hill, New York, USA, 14th edition, 1992.

[71] Craig, Bruce D.; Anderson, David S.; International, A. S. M. (January 1995). Handbook of corrosion data. p. 126. ISBN 978-0-87170-518-1. Archived from the original on 2016-05-11.

[72] Okamoto, H. (2007). Au-Sn (Gold-Tin). Journal of Phase Equilibria and Diffusion, 28(5), 490–490.

[73] Vnuk, F., Ainsley, M. H., & Smith, R. W. (1981). The solid solubility of silver, gold and zinc in metallic tin. Journal of Materials Science, 16(5), 1171–1176.

[74] Karakaya, I., & Thompson, W. T. (1987). The Ag-Sn (Silver-Tin) system. Bulletin of Alloy Phase Diagrams, 8(4), 340–347.

[75] Saunders, N., & Miodownik, A. P. (1990). The Cu-Sn (Copper-Tin) system. Bulletin of Alloy Phase Diagrams, 11(3), 278–287.

[76] Knight, J. R., & Rhys, D. W. (1959). The systems palladium - indium and palladium - tin. Journal of the Less Common Metals, 1(4), 292–303.

[77] Okamoto, H. (2012). Pd-Sn (Palladium-Tin). Journal of Phase Equilibria and Diffusion, 33(3), 253–254.

[78] Ishida, K., & Nishizawa, T. (1991). The Co-Sn (Cobalt-Tin) System. Journal of Phase Equilibria, 12(1), 88–93.

[79] Okamoto, H. (2006). Co−Sn (Cobalt-Tin). Journal of Phase Equilibria and Diffusion, 27(3), 308–308.

[80] Nash, P., & Nash, A. (1985). The Ni−Sn (Nickel-Tin) system. Bulletin of Alloy Phase Diagrams, 6(4), 350–359.

[81] Schmetterer, C., Flandorfer, H., Richter, K. W., Saeed, U., Kauffman, M., Roussel, P., & Ipser, H. (2007). A new investigation of the system Ni–Sn. Intermetallics, 15(7), 869–884.

[82] Massalski TB, Okamoto H, Subramanian PR, Kacprzak L. Binary alloy phase diagrams. ASM International; 1996.

[83] Okamoto, H. (2008). Ni-Sn (Nickel-Tin). Journal of Phase Equilibria and Diffusion, 29(3), 297–298.

[84] Lee, BJ., Oh, CS. & Shim, JH. Thermodynamic assessments of the Sn-In and Sn-Bi binary systems. J. Electron. Mater. 25, 983–991 (1996).

[85] Okamoto, H. (2010). Bi-Sn (Bismuth-Tin). Journal of Phase Equilibria and Diffusion, 31(2), 205–205.

[86] Rubinšteĭn, L. I. (2000). The stefan problem (Vol. 8). American Mathematical Soc.

[87] Lee, L. M., & Mohamad, A. A. (2013). Interfacial Reaction of Sn-Ag-Cu Lead-Free Solder Alloy on Cu: A Review. Advances in Materials Science and Engineering, 2013, 1–11.

[88] Fubin Song, Lo, J. C. C., Lam, J. K. S., Tong Jiang, & Lee, S. W. R. (2008). A comprehensive parallel study on the board level reliability of SAC, SACX and SCN solders. 2008 58th Electronic Components and Technology Conference.

[89] Geng Ni, Patrick F. Thompson, Choong-Un Kim, Pilin Liu and Allison Theresa Osmanson. Mechanism of Alloying Elements Affecting the Rate of Electromigration of Sn Based Solder Interconnect, TechCon 2022.

[90] Okamoto, H. (2006). In−Sn (Indium-Tin). Journal of Phase Equilibria and Diffusion, 27(3), 313–313.

[91] D.S. Evans and A. Prince, Alloy Phase Diagrams, eds. L.H. Bennett, T.B. Massalski and B.C. Giessen, MRS Symp. Proc. Vo1.19, 389 (Elsevier North-Holland, 1983).

[92] Heumann, T., & Alpaut, O. (1964). Das Zustandsdiagramm Indium-Zinn. Journal of the Less Common Metals, 6(2), 108–117.

Biographical Information

Geng Ni obtained his B.E. in Materials Forming and Controlling Engineering from the Jiangsu University of Science and Technology (JUST) in China in 2016. In 2017, he joined the University of Texas at Arlington (UTA) as a Master student in Materials Science and Engineering. Recognizing his solid foundation and exceptional academic performance, he transitioned to the Ph.D. program in Materials Science and Engineering under the guidance of Prof. Choong-un Kim in 2018.

Throughout his Ph.D. studies, Geng Ni actively engaged in various research projects encompassing failure analysis, electrochemistry, and semiconductor fields. In 2022, he took on the role of Sabre 3D Process Engineering Intern at Lam Research, where he gained valuable hands-on experience in Wafer Level Packaging (WLP) techniques.

Upon completion of his Ph.D., Geng Ni was offered a position as a Senior Engineer – Integration Engineering at GlobalFoundries. He eagerly accepted the offer and looks forward to contributing his knowledge and skills to their operations after graduating.